Focal Plane Wavefront Sensing and Control Strategies for High-Contrast Imaging on the MagAO-X Instrument

KELSEY MILLER
PHD CANDIDATE, 2018
UNIVERSITY OF ARIZONA
COLLEGE OF OPTICAL SCIENCES & STEWARD OBSERVATORY

[10703-66]

THE UNIVERSITY OF ARIZONA

Center for Astronomical Adaptive Optics

Universiteit Leiden

SPIE.

14 JUNE 2018

AUSTIN, TEXAS

Outline

- Wavefront sensing on MagAO-X
- Focal plane wavefront sensing with a vAPP
  - Low-order wavefront sensing (LOWFS)
  - Linear dark field control (LDFC)
- Future on MagAO-X
- Conclusions and ongoing work

Wavefront sensing on MagAO-X

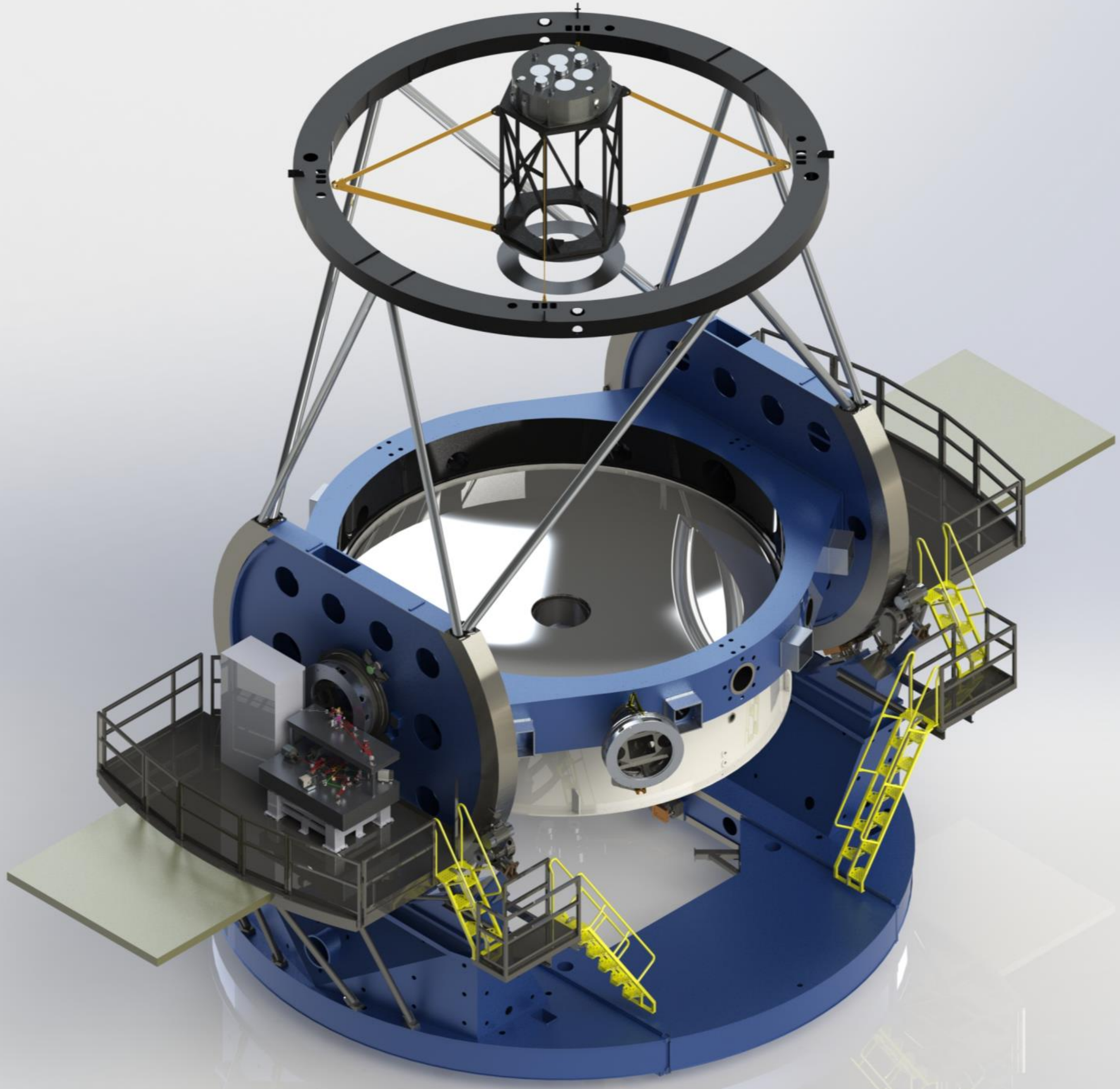

Primary wavefront sensor:

- Pyramid wavefront sensor (PyWFS)
- Operating at up to 3.63 kHz

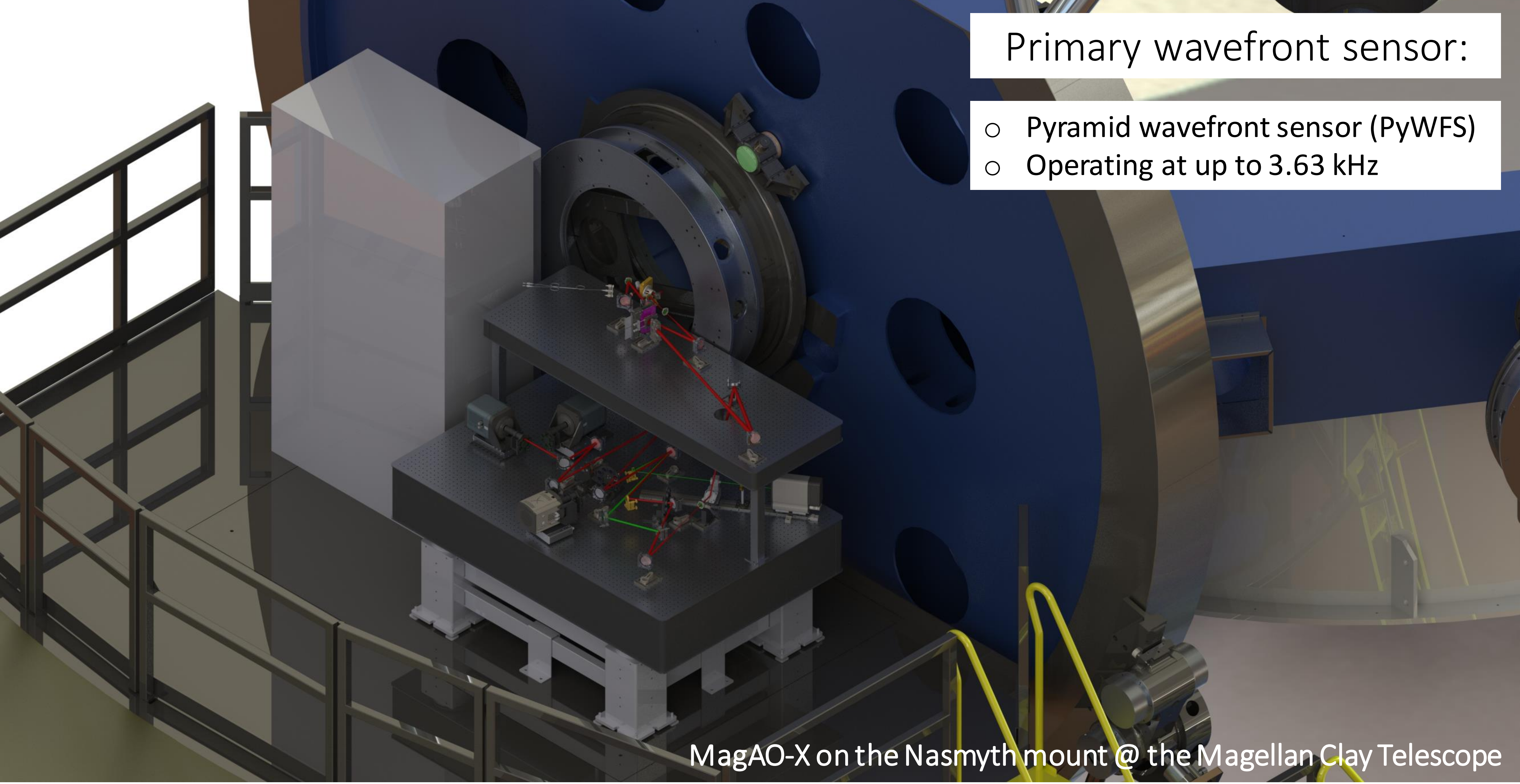

MagAO-X on the Nasmyth mount @ the Magellan Clay Telescope

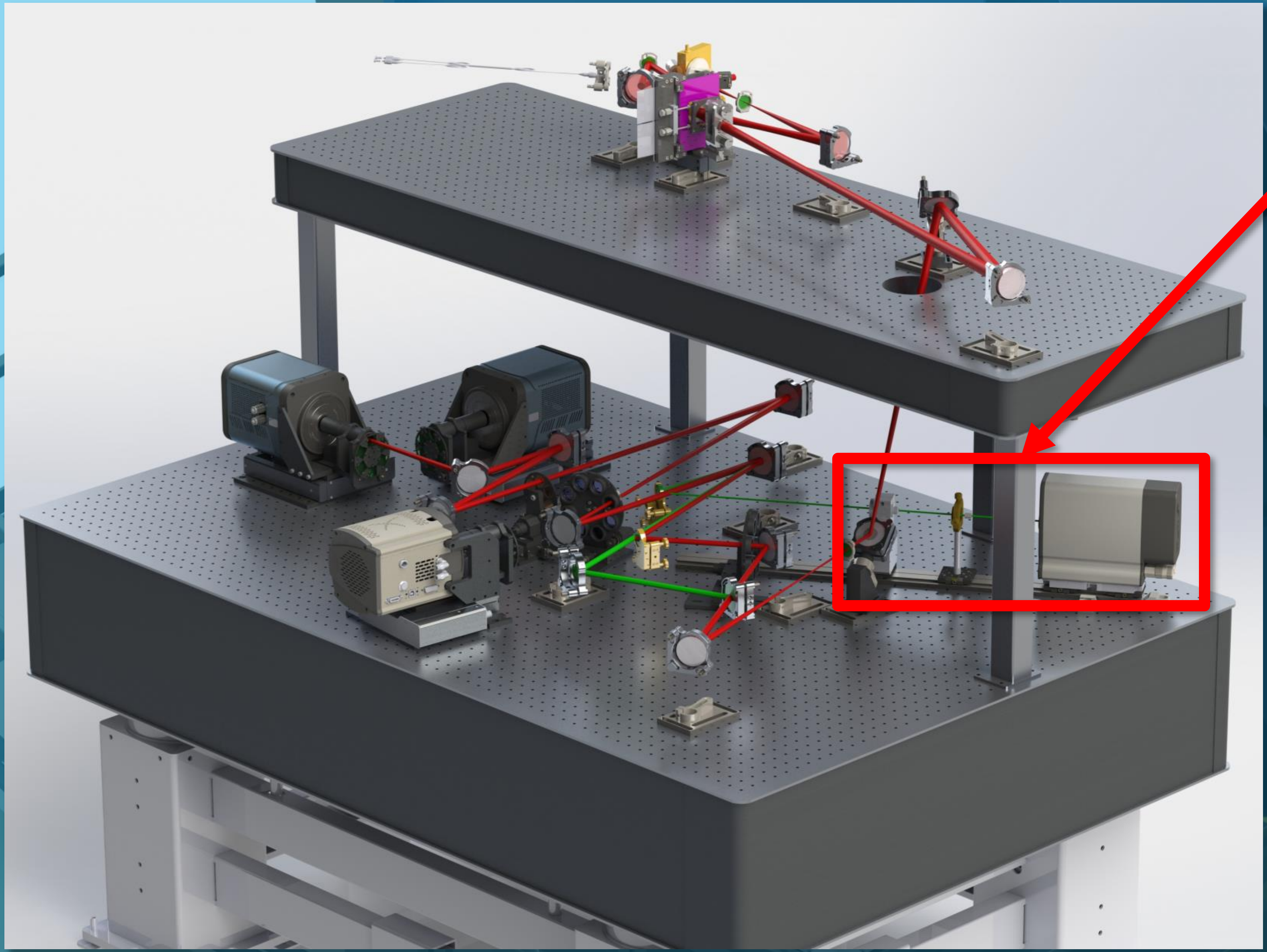

Primary wavefront sensor:

- Pyramid wavefront sensor (PyWFS)
- Operating at up to 3.63 kHz

Schatz [10703-74] 4:50 – 5:10 pm

MagAO-X on the Nasmyth mount @ the Magellan Clay Telescope

Why focal plane wavefront sensing?

Why focal plane wavefront sensing?

- Enable continuous high-contrast imaging performance at the raw contrast level delivered by the coronagraph

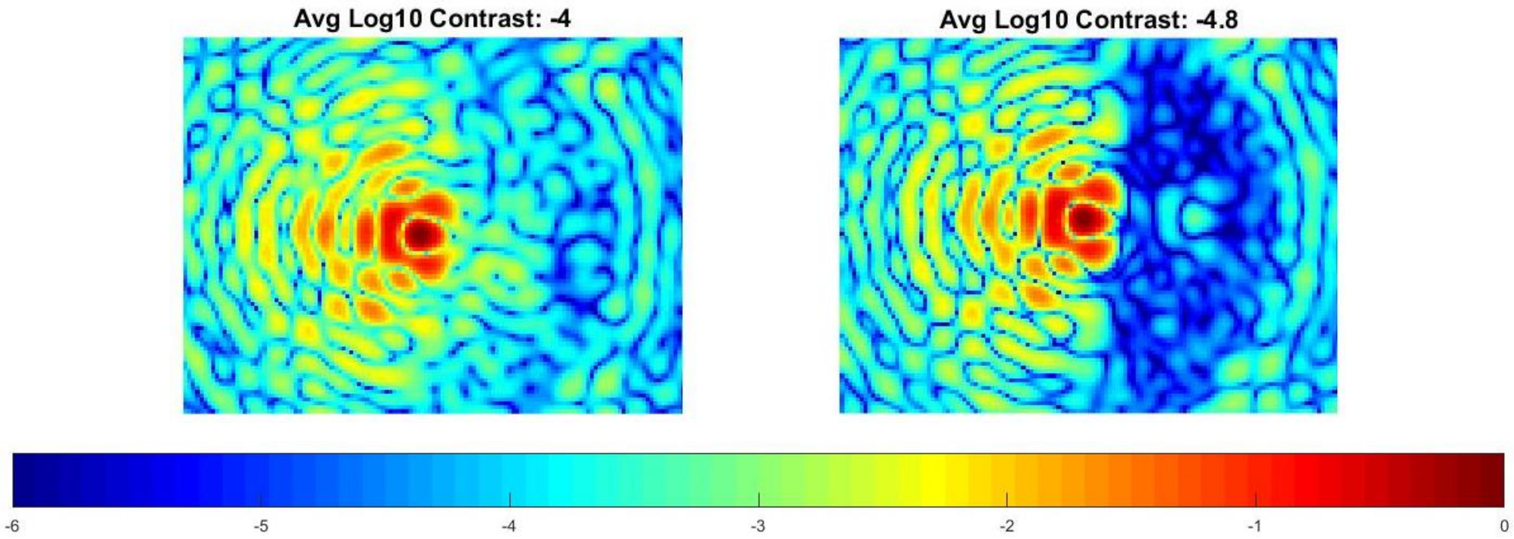

Why focal plane wavefront sensing?

- Enable continuous high-contrast imaging performance at the raw contrast level delivered by the coronagraph
  - Mitigate the impact of quasi-static and non-common path (NCP) aberrations

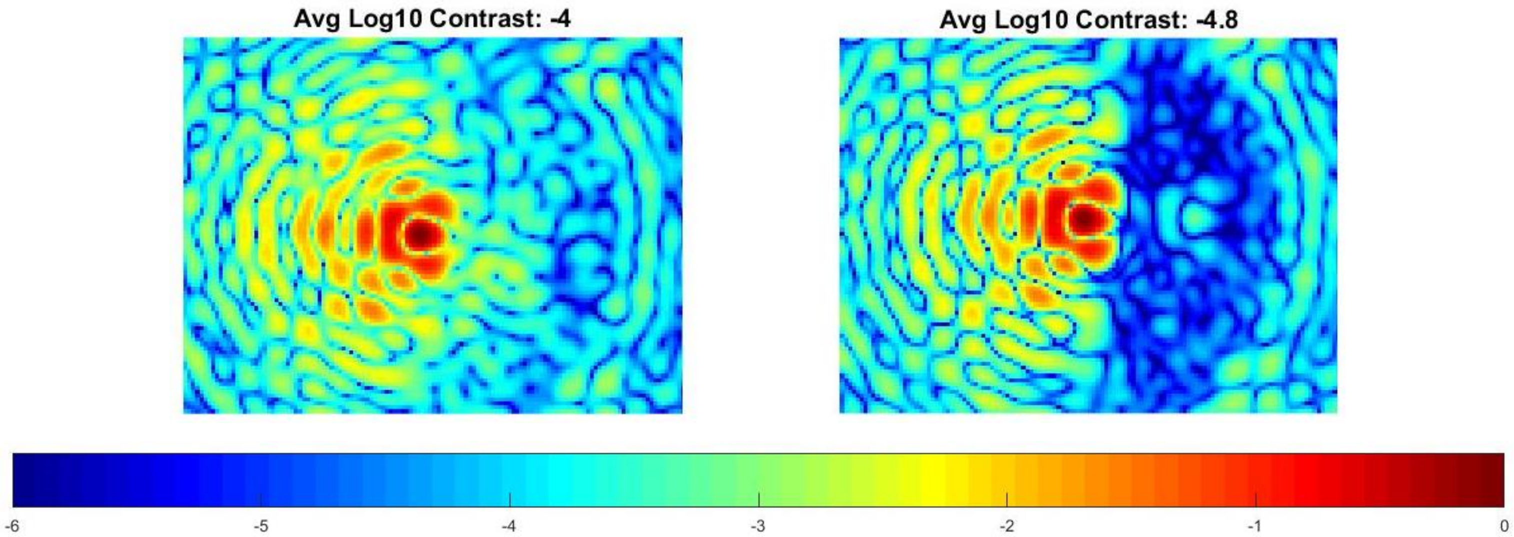

Why focal plane wavefront sensing?

- Enable continuous high-contrast imaging performance at the raw contrast level delivered by the coronagraph
  - Mitigate the impact of quasi-static and non-common path (NCP) aberrations
    - Low-order aberrations

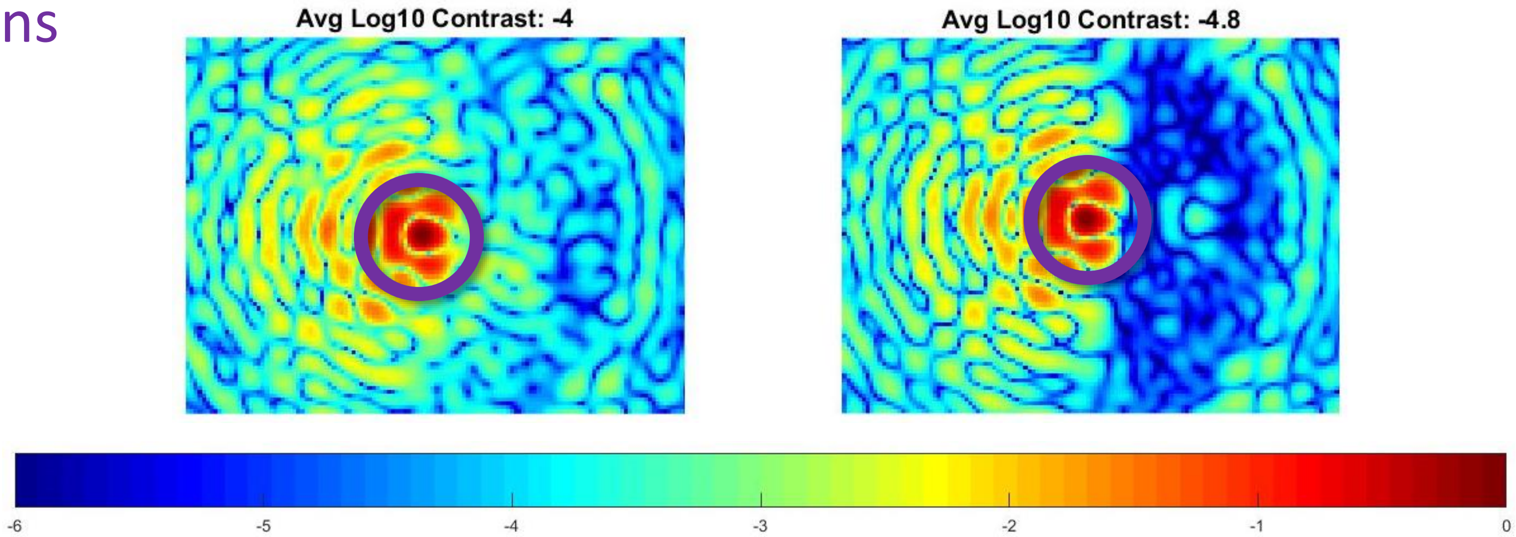

Why focal plane wavefront sensing?

- Enable continuous high-contrast imaging performance at the raw contrast level delivered by the coronagraph
  - Mitigate the impact of quasi-static and non-common path (NCP) aberrations
    - Low-order aberrations
    - Mid-spatial frequencies

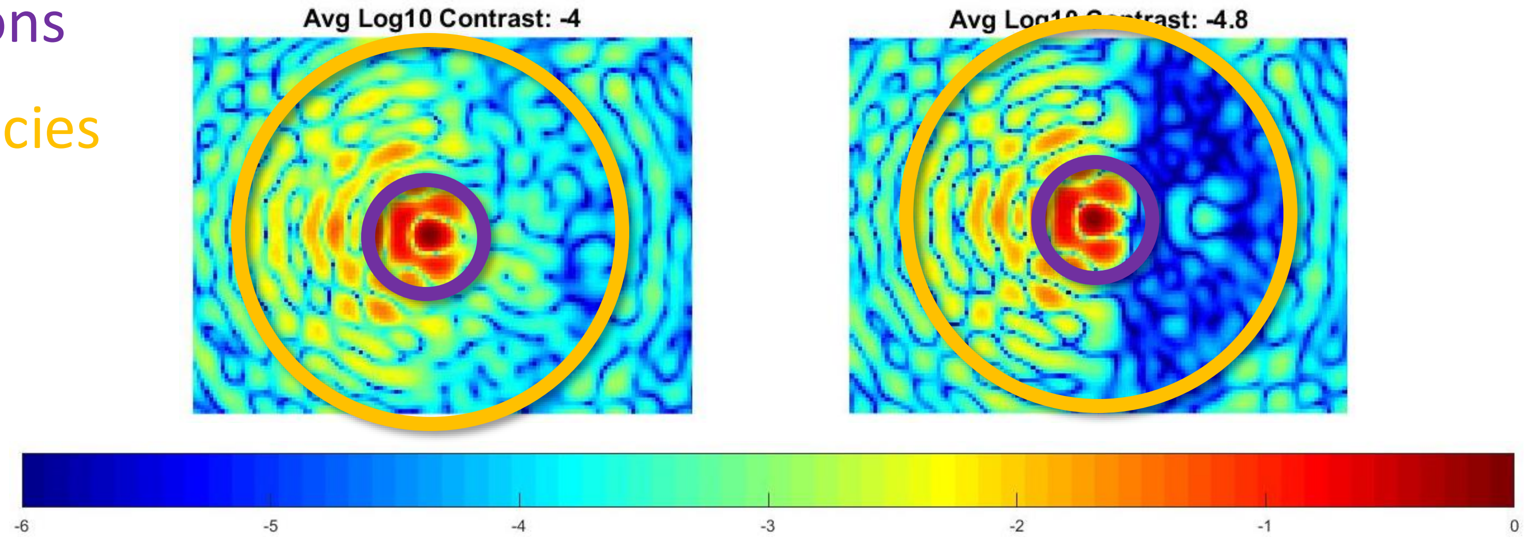

FPWFS w/ a vAPP

Focal plane wavefront sensing of low and mid-spatial frequencies with a vAPP coronagraph

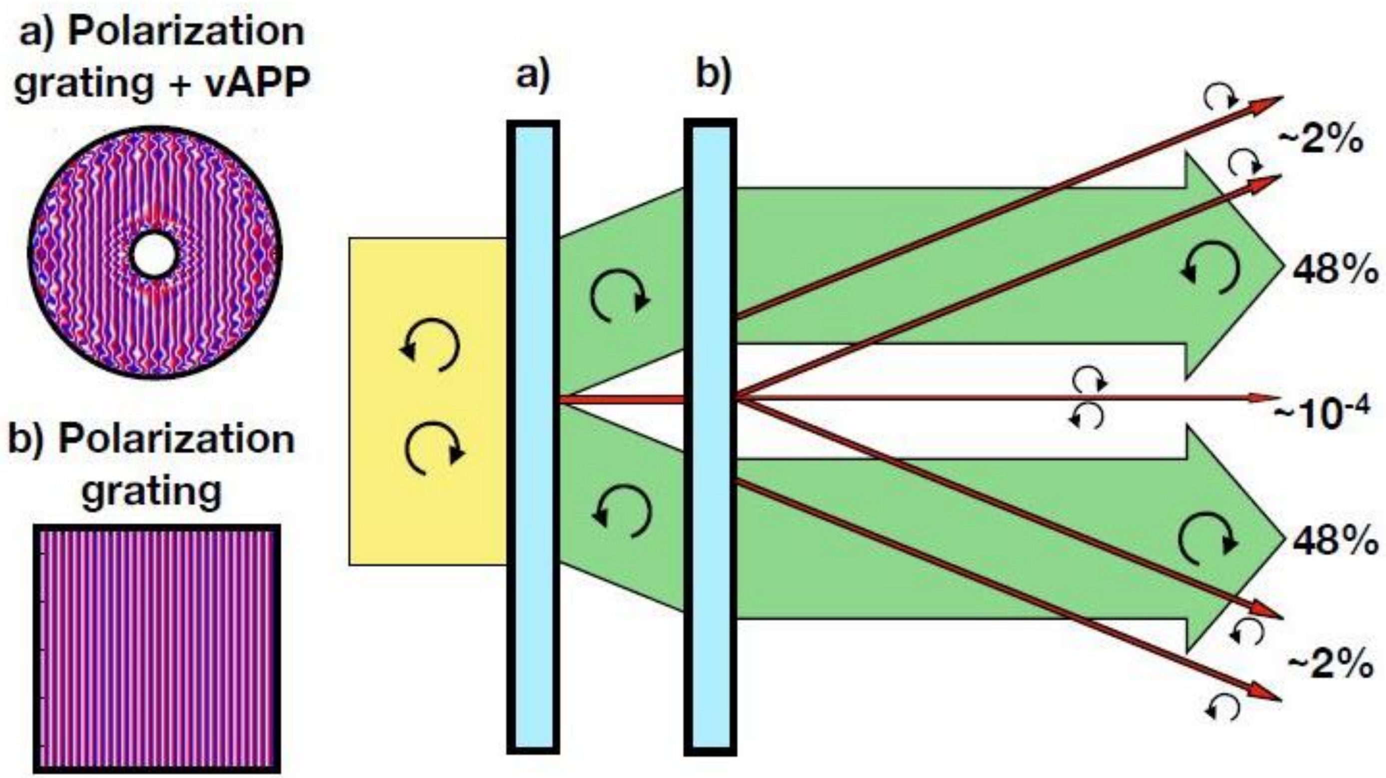

vAPP coronagraph
(vector Apodizing Phase Plate)

vAPP coronagraph (courtesy of D. Doelman, F. Snik, et. al.)

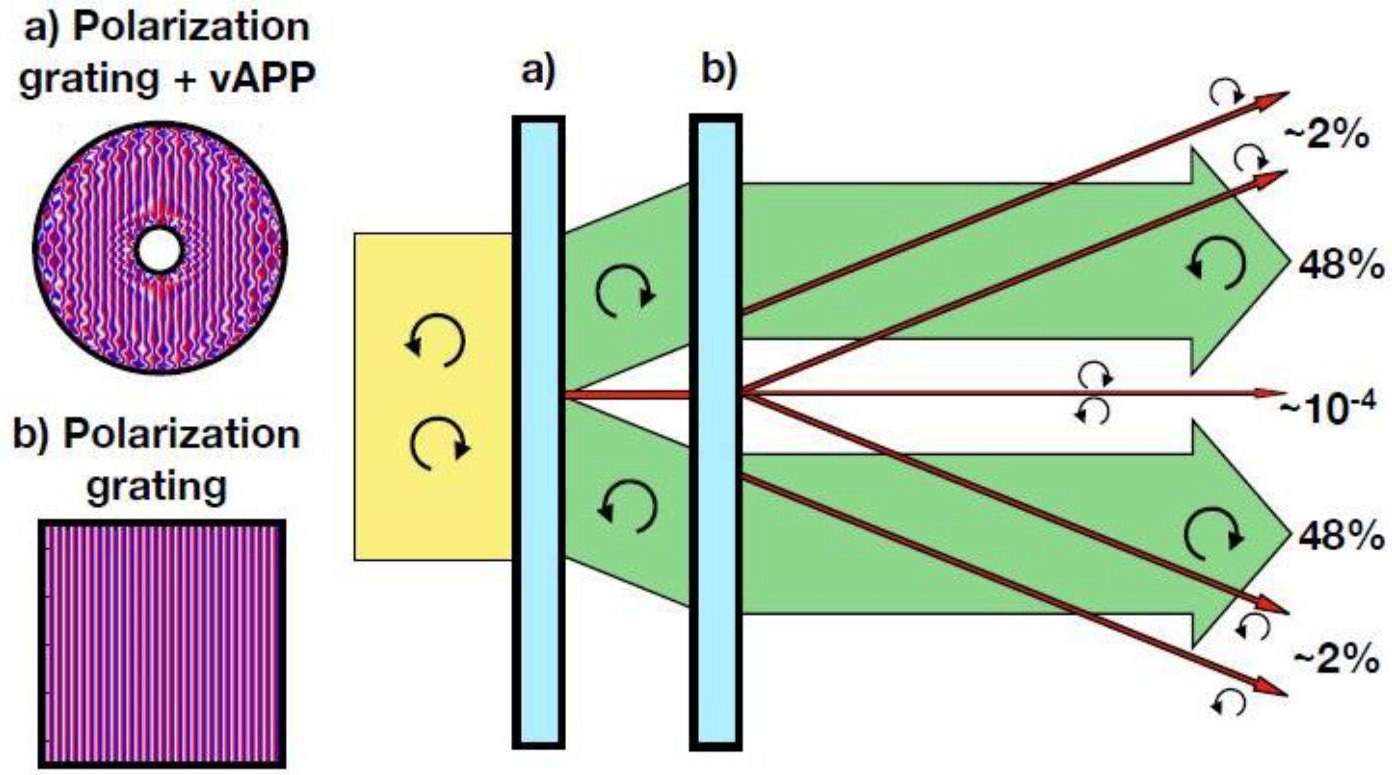

Figure 1: Schematic diagram of the double-grating. Unpolarized light (yellow) enters the grating-vAPP. The grating-vAPP consists of a two patterns added together: a polarization grating and a vAPP that generates a 360-degree dark zone. The combined pattern splits the two circular polarization states and applies the phase that generates the dark zone (green). The second polarization grating reverses the tilt from the first polarization grating pattern and the apodized light continues without tilt. A leakage term (red) goes through the grating-vAPP without acquiring any phase. This leakage term is apodized by the second grating and is diffracted. Any offset from half-wave retardance for the second polarization grating generates three leakage terms. The first is a double leakage term, that only contains 0.01% of the light and the other two are diffracted beams of the grating-vAPP. Note that the latter leakage terms have been apodized by the first grating-vAPP and have a dark zone.

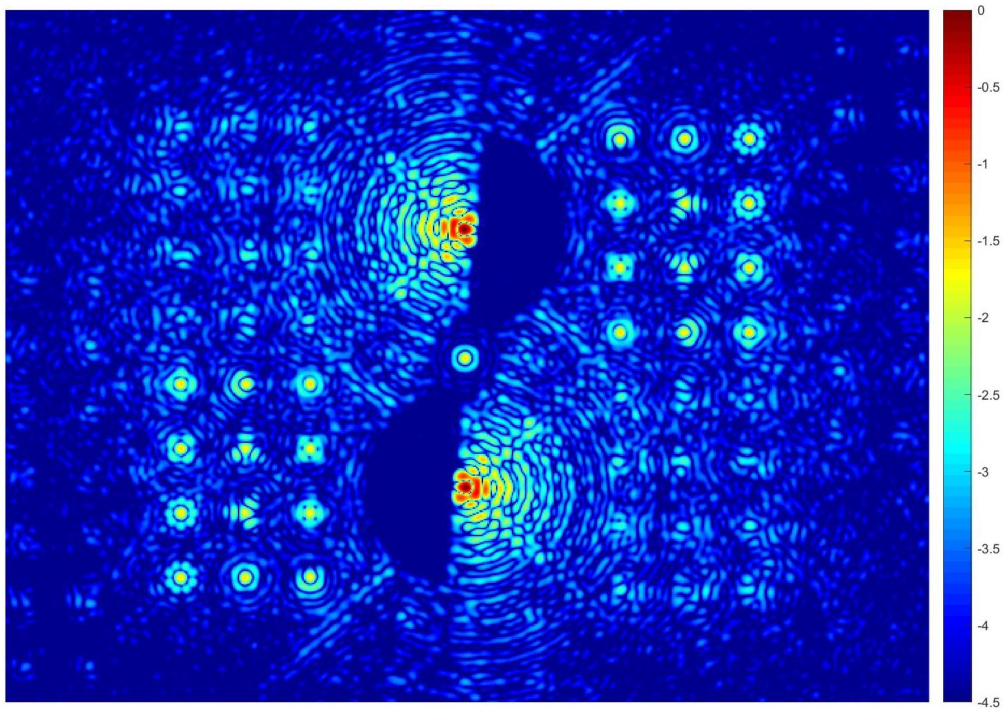

“Patterned liquid-crystal optics for broadband coronagraphy and wavefront sensing”, Doelman et. al 2017

vAPP coro

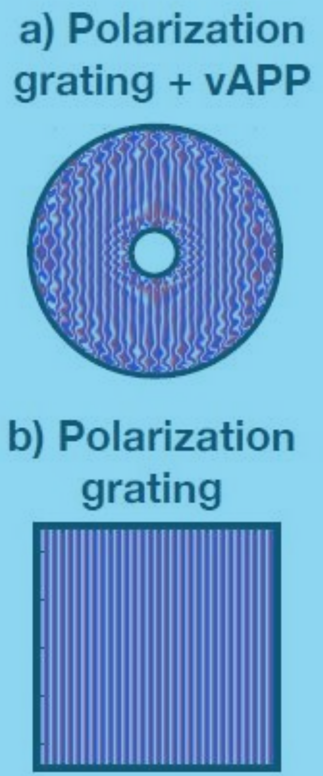

Figure 1: Schematic diagr
grating-vAPP consists of a
360-degree dark zone. The
that generates the dark zon
grating pattern and the ap
vAPP without acquiring an
offset from half-wave retar
is a double leakage term, t
grating-vAPP. Note that th
zone.

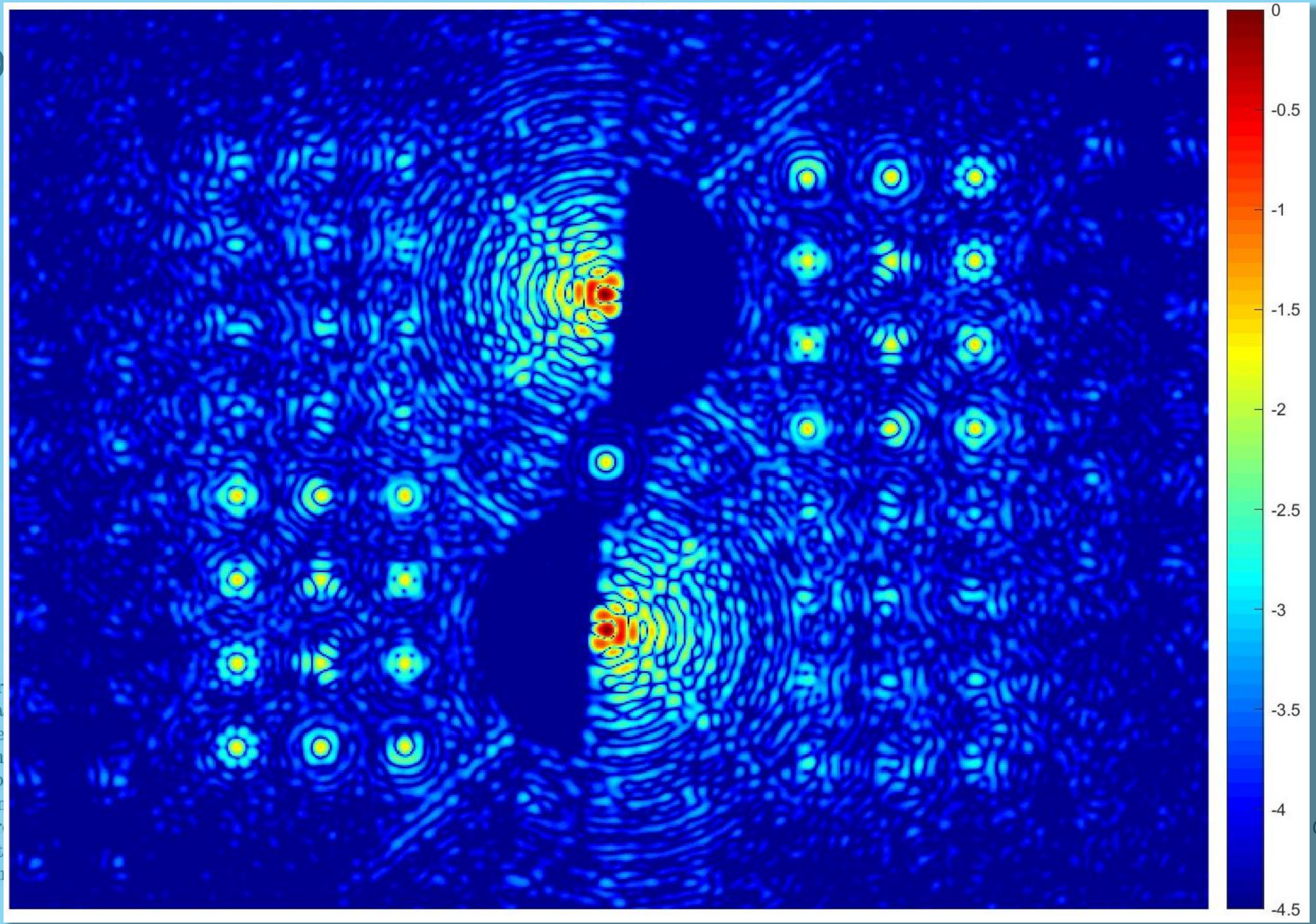

coronagraphy

vAPP coro

a) Polarization grating + vAPP

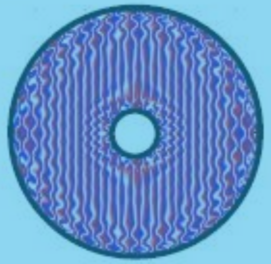

b) Polarization grating

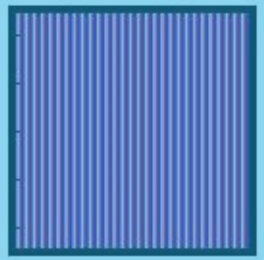

Figure 1: Schematic diagr
grating-vAPP consists of a
360-degree dark zone. The
that generates the dark zon
grating pattern and the ap
vAPP without acquiring an
offset from half-wave retar
is a double leakage term, t
grating-vAPP. Note that th
zone.

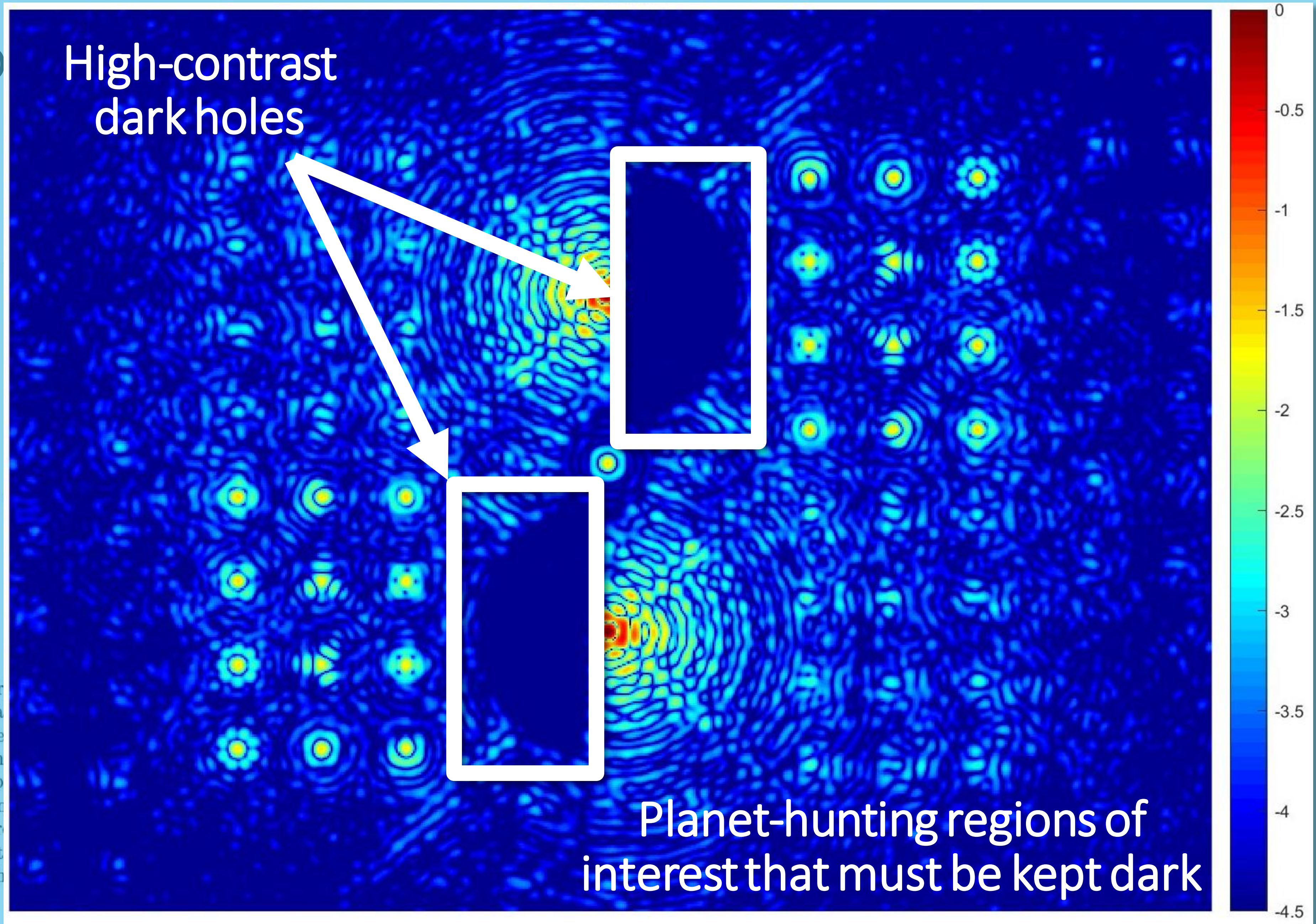

coronagraphy

vAPP coro

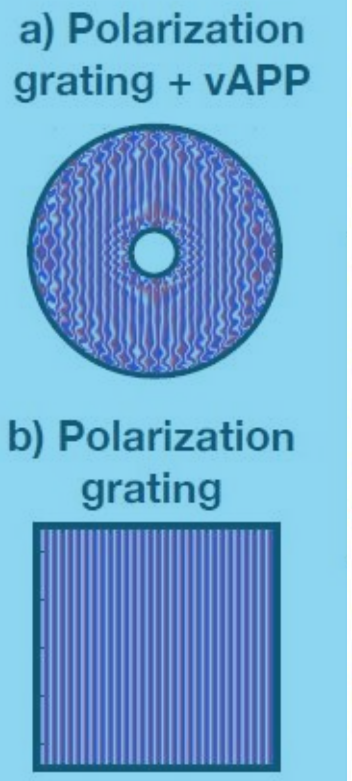

Figure 1: Schematic diagr
grating-vAPP consists of a
360-degree dark zone. The
that generates the dark zon
grating pattern and the ap
vAPP without acquiring ar
offset from half-wave retar
is a double leakage term, t
grating-vAPP. Note that th
zone.

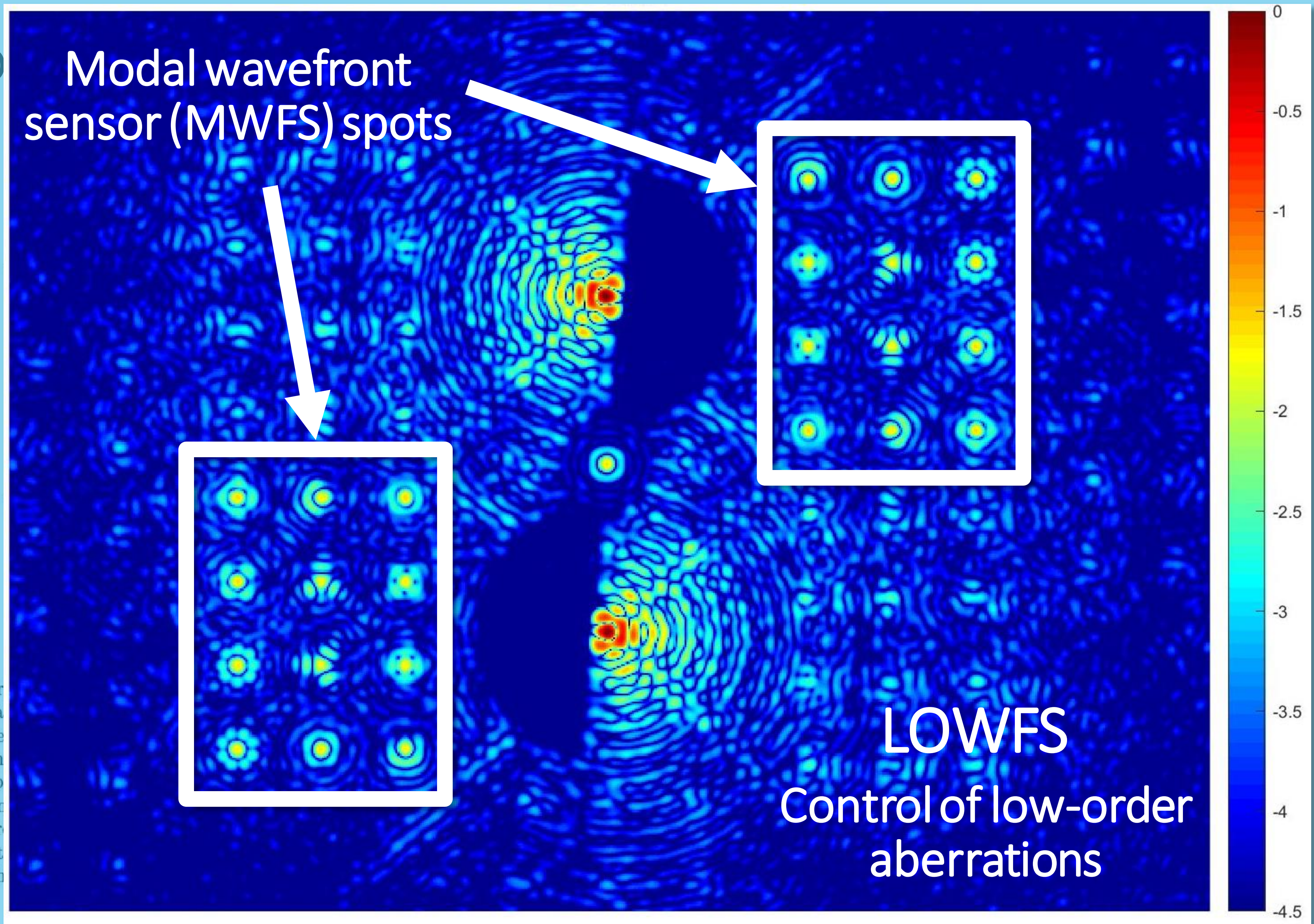

coronagraphy

vAPP coro

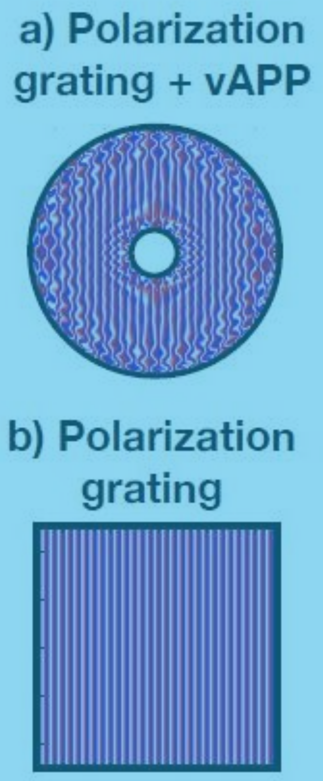

Figure 1: Schematic diagr
grating-vAPP consists of a
360-degree dark zone. The
that generates the dark zon
grating pattern and the ap
vAPP without acquiring ar
offset from half-wave retar
is a double leakage term, t
grating-vAPP. Note that th
zone.

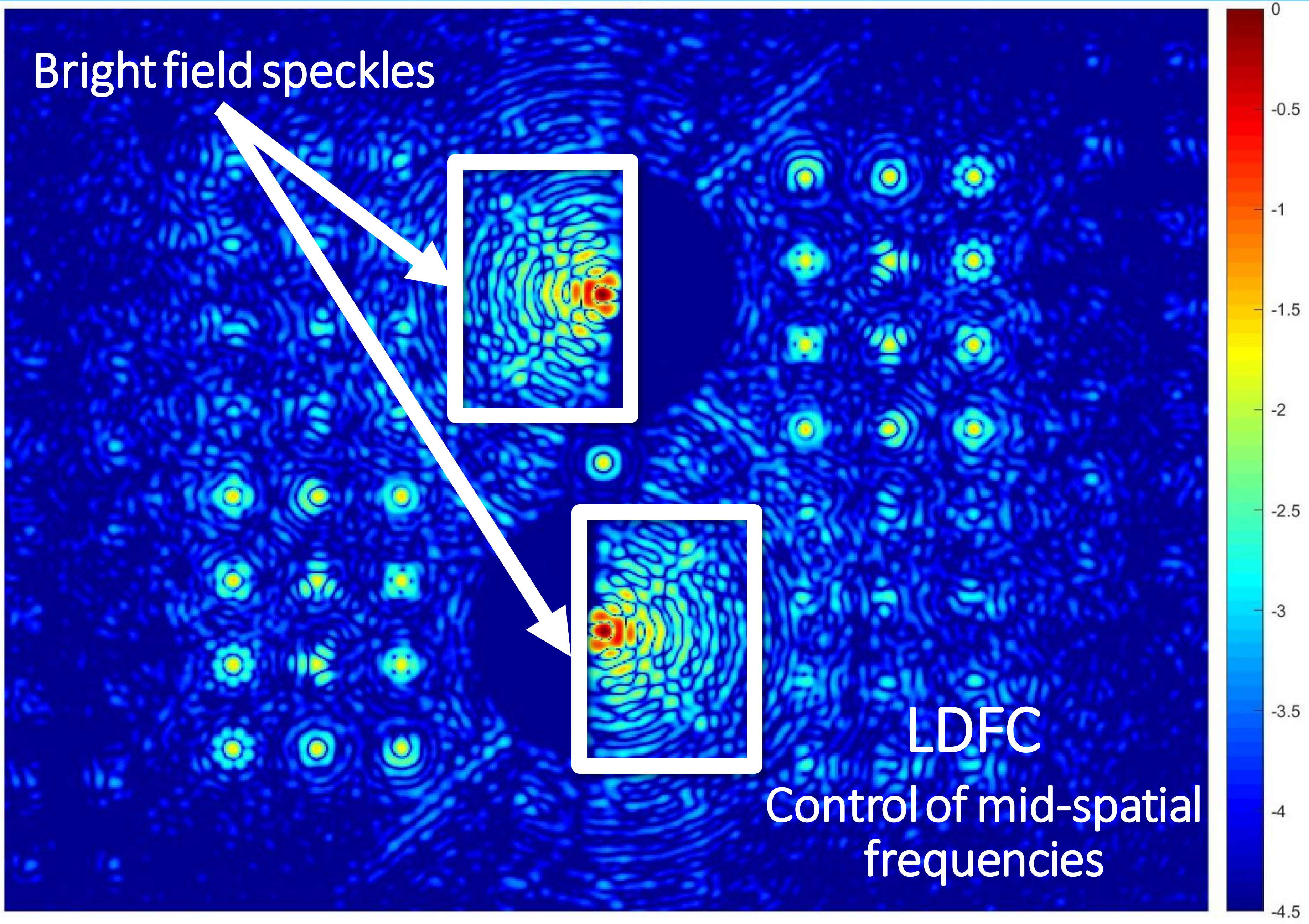

coronagraphy

Low-order wavefront sensing (LOWFS)

Low-order wavefront sensing (LOWFS) using modal wavefront sensor (MWFS) spots created in the image plane by the vAPP coronagraph

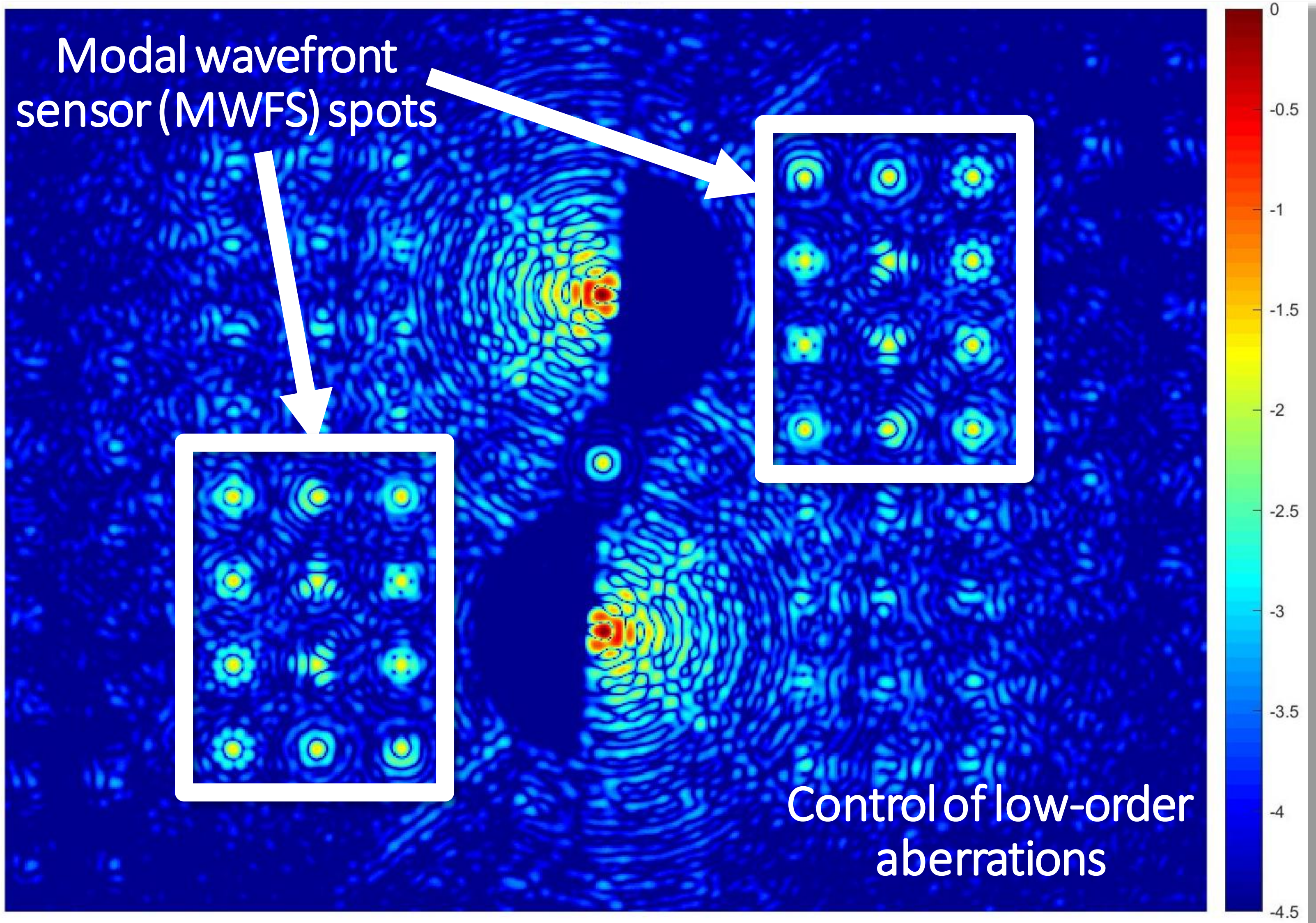

LOWFS w/ a MWFS

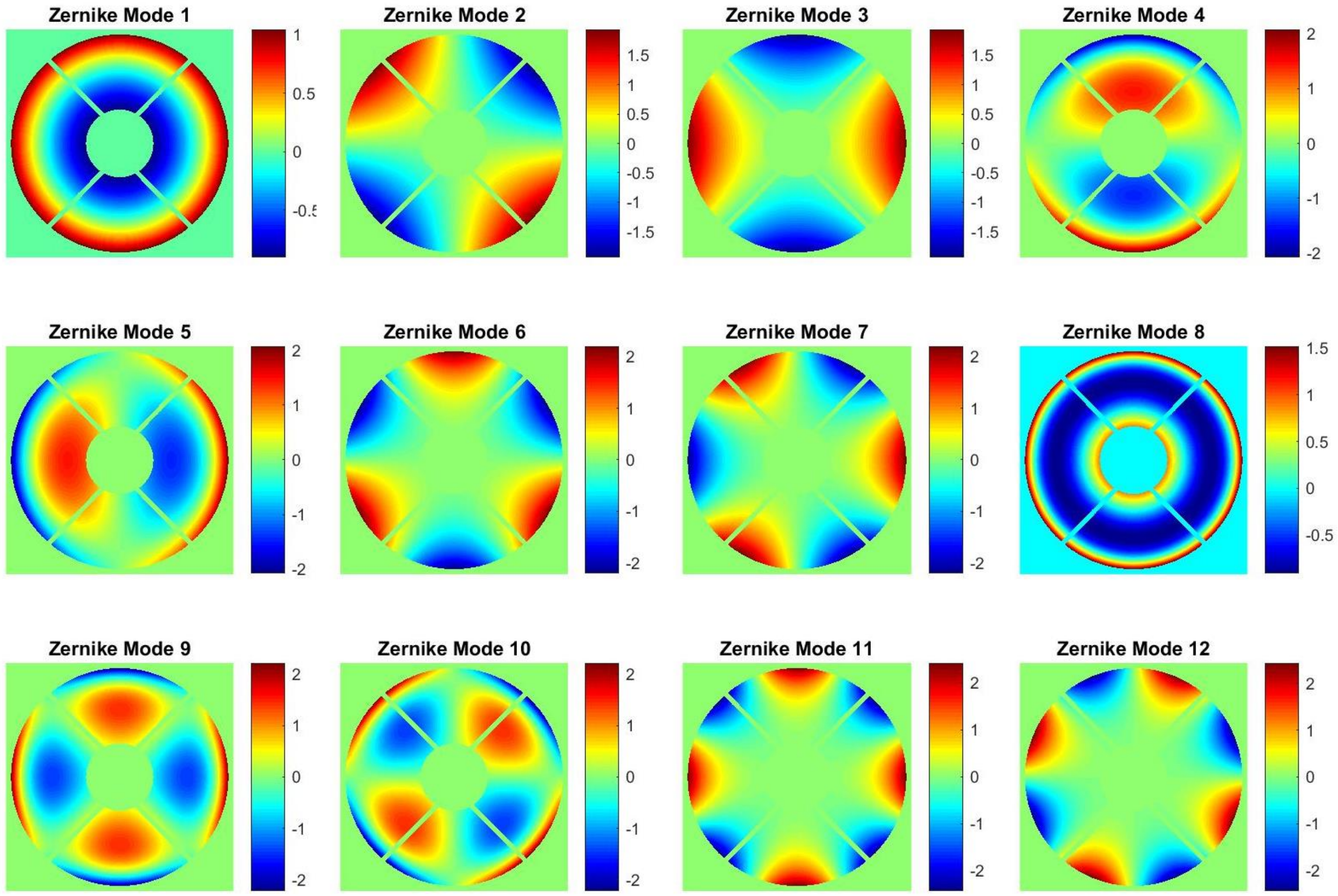

Applied Zernike modes

LOWFS w/ a MWFS

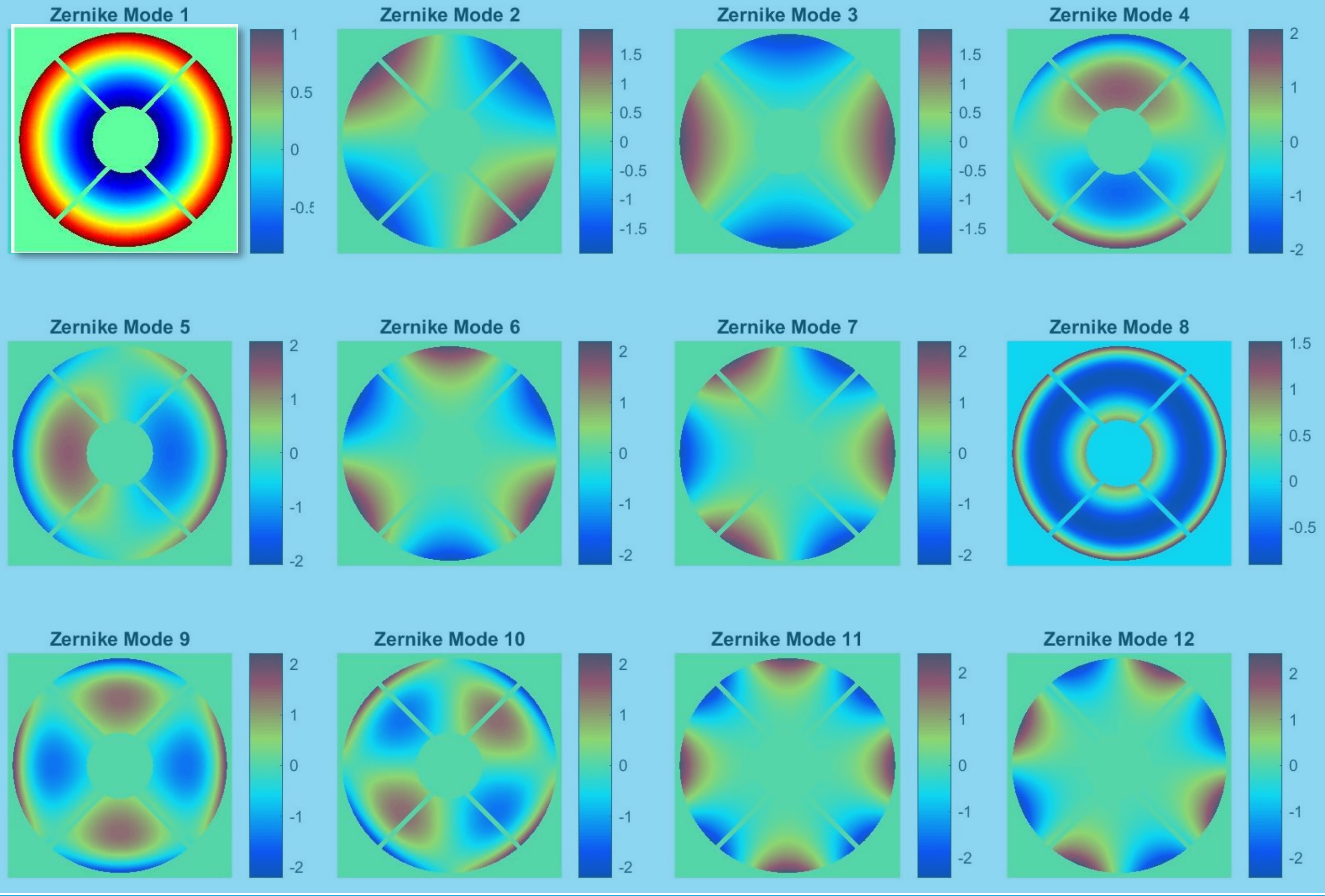

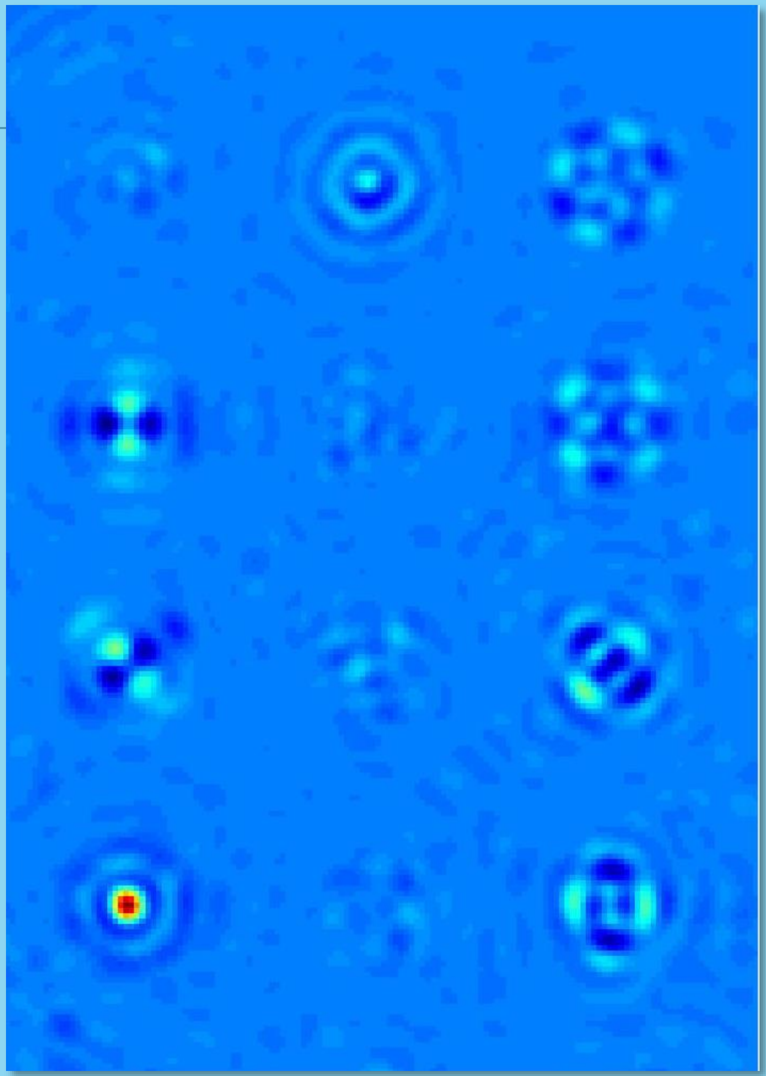

LOWFS w/ a MWFS

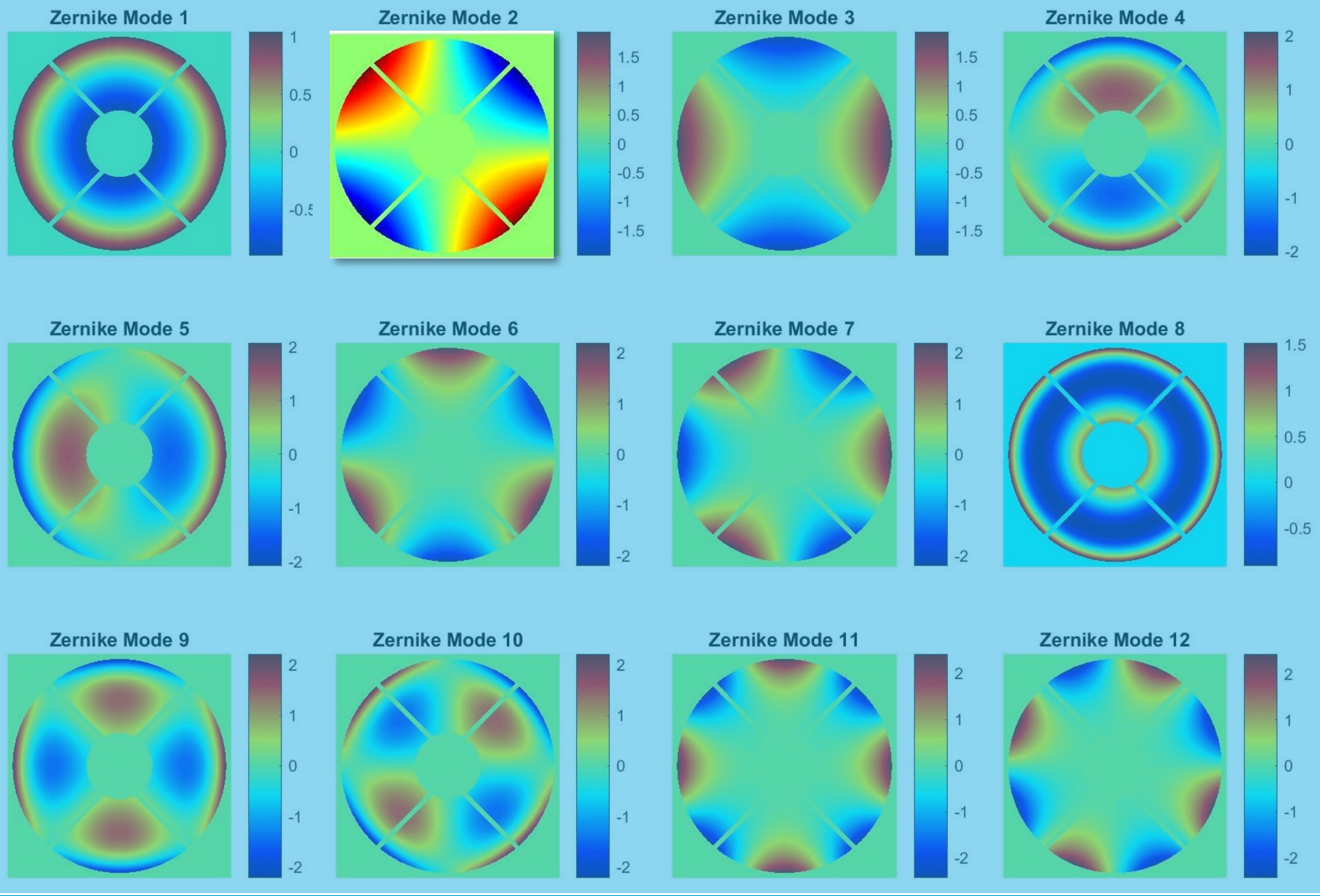

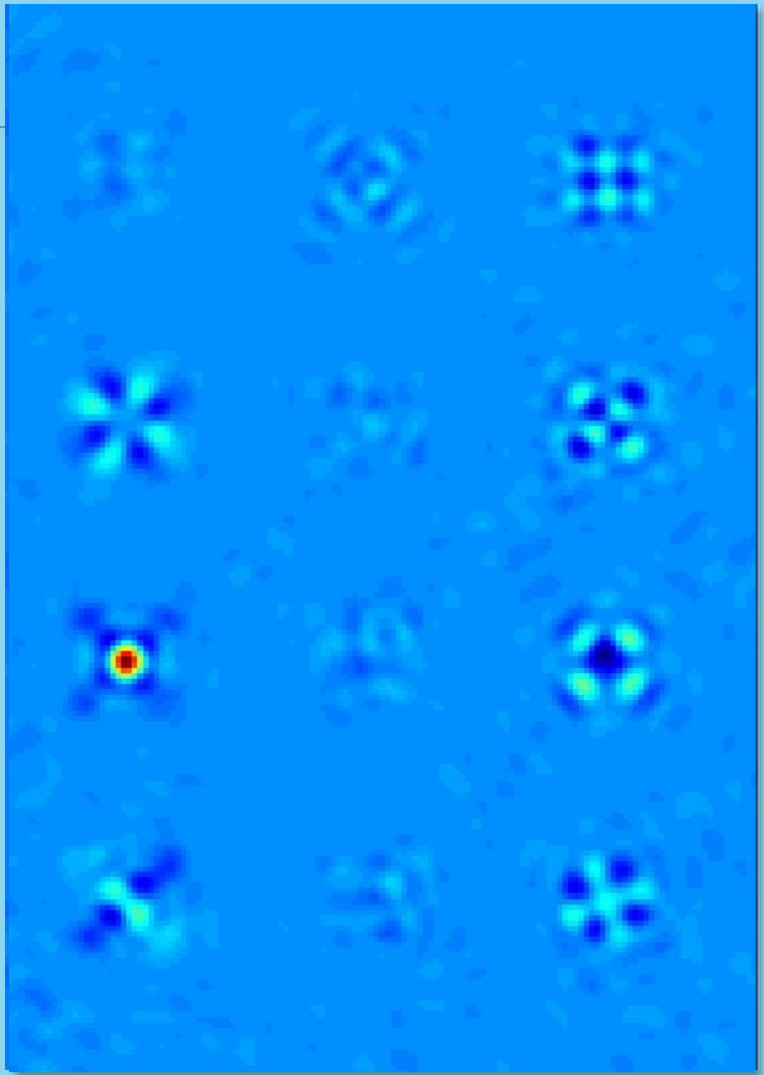

LOWFS w/ a MWFS

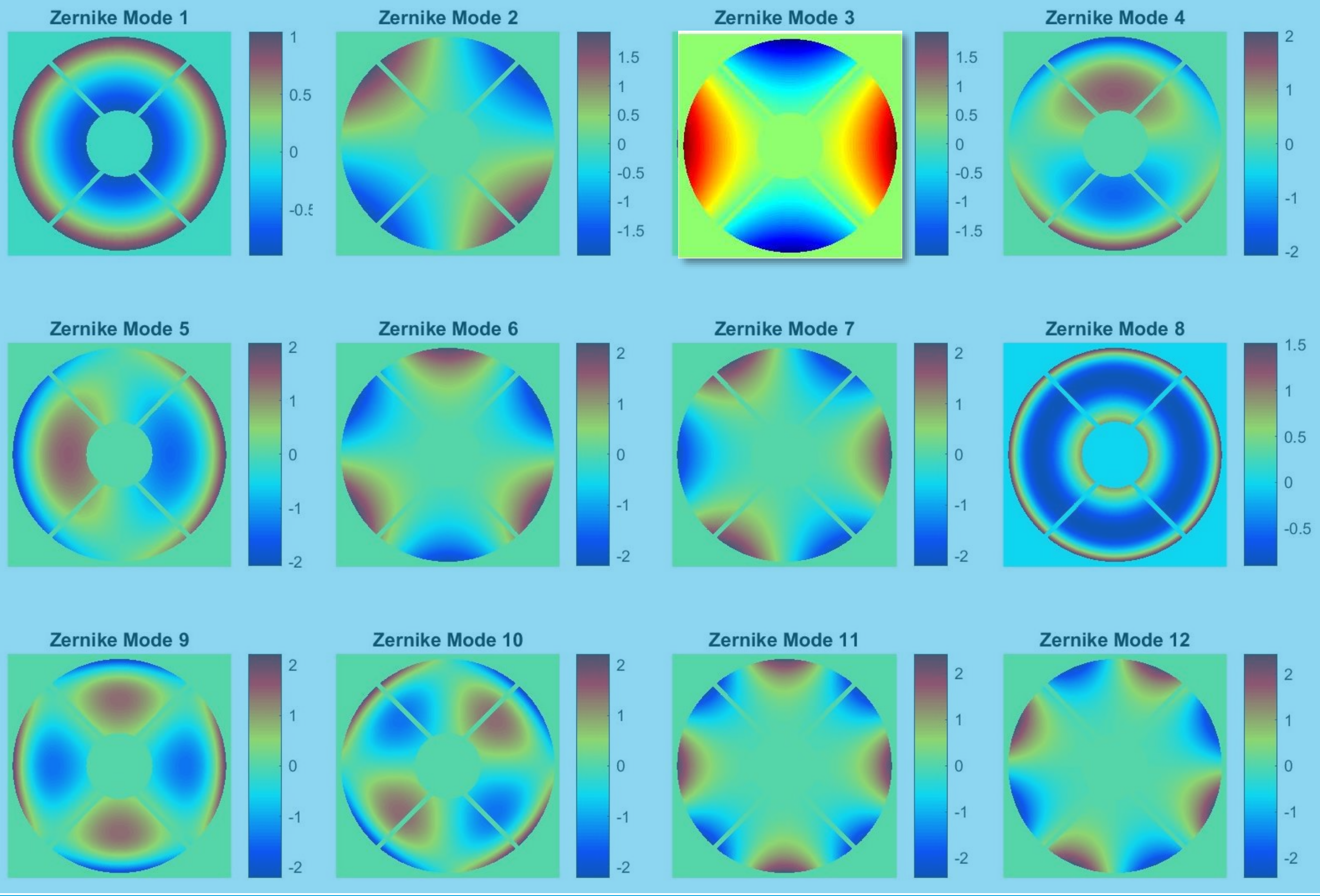

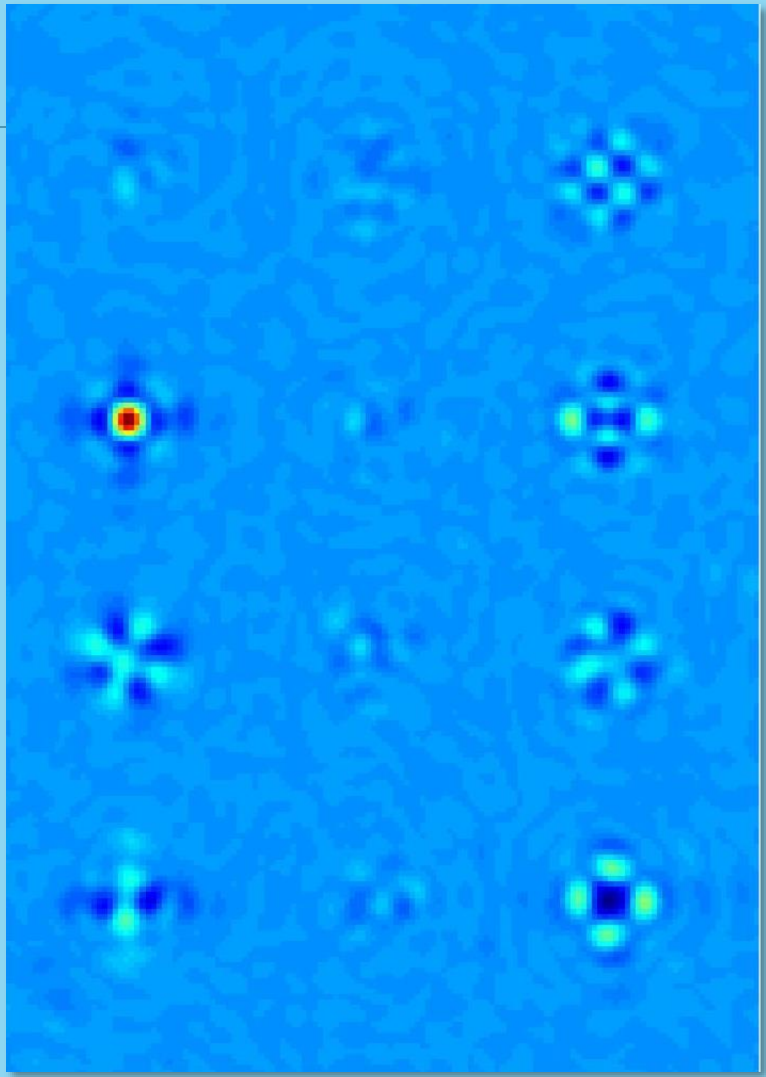

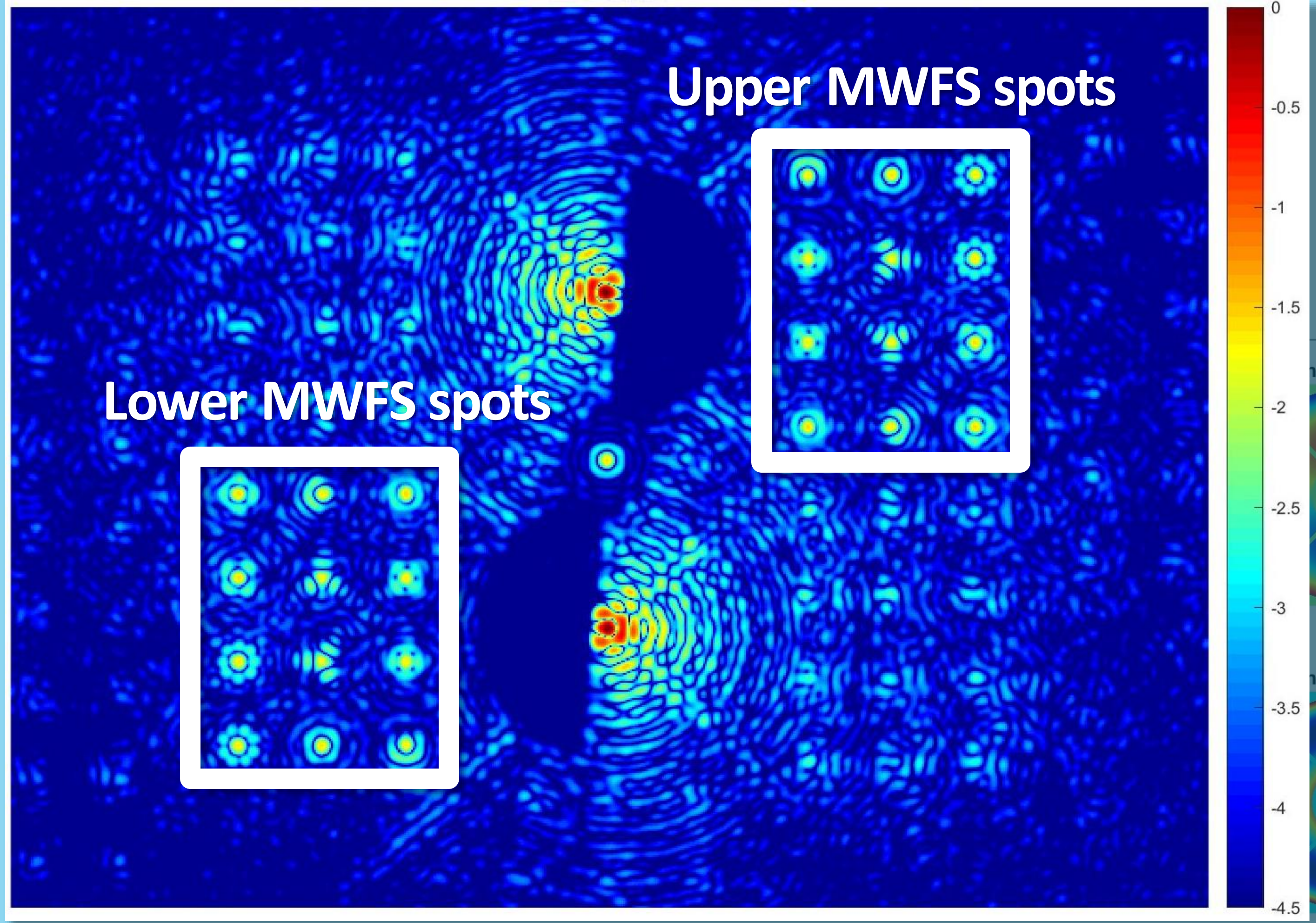

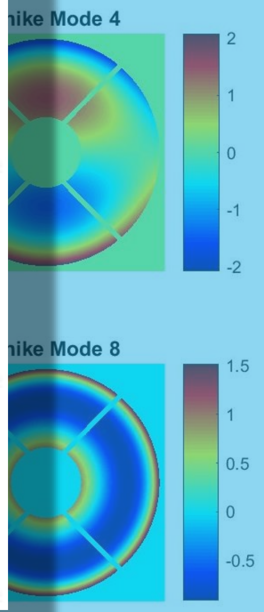

Applied Zernike modes

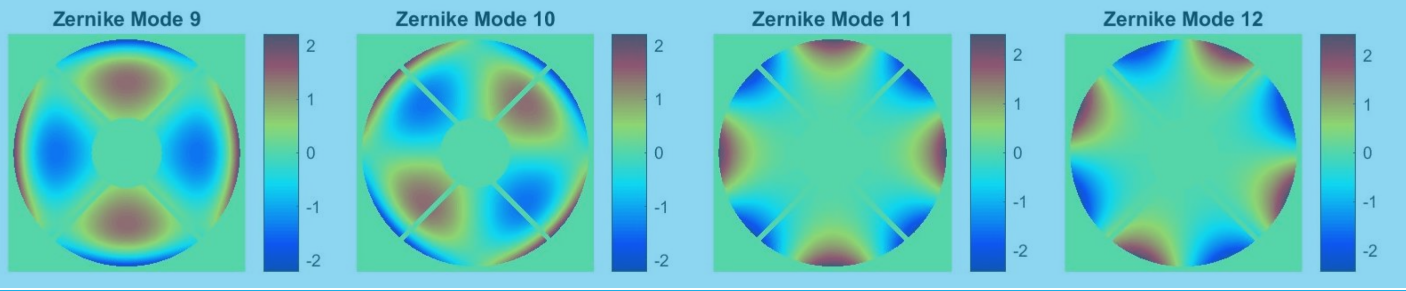

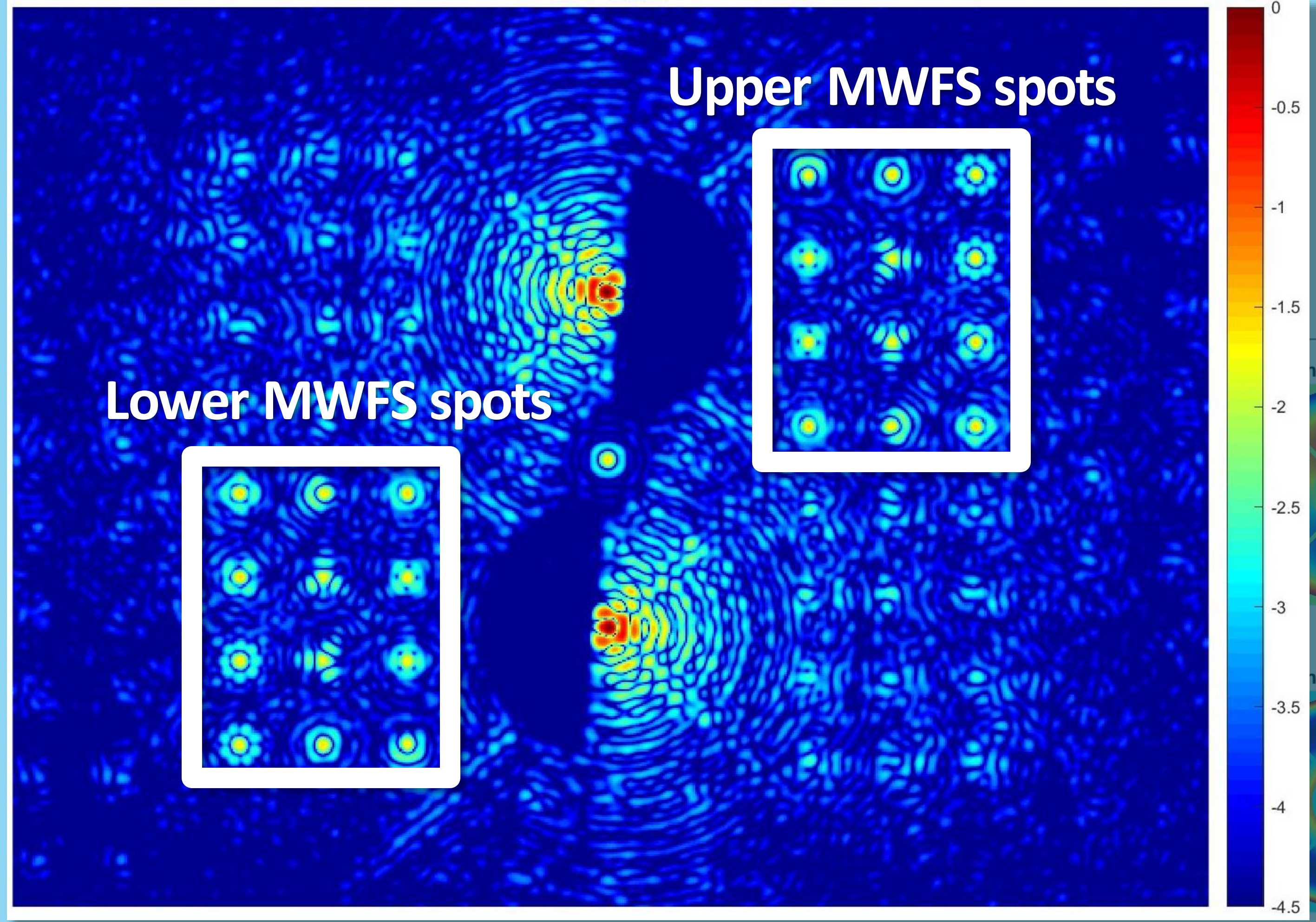

LOWFS signal

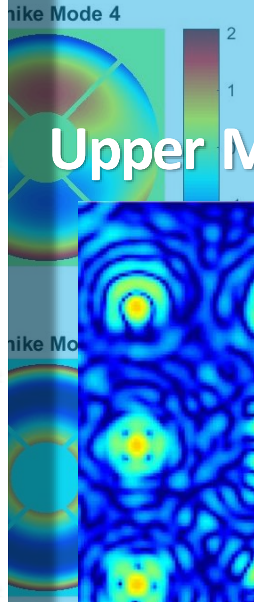

Upper MWFS spots

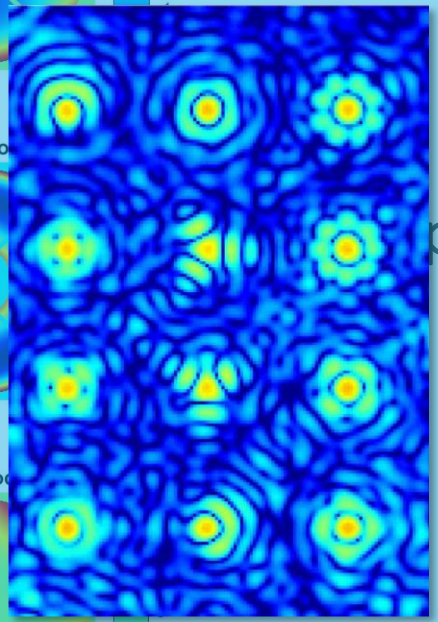

$-$

Lower MWFS spots

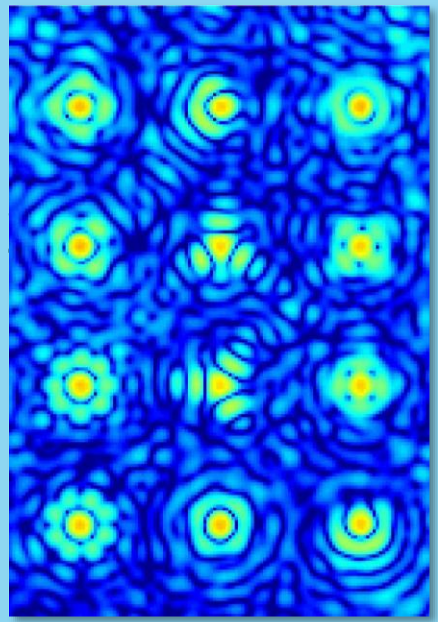

plied

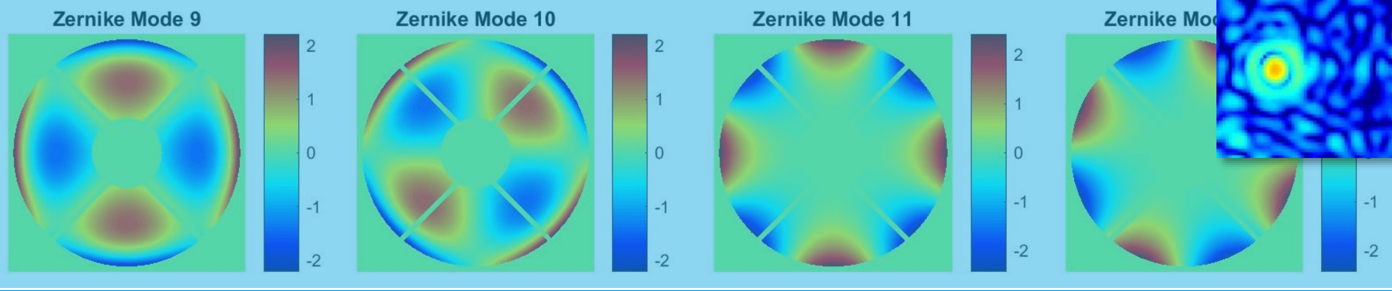

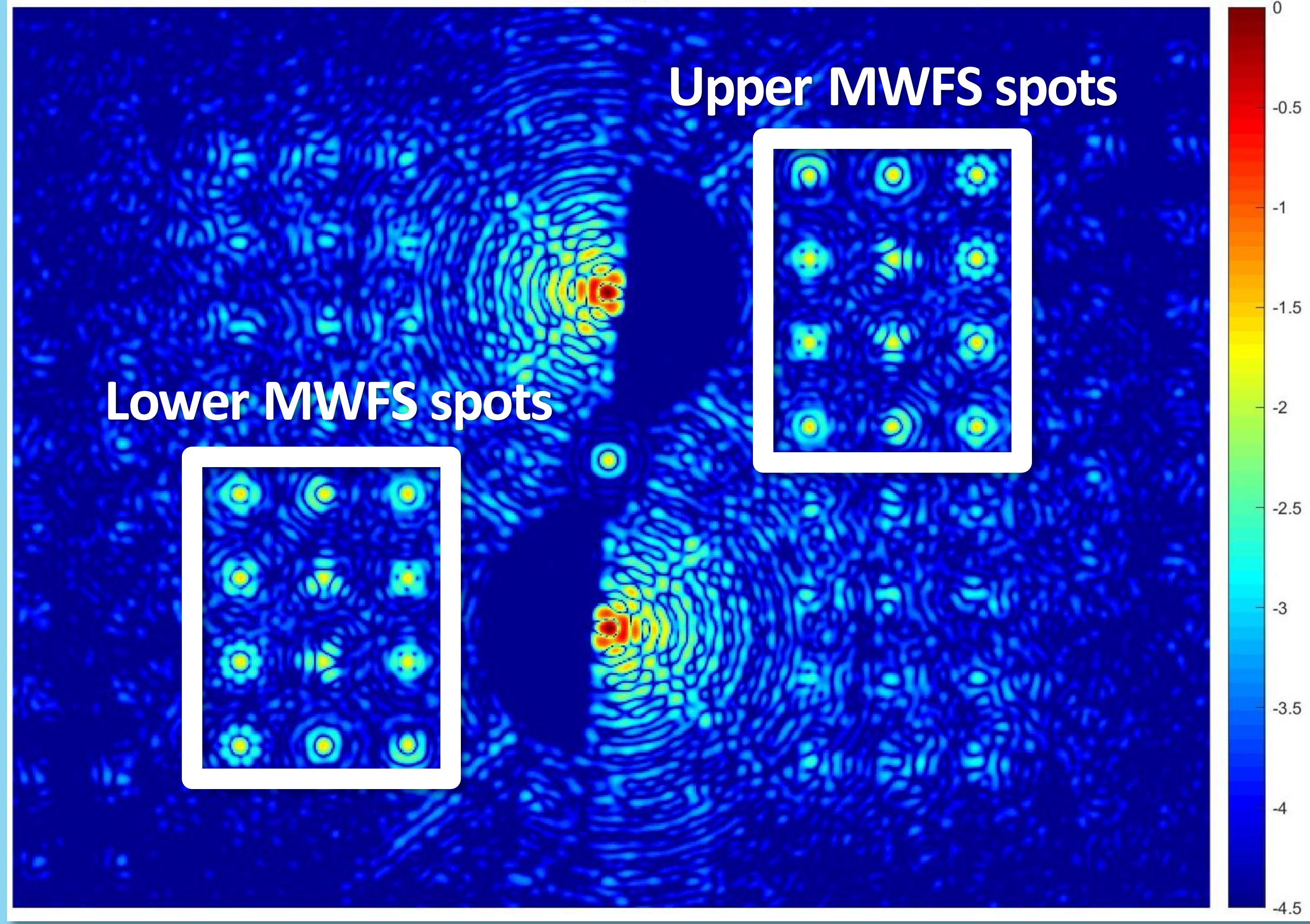
Upper MWFS spots
Lower MWFS spots
0
-0.5
-1
-1.5
-2
-2.5
-3
-3.5
-4
-4.5

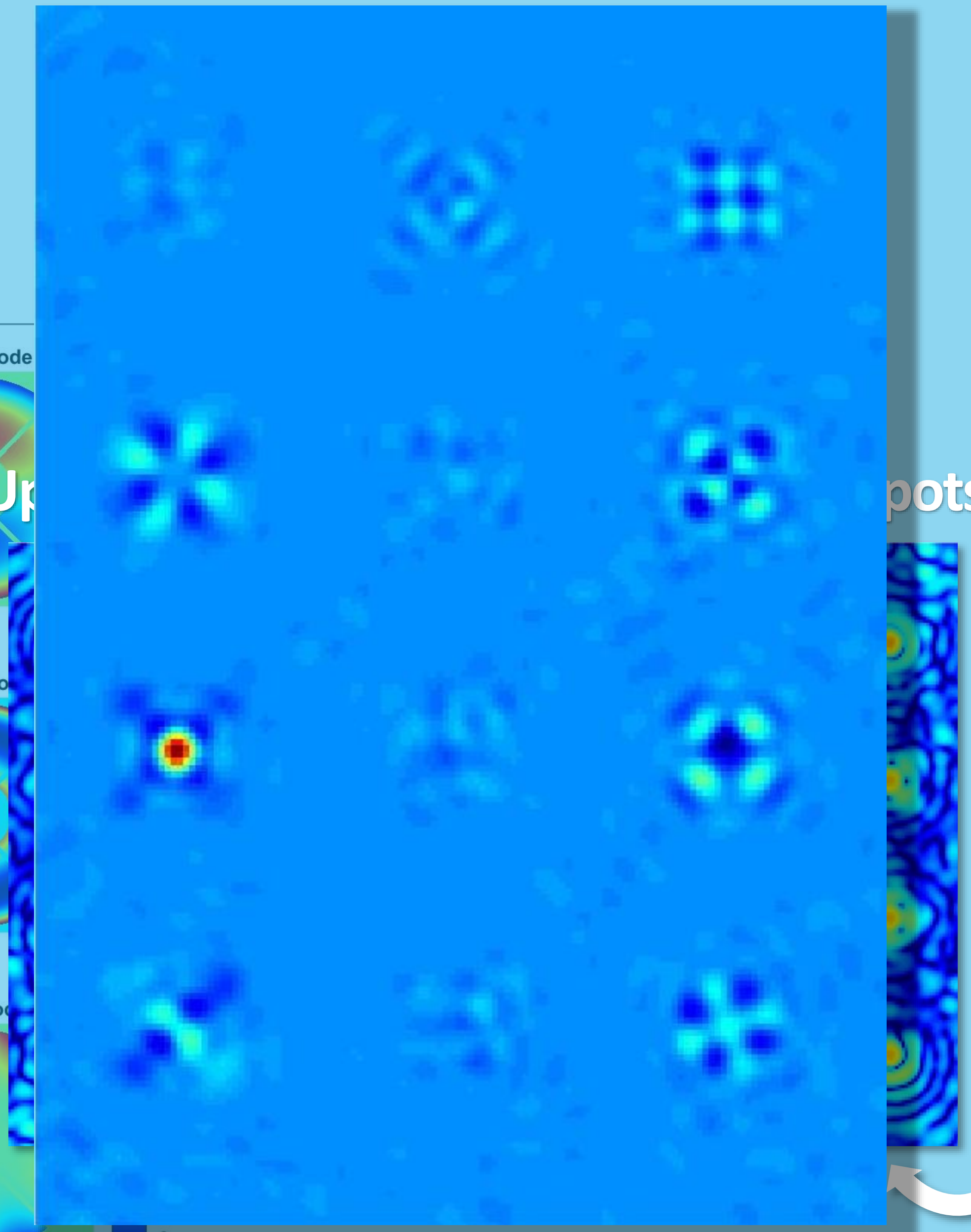

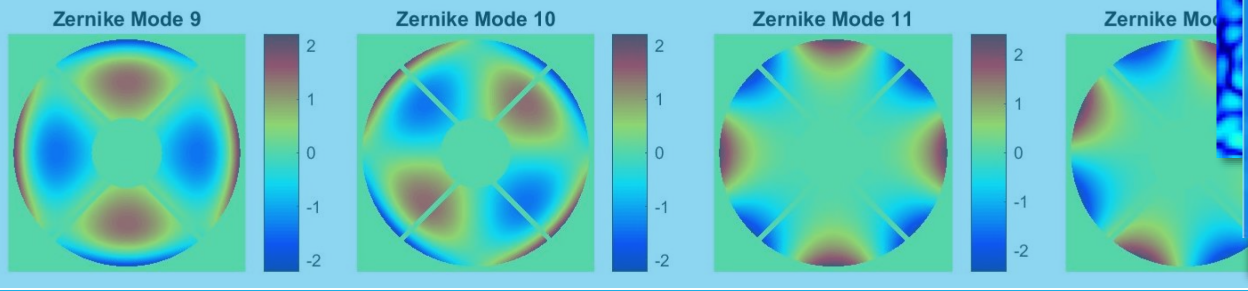
Zernike Mode 9
Zernike Mode 10
Zernike Mode 11
2
1
0
-1
-2

Simulated data: Linear response curves for the Zernike MWFS

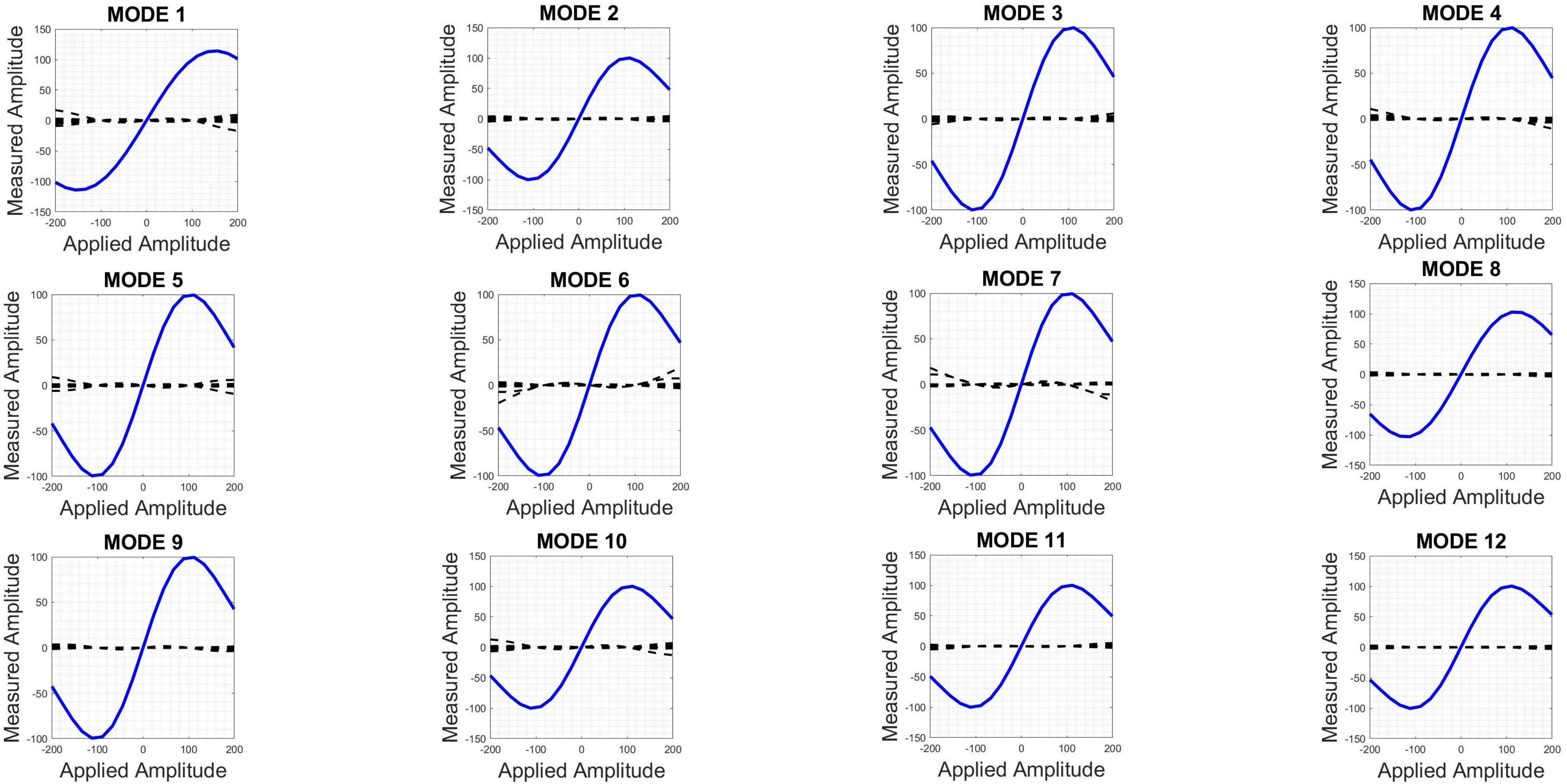

Lab data: Linear response curves for the Zernike MWFS

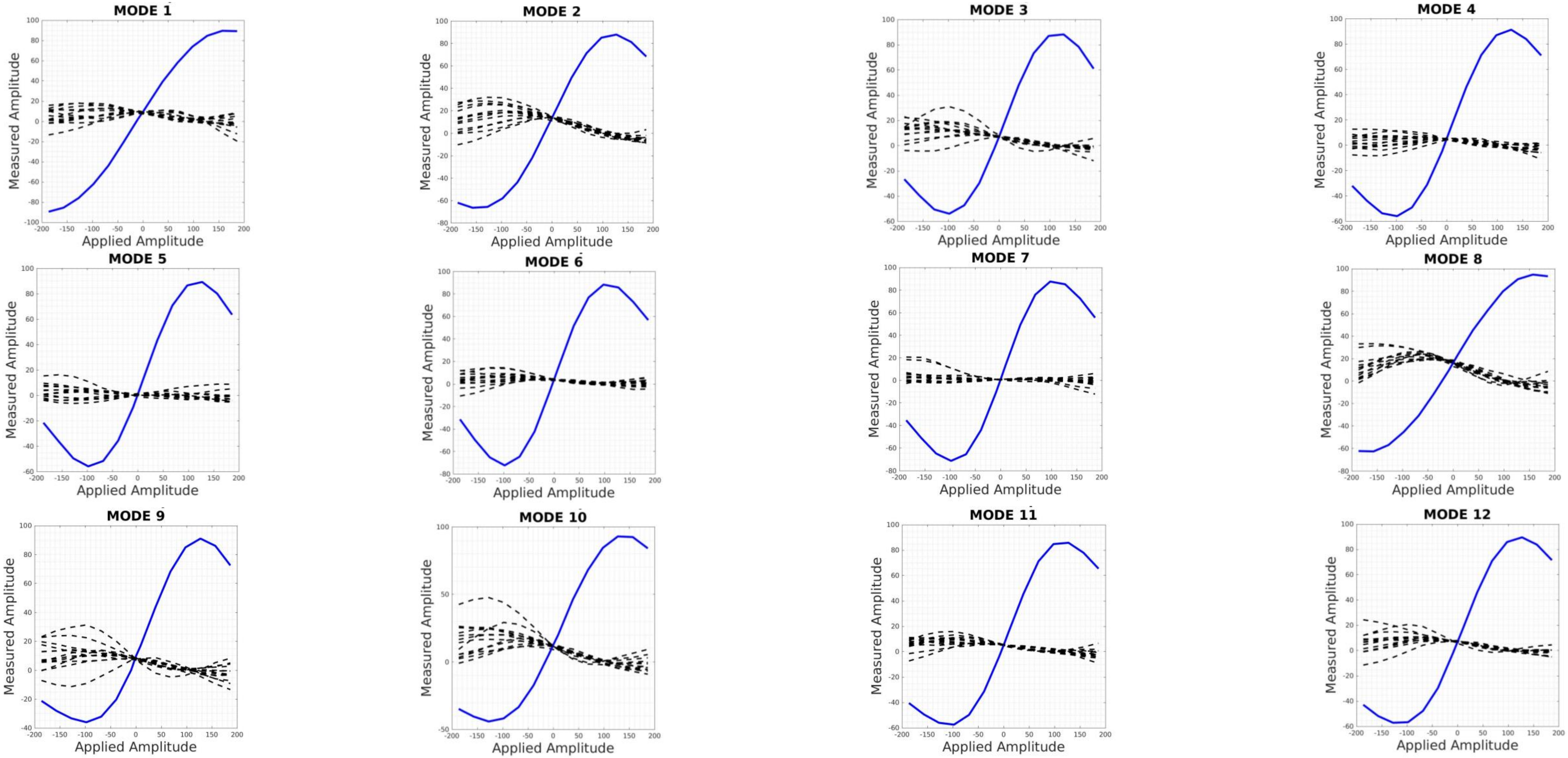

Simulated closed-loop MWFS LOWFS

Applied aberration | MWFS – sensed shape | Residual wavefront error

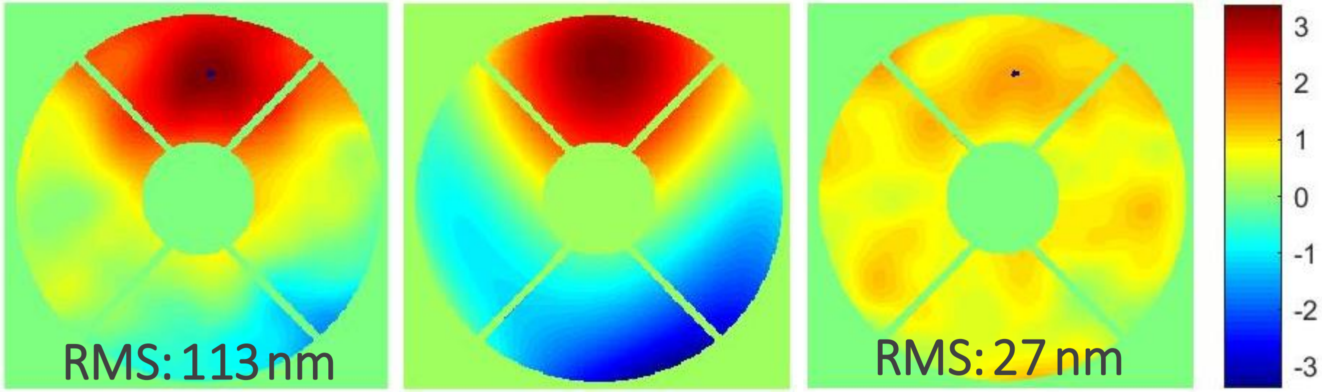

Aberrated PSF

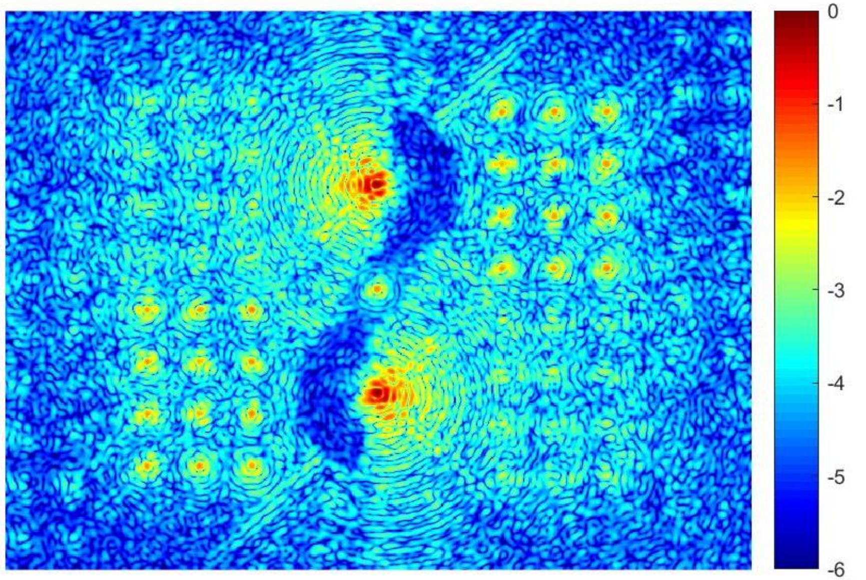

Upper MWFS

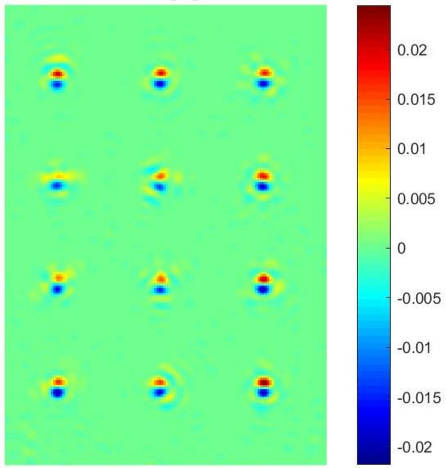

Lower MWFS

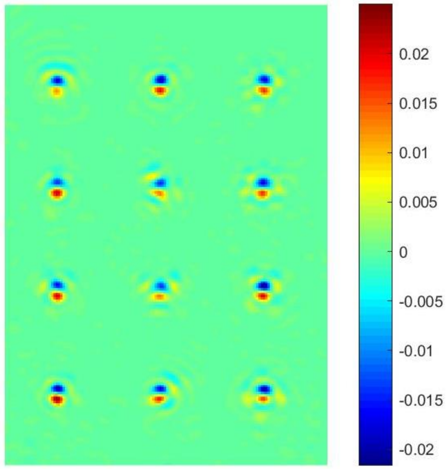

MWFS LOWFS signal

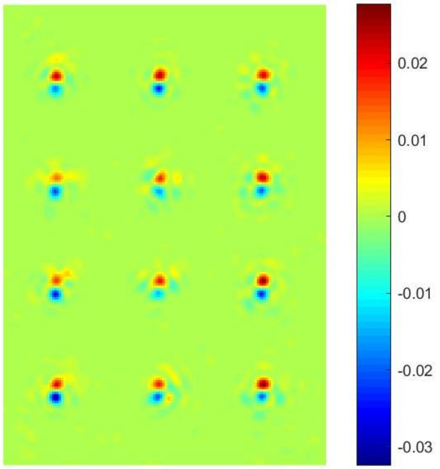

Corrected PSF

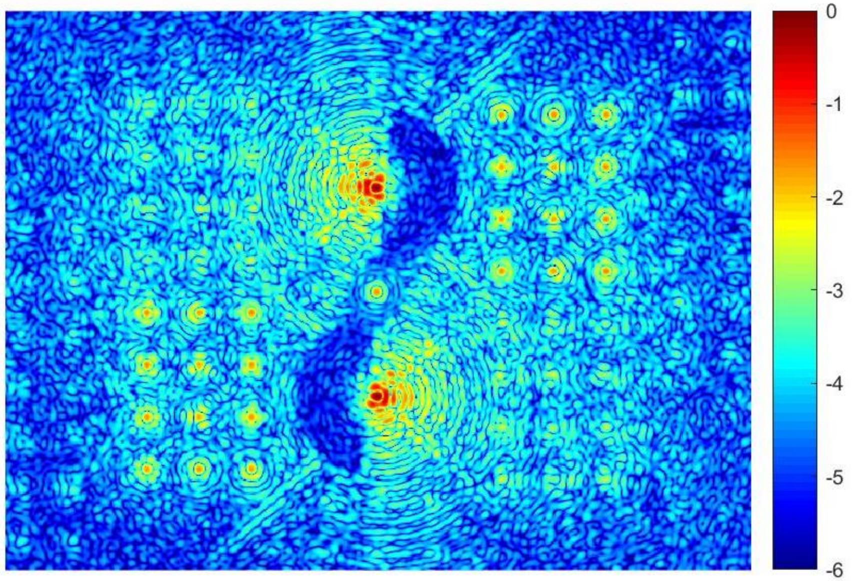

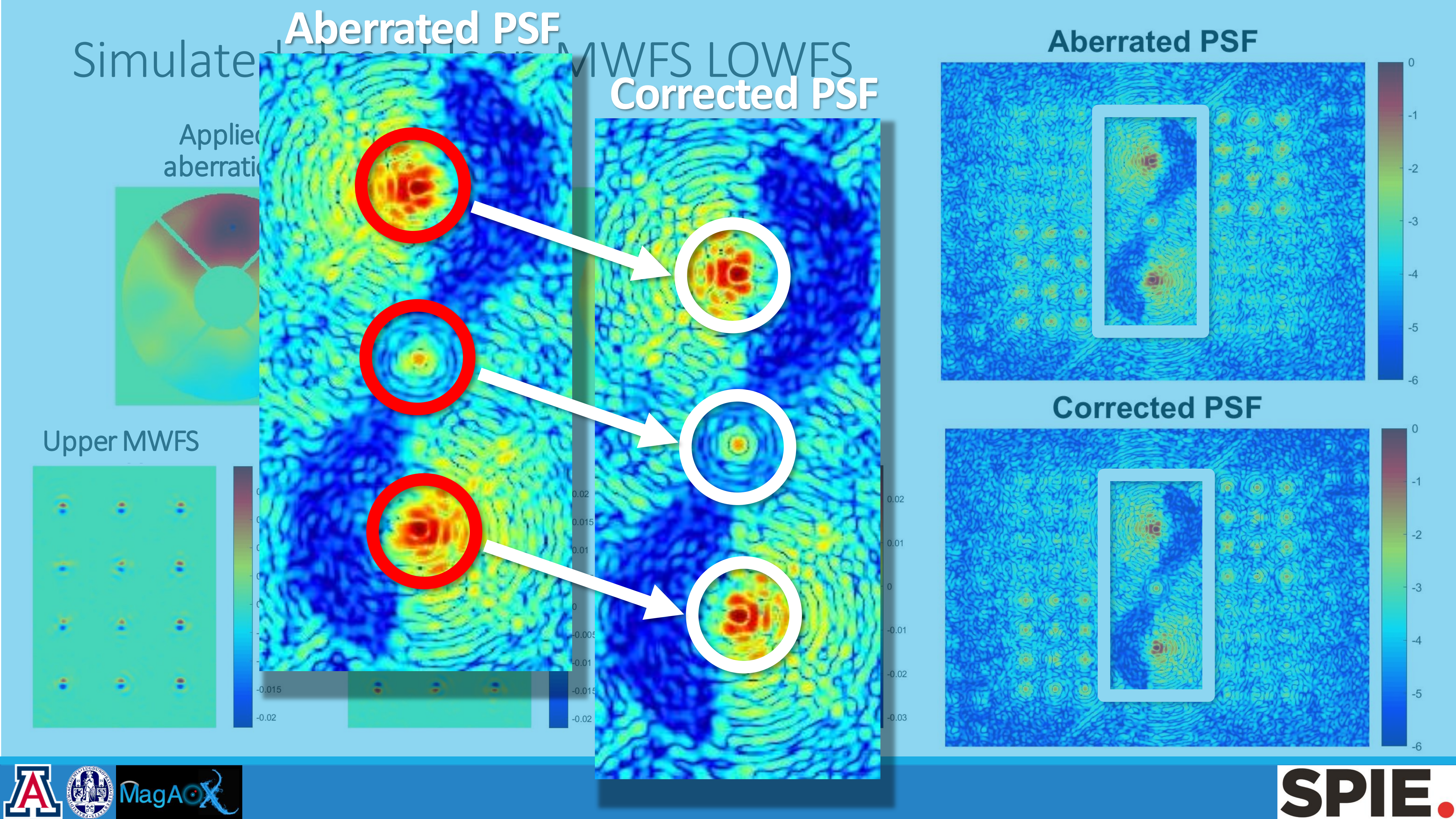
Aberrated PSF
Corrected PSF
Upper MWFS
Aberrated PSF
0
-1
-2
-3
-4
-5
-6
Corrected PSF
0
-1
-2
-3
-4
-5
-6
SPIE.

vAPP testing on the UA Wavefront Control Testbed

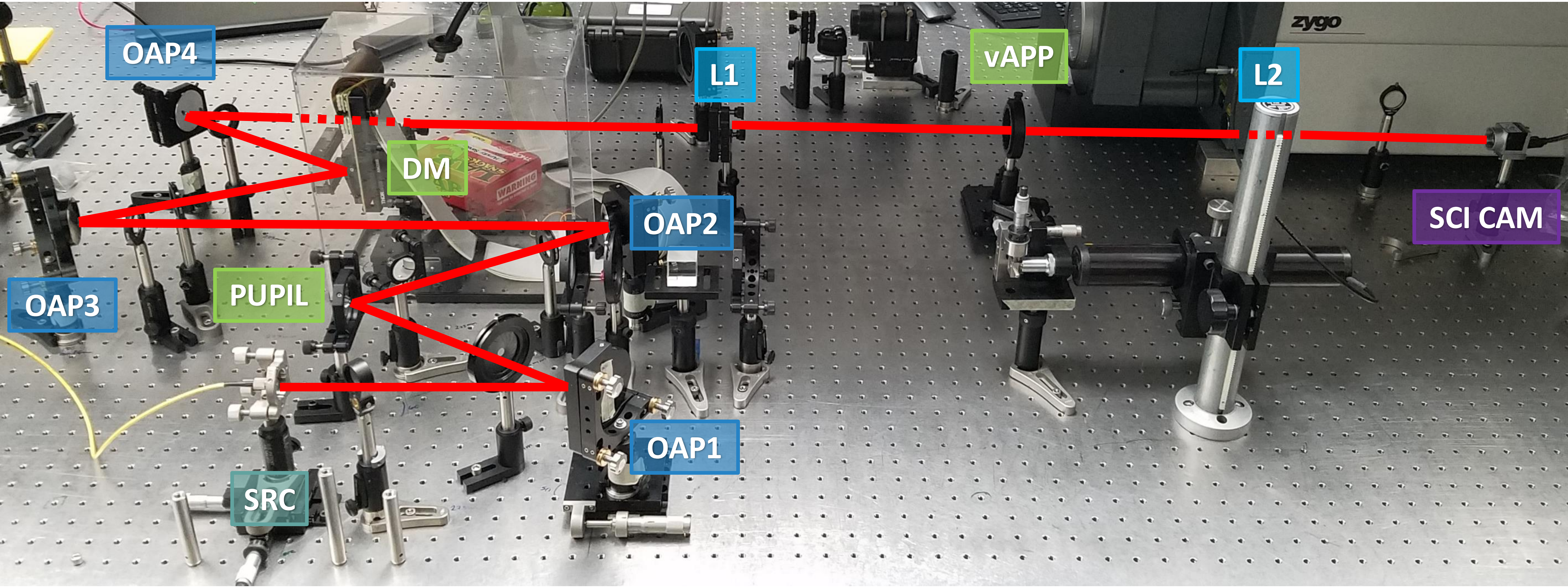

vAPP testing on the UA Wavefront Control Testbe

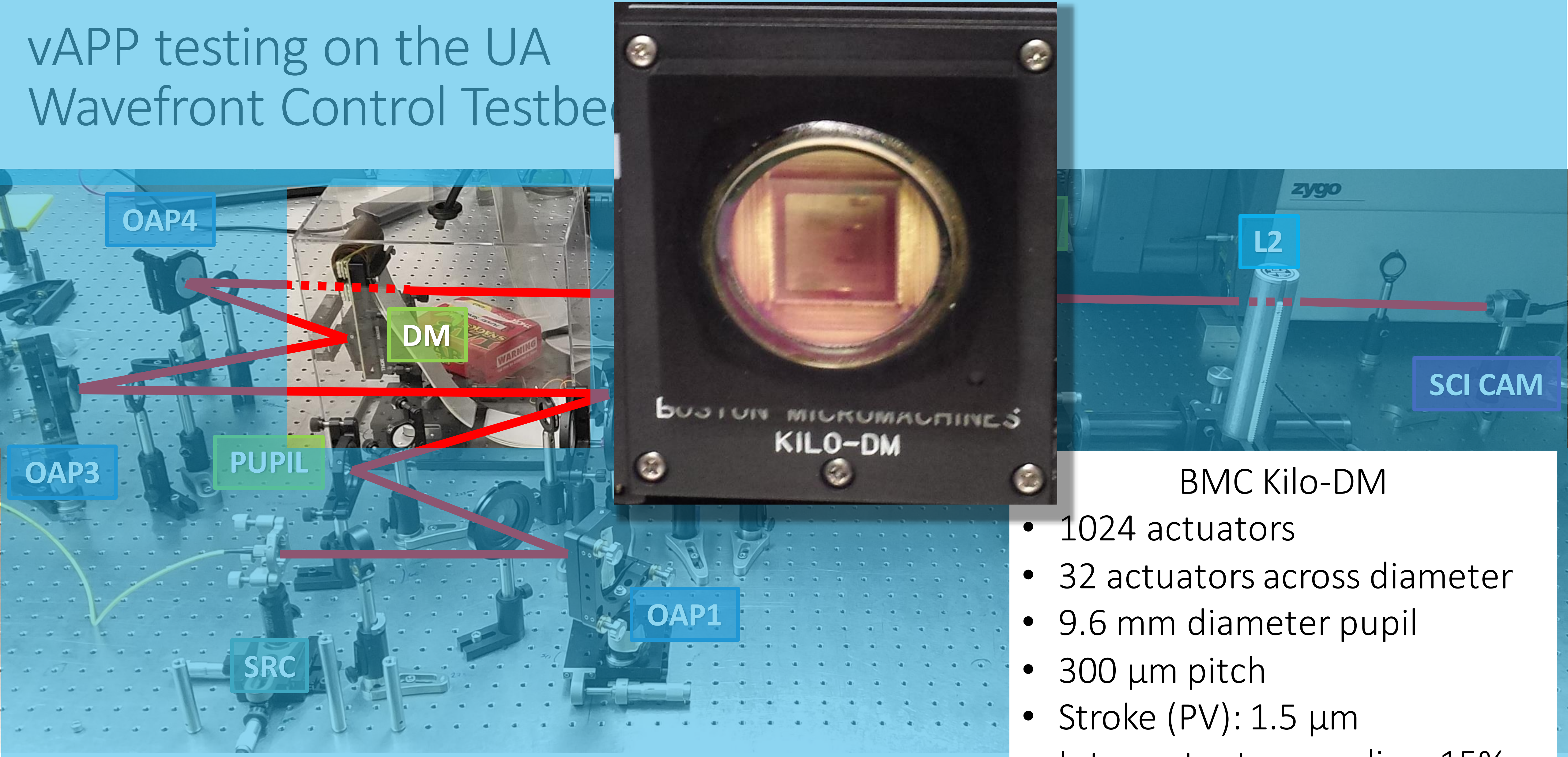

BMC Kilo-DM

- 1024 actuators
- 32 actuators across diameter
- 9.6 mm diameter pupil
- 300 μm pitch
- Stroke (PV): 1.5 μm
- Inter-actuator coupling: 15%

vAPP testing on the UA Wavefront Control Testbed

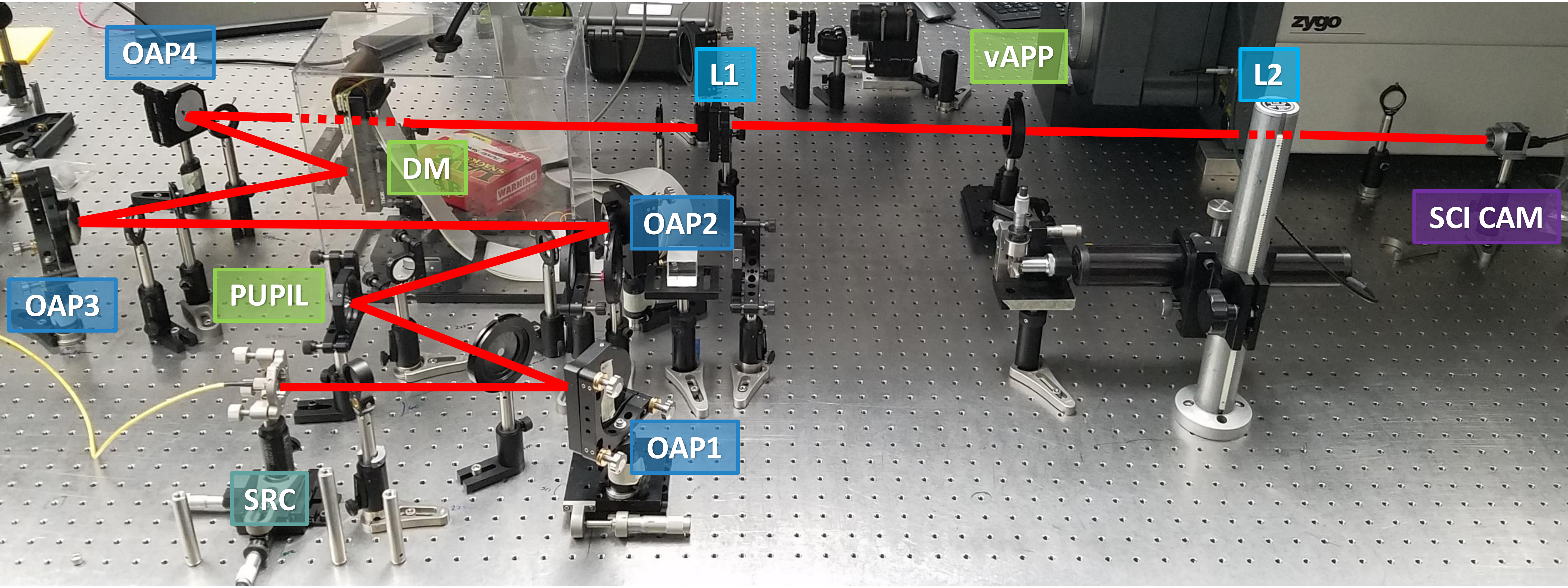

vAPP testing on the UA Wavefront Control Testbed

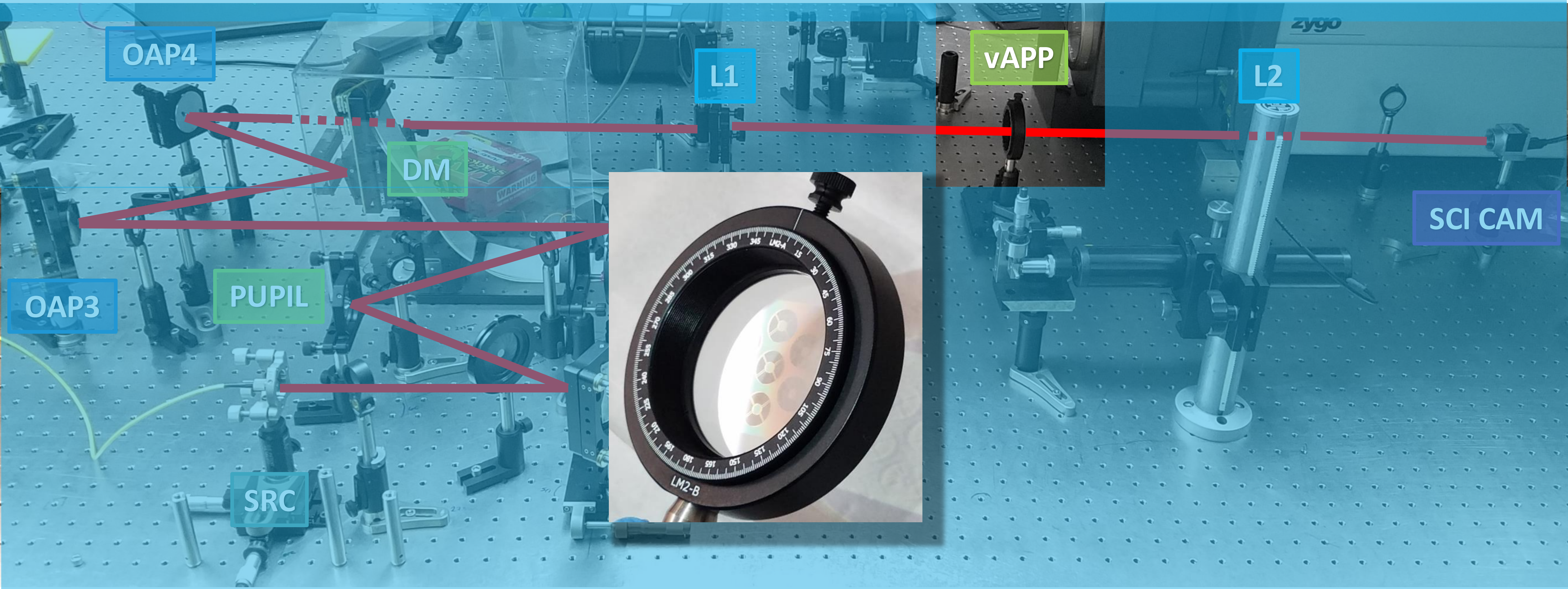

vAPP testing on the UA Wavefront Control Testbed

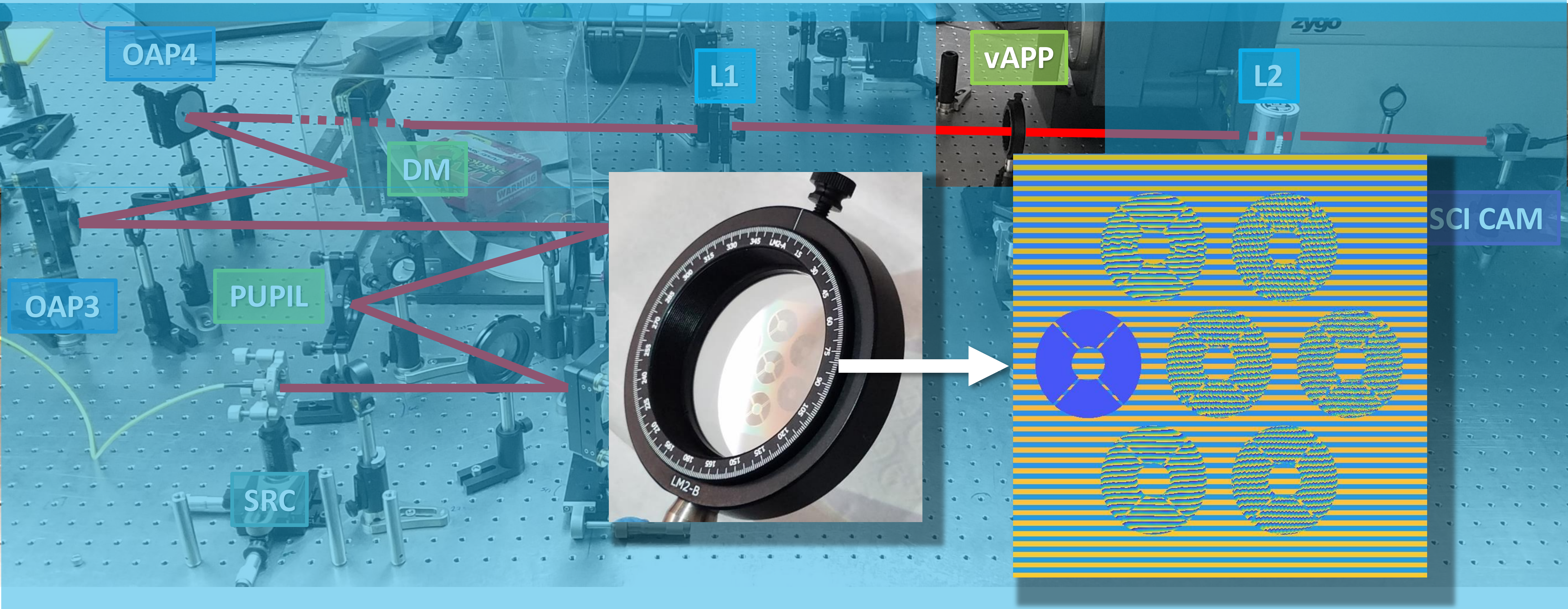

vAPP coronagraphs @ UA Wavefront Control Lab

7 vAPP masks

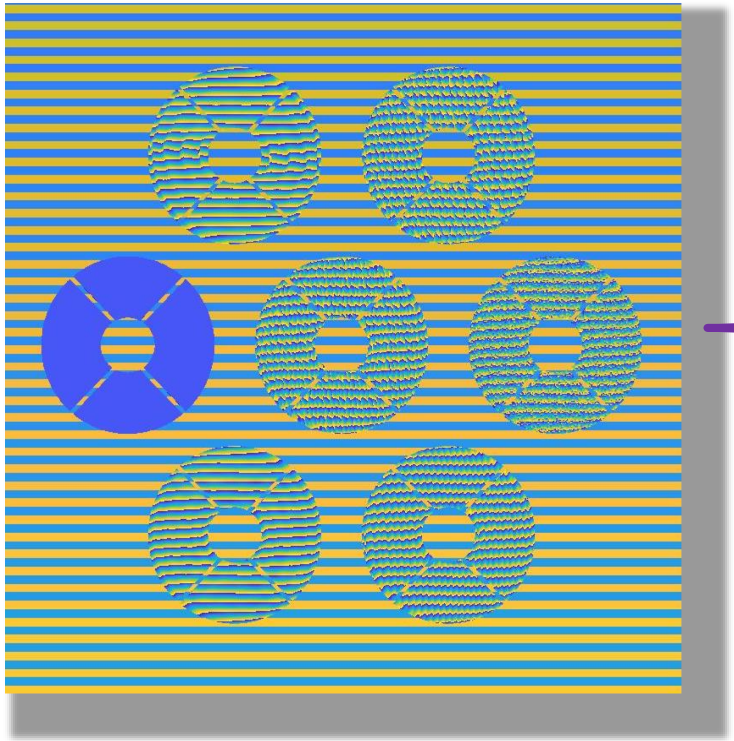

7 PSFs & MWFS spots on the science camera

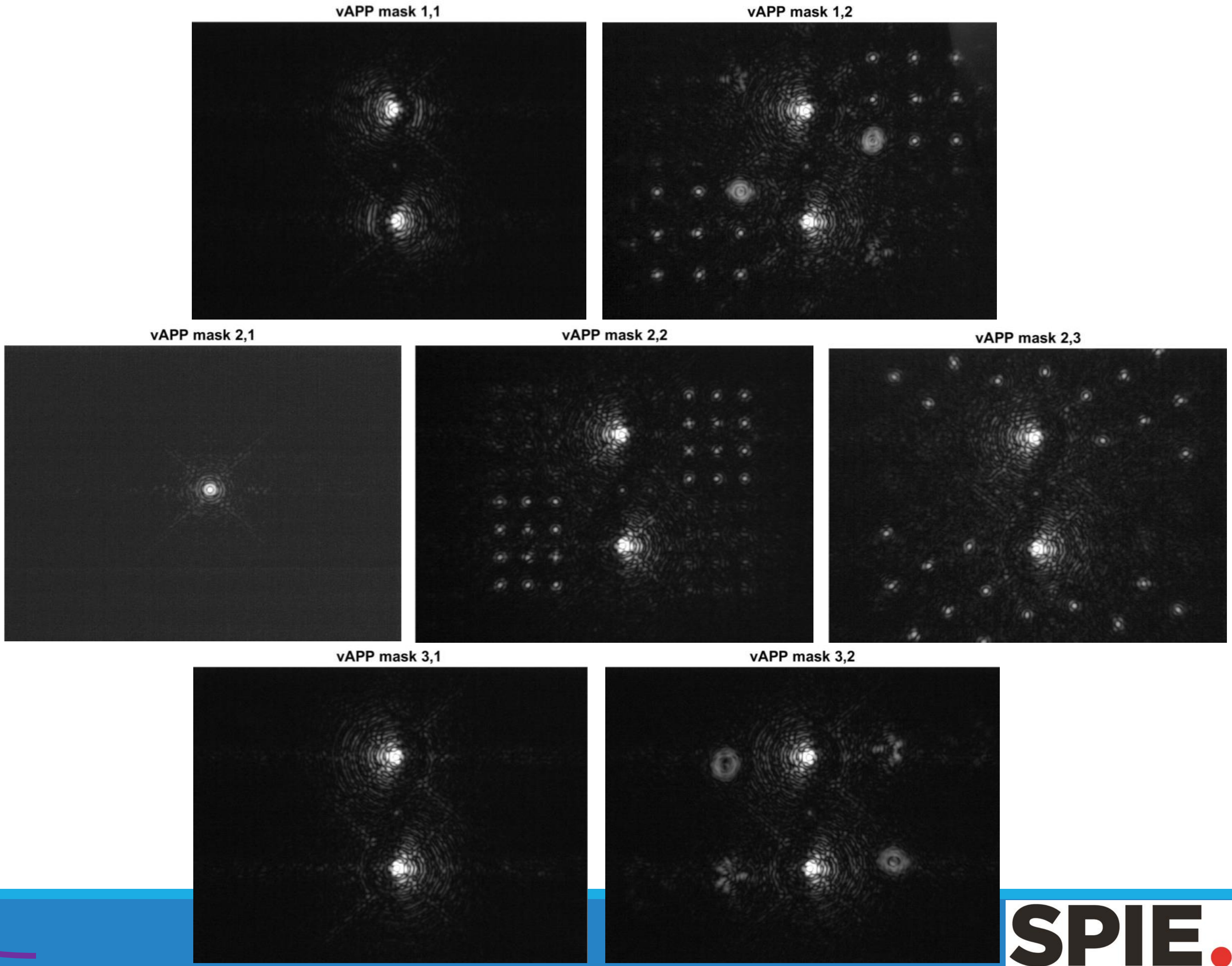

SPIE.

vAPP coronagraphs @ UA Wavefront Control Lab

7 vAPP masks

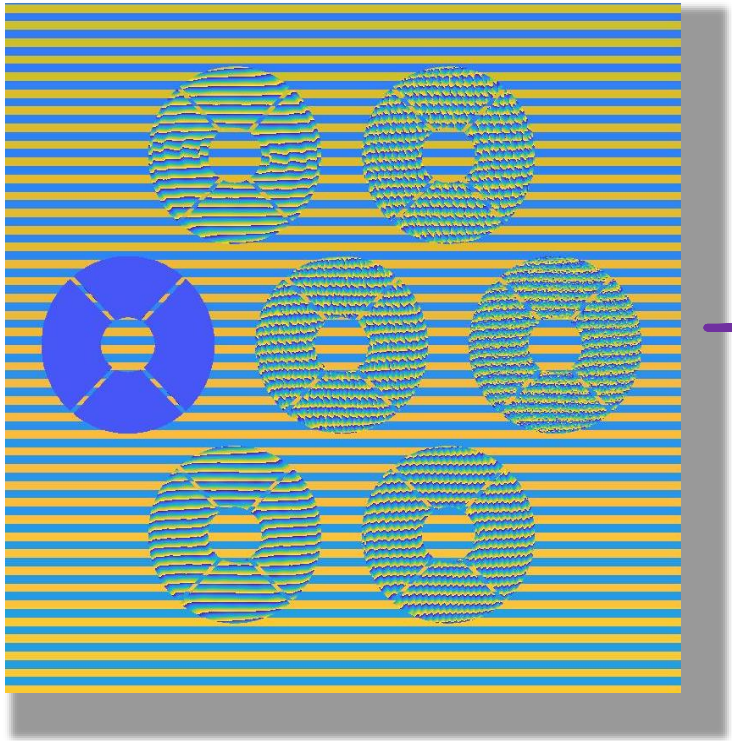

7 PSFs & MWFS spots on the science camera

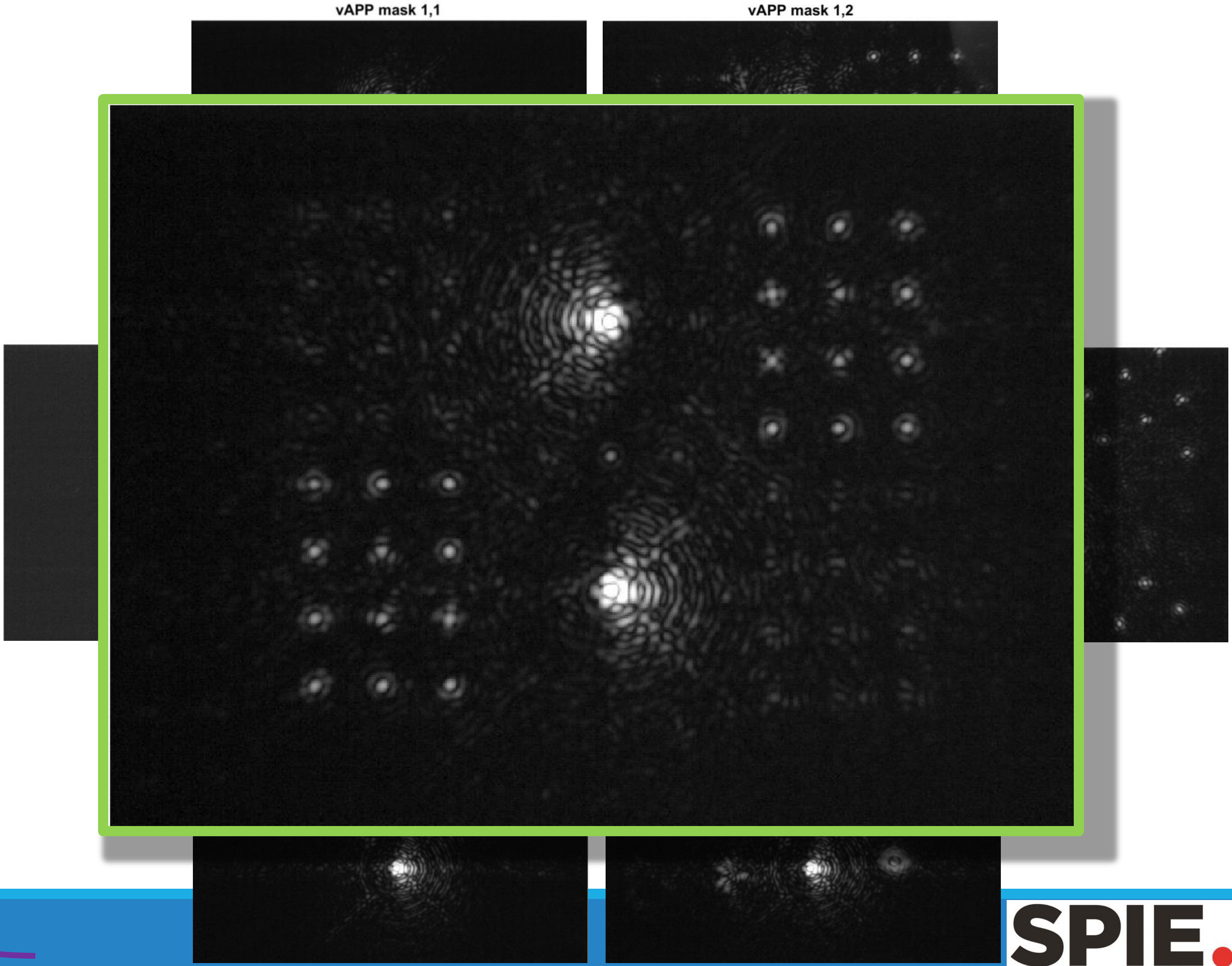

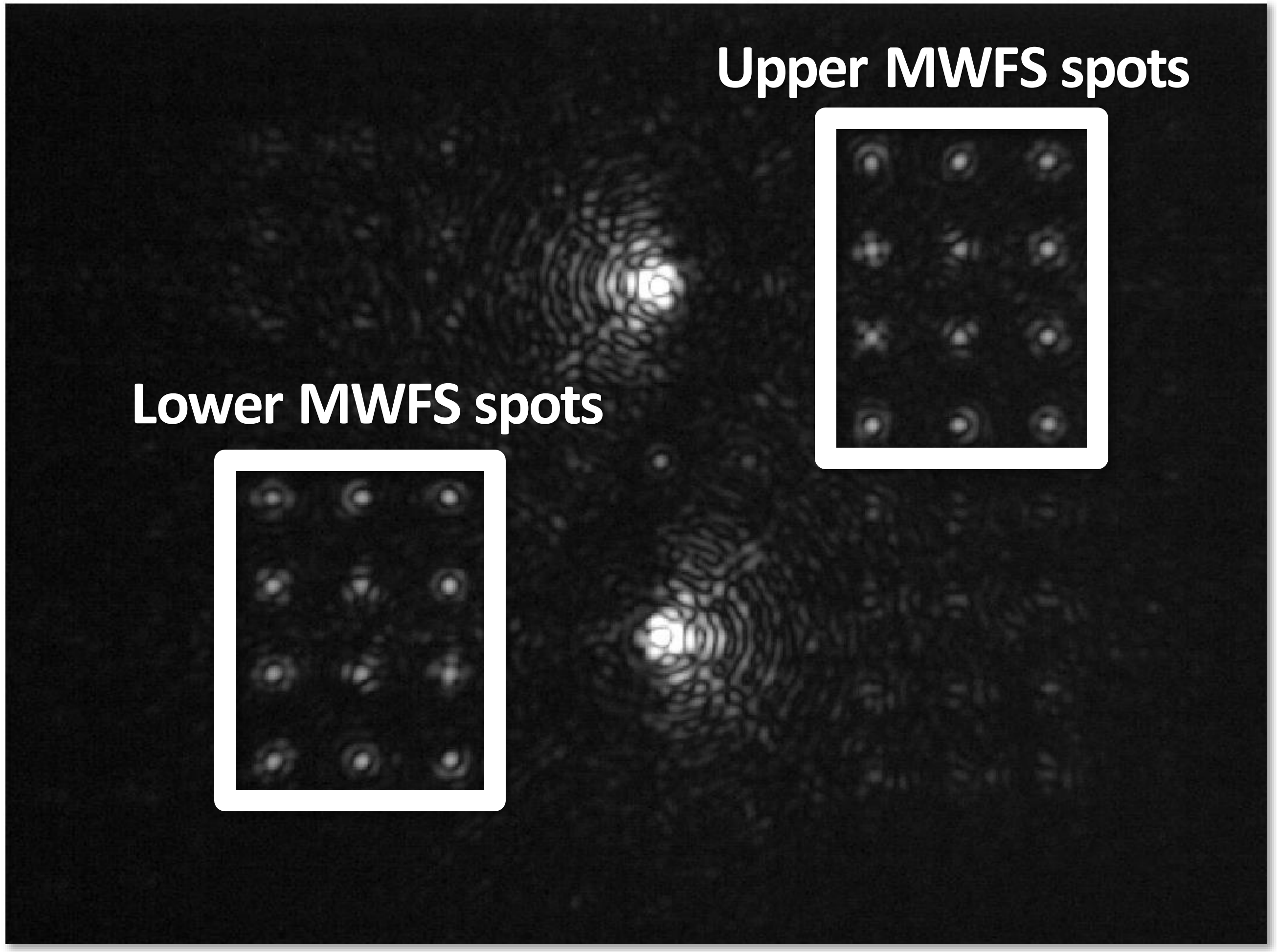
Upper MWFS spots
Lower MWFS spots

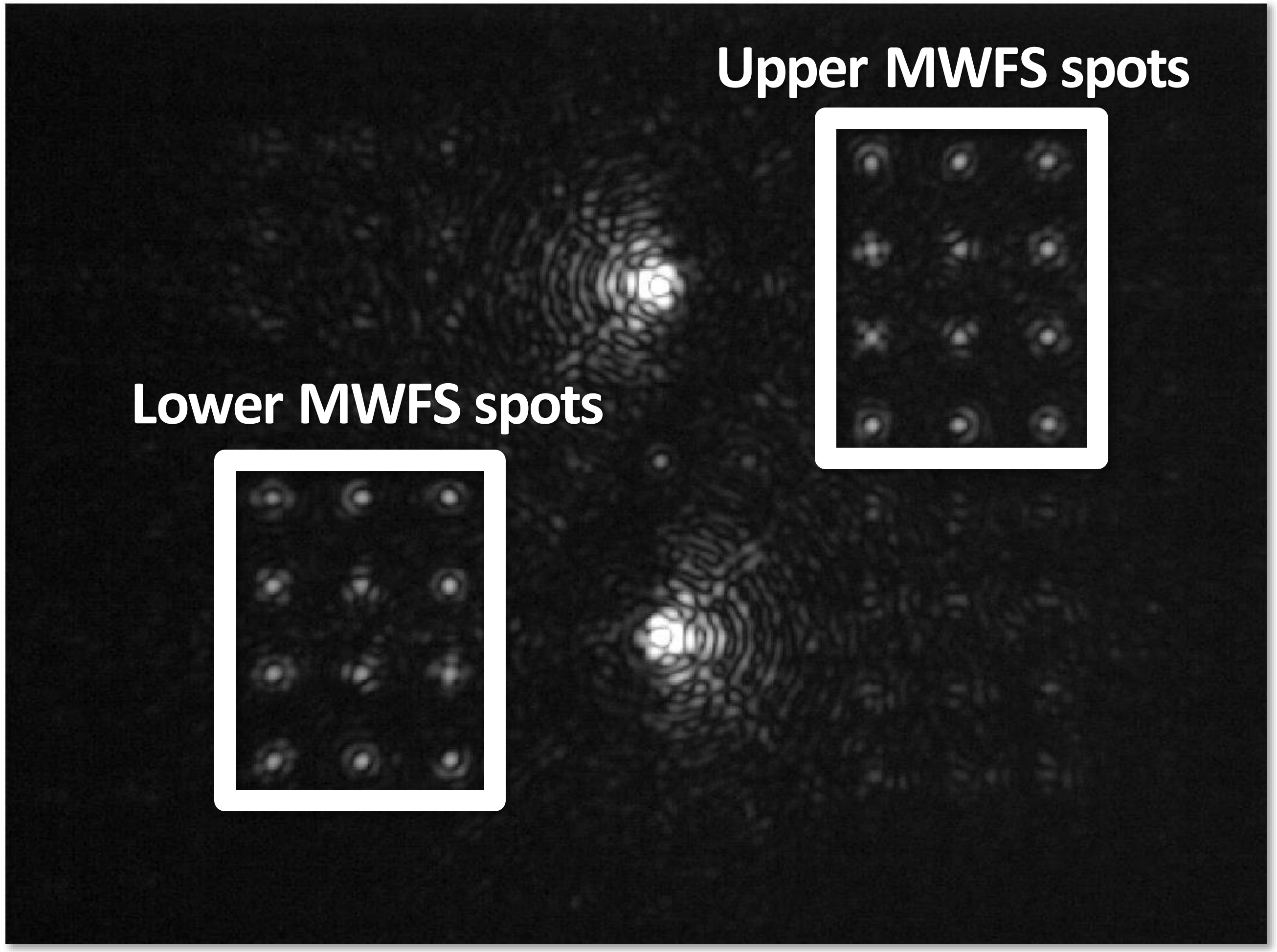

LOWFS signal

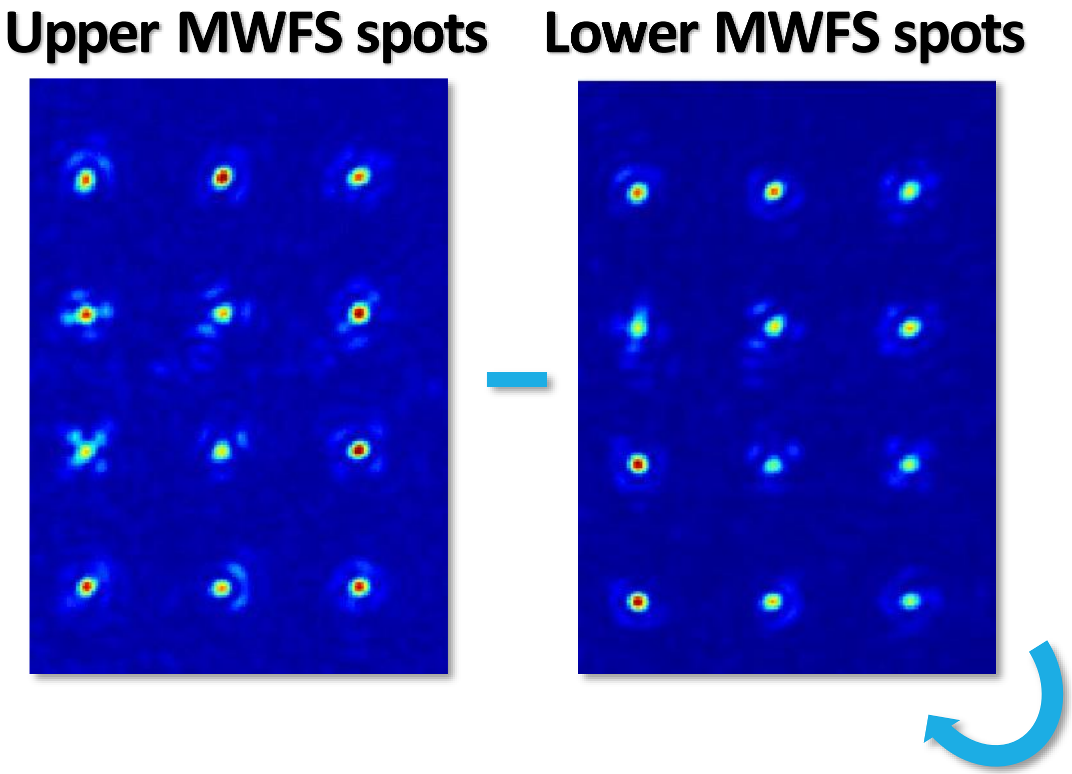

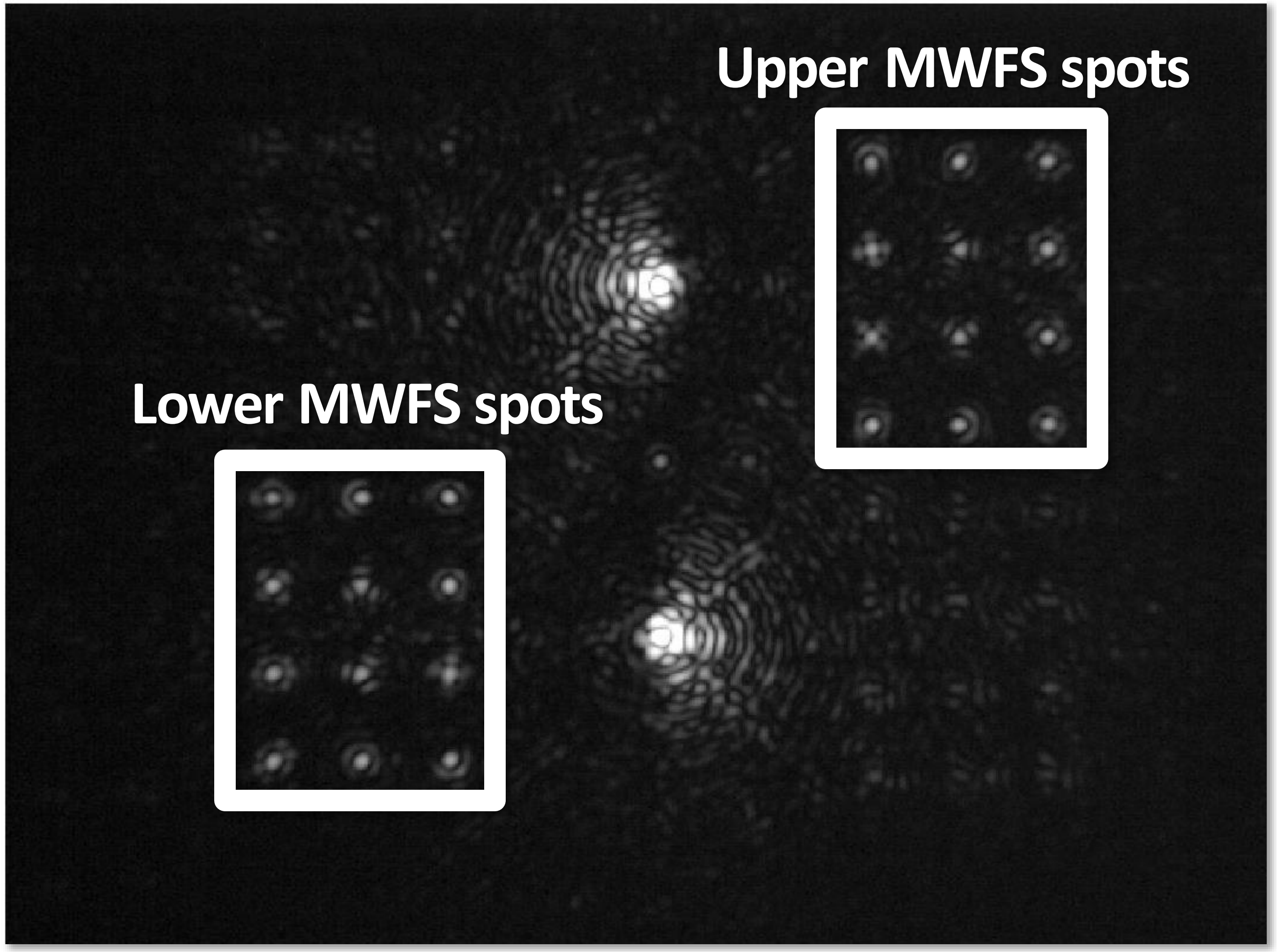
Upper MWFS spots
Lower MWFS spots

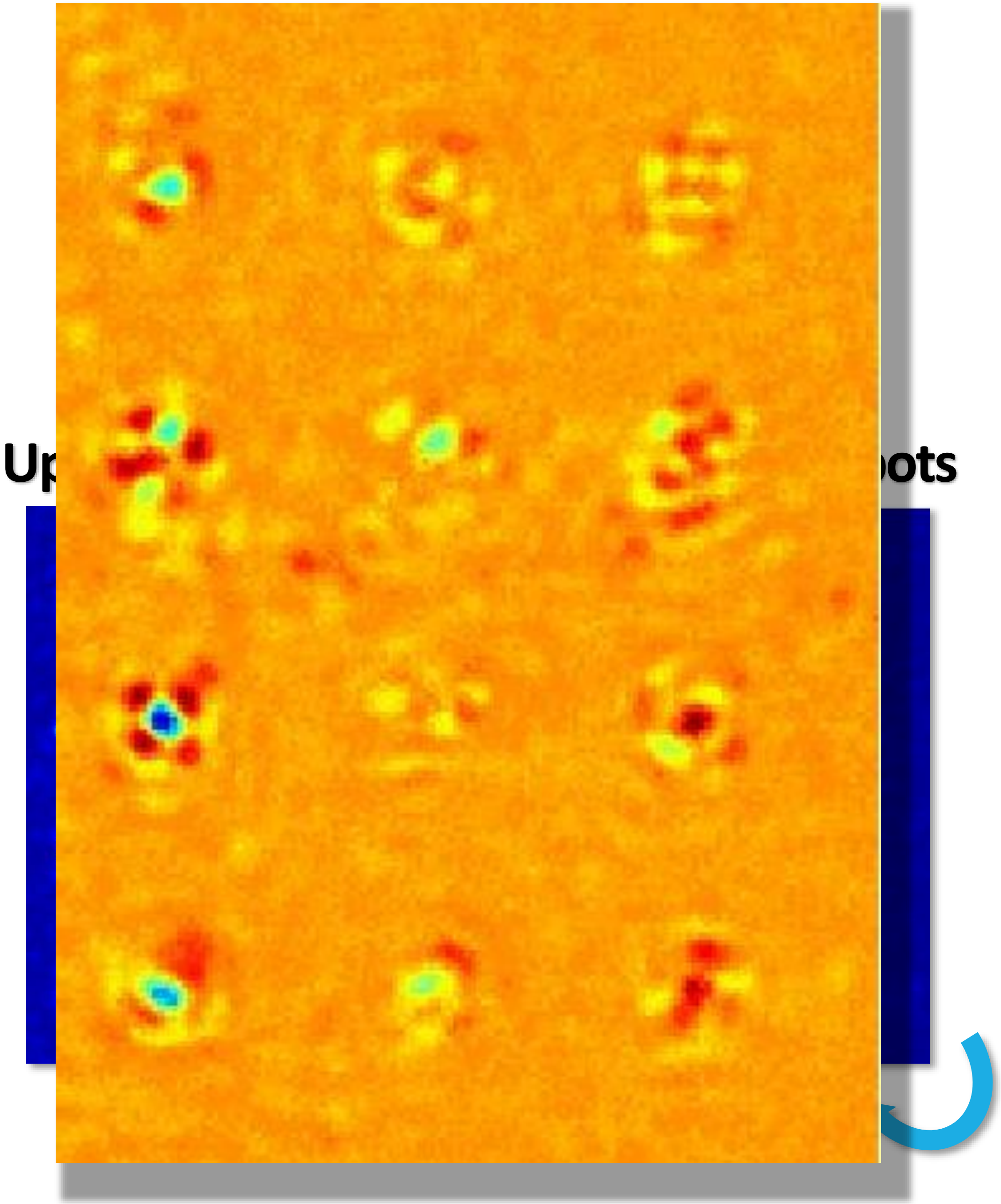

In-lab closed-loop MWFS LOWFS

Applied aberration

MWFS - sensed shape after 2 iterations

Residual wavefront error

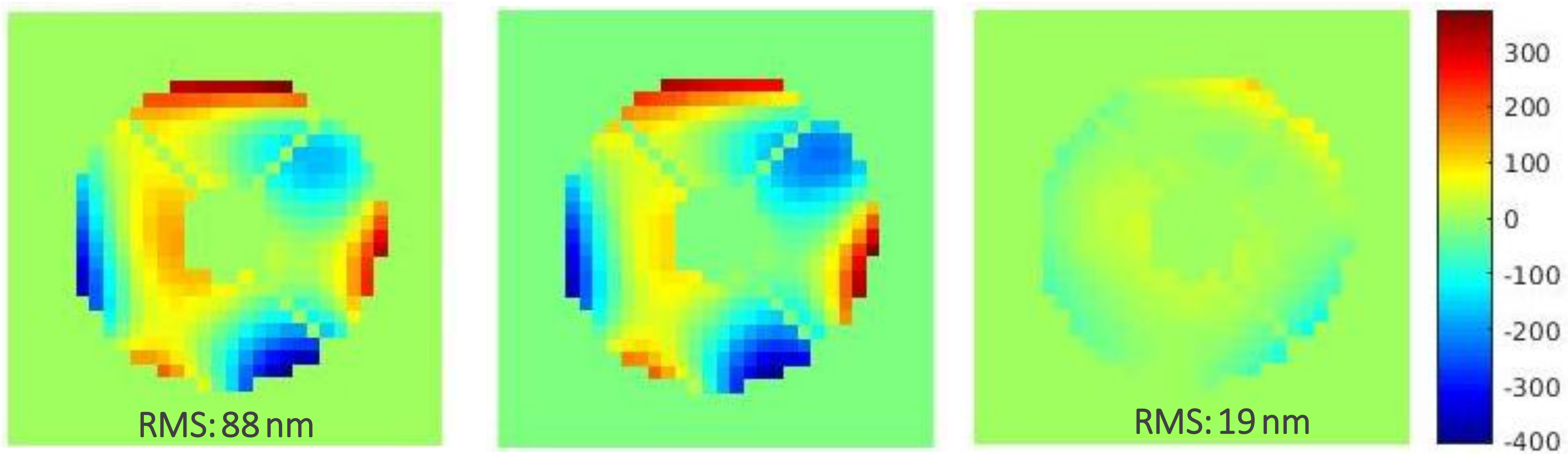

Linear dark field control (LDFC)

Linear dark field control (LDFC) using the bright speckle field outside of the dark hole for suppression of mid-spatial frequency aberrations in the dark hole

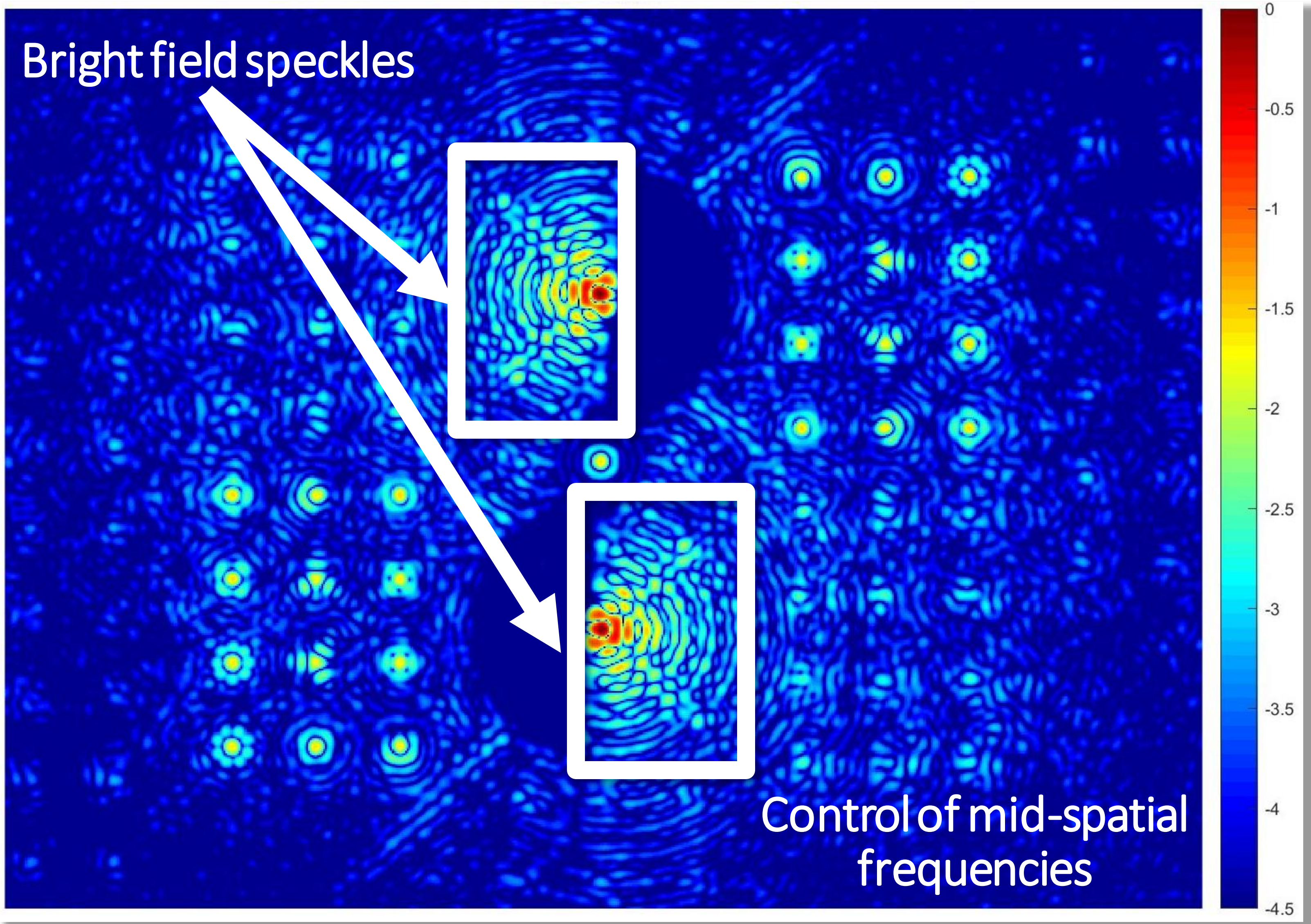

Linear Dark Field Control: Theory

- Stabilizes the dark hole
- Does not require field modulation; still fundamentally relies on coherent mixing of stellar speckles and aberration-induced speckles
- Uses the intensity variation in bright field speckles in the image plane
- Relies on the linear response of the bright field to wavefront perturbations that modify both the bright and dark field and decrease the contrast in the dark hole

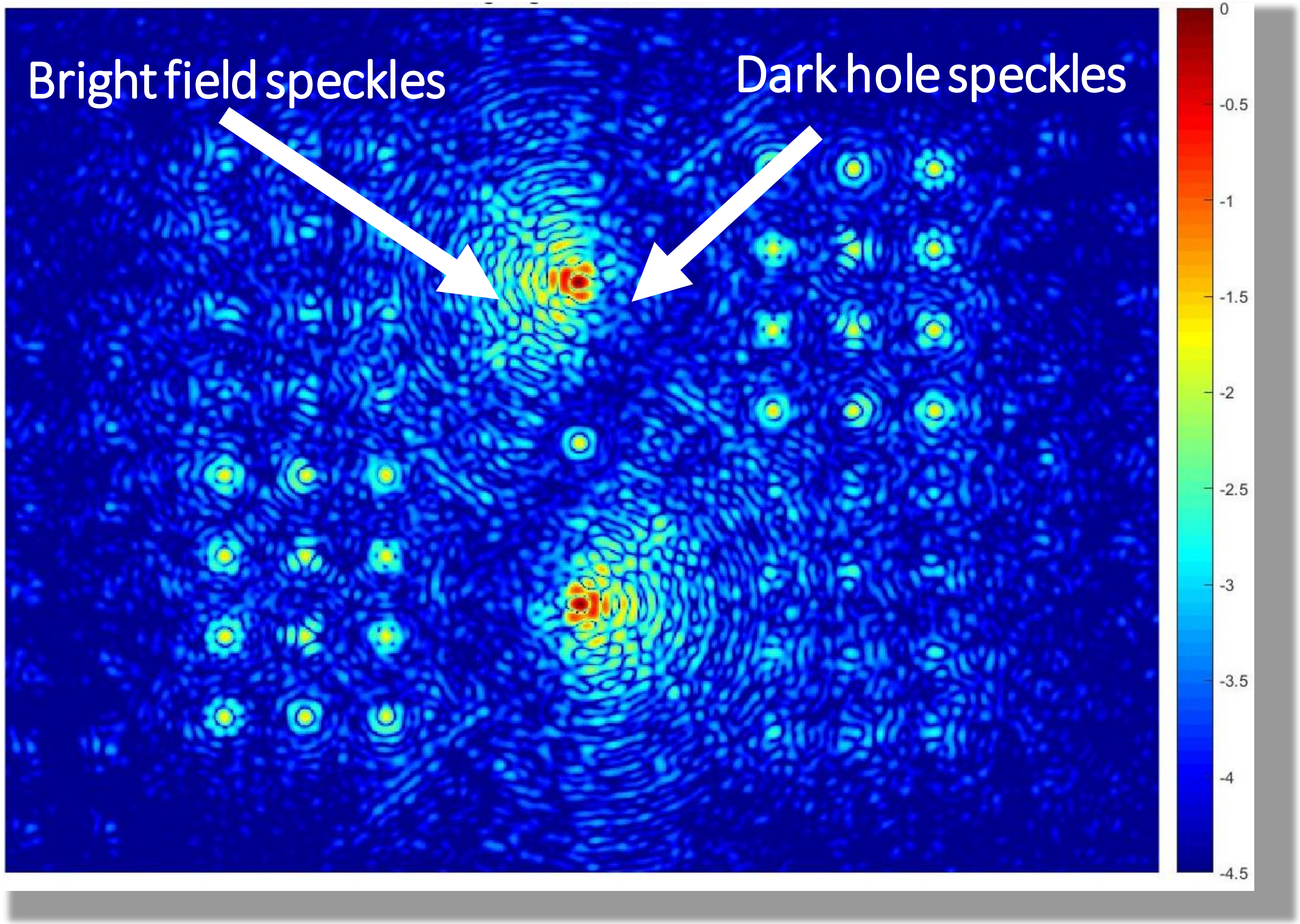

Linear Dark Field Control: Theory

- Stabilizes the dark hole

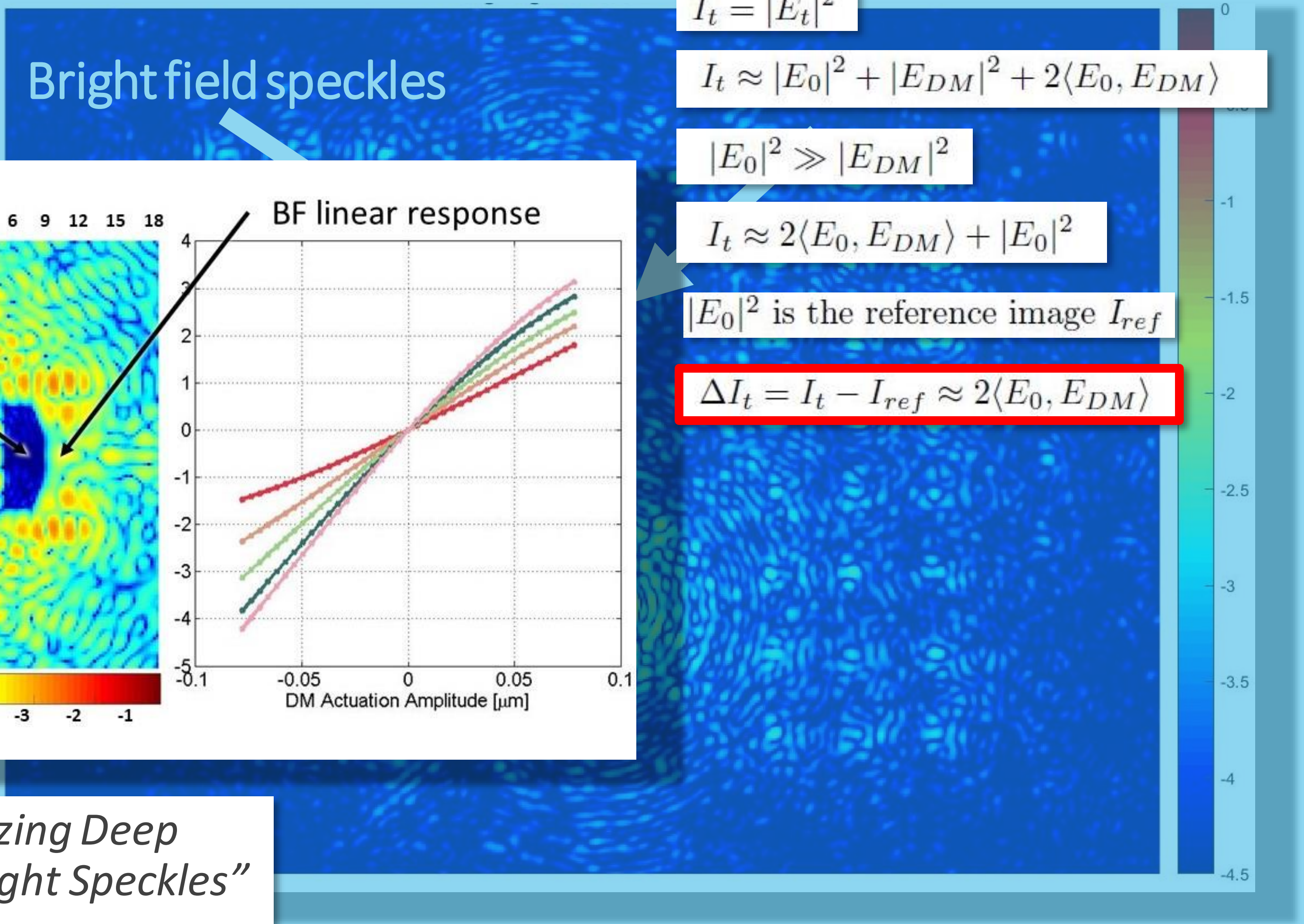

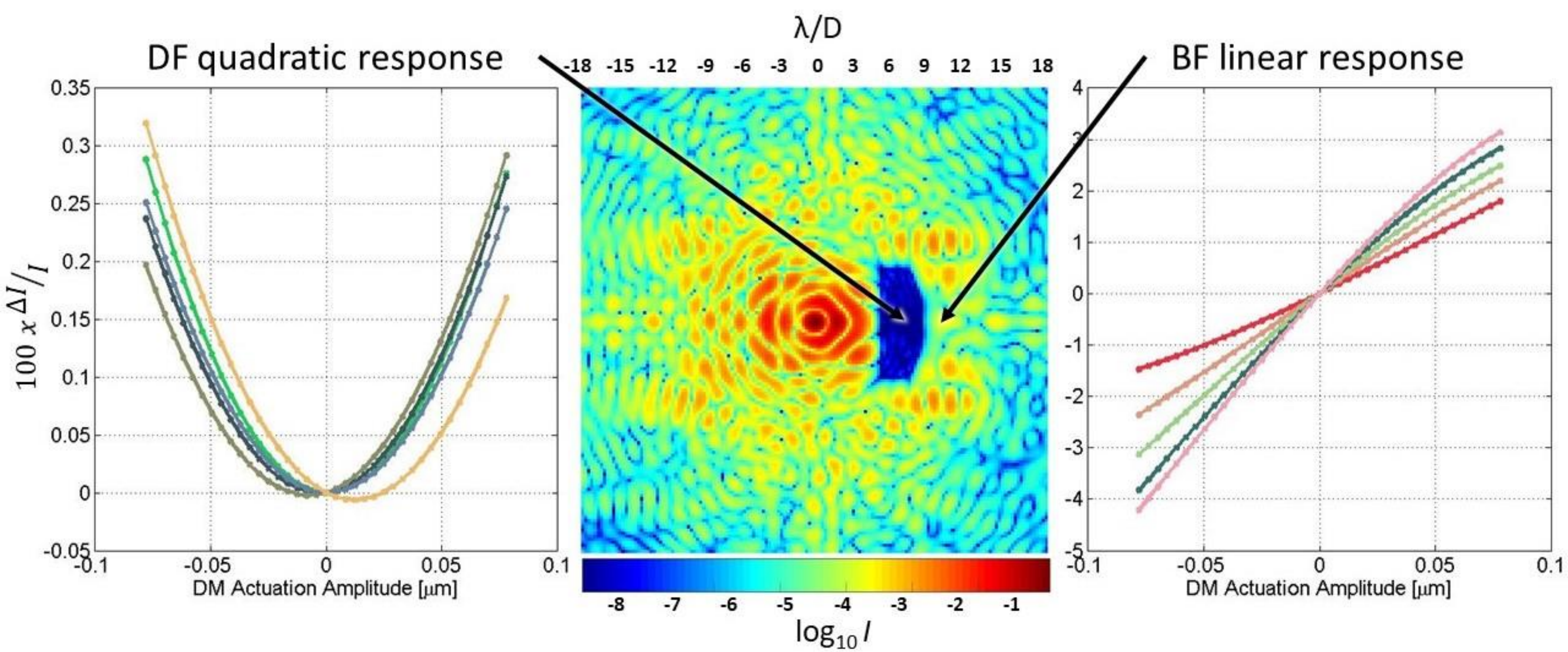

that modify both the bright and dark

$E_t \approx E_0 + E_{DM}$

$I_t = |E_t|^2$

$I_t \approx |E_0|^2 + |E_{DM}|^2 + 2\langle E_0, E_{DM}\rangle$

$|E_0|^2 \gg |E_{DM}|^2$

$I_t \approx 2\langle E_0, E_{DM}\rangle + |E_0|^2$

$|E_0|^2$ is the reference image I_{ref}

$\boxed{\Delta I_t = I_t - I_{ref} \approx 2\langle E_0, E_{DM}\rangle}$

“Spatial Linear Dark Field Control: Stabilizing Deep Contrast for Exoplanet Imaging Using Bright Speckles” (Miller et al 2017, JATIS)

LDFC with a vAPP coronagraph

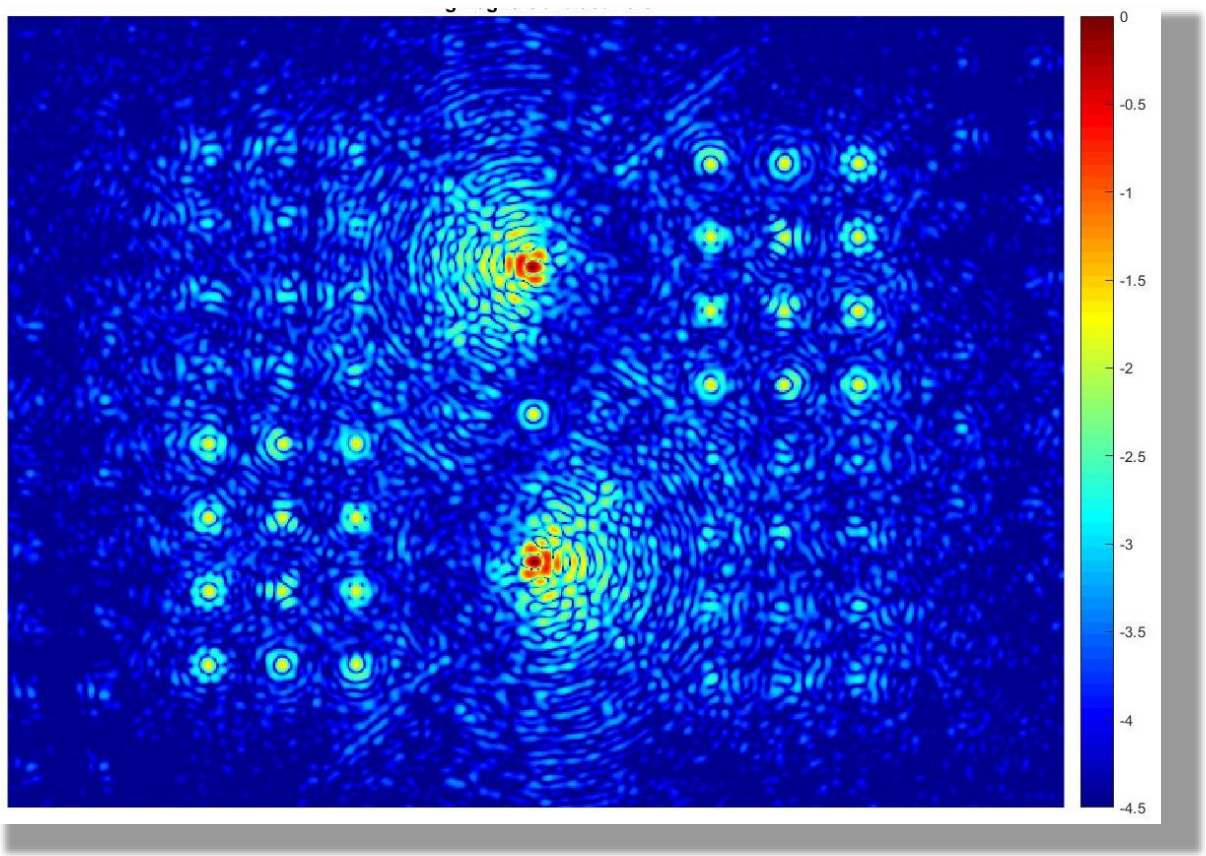

LDFC with a vAPP coronagraph

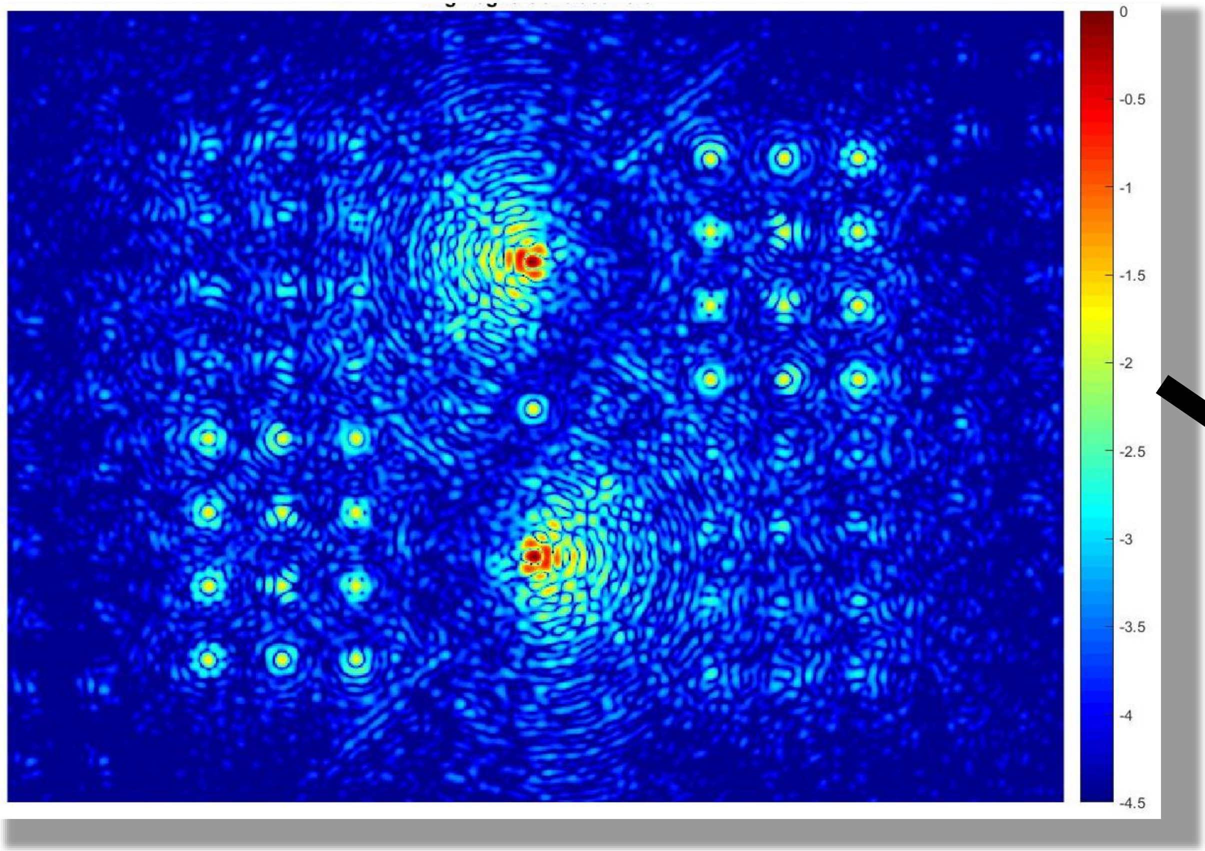

Defocused image

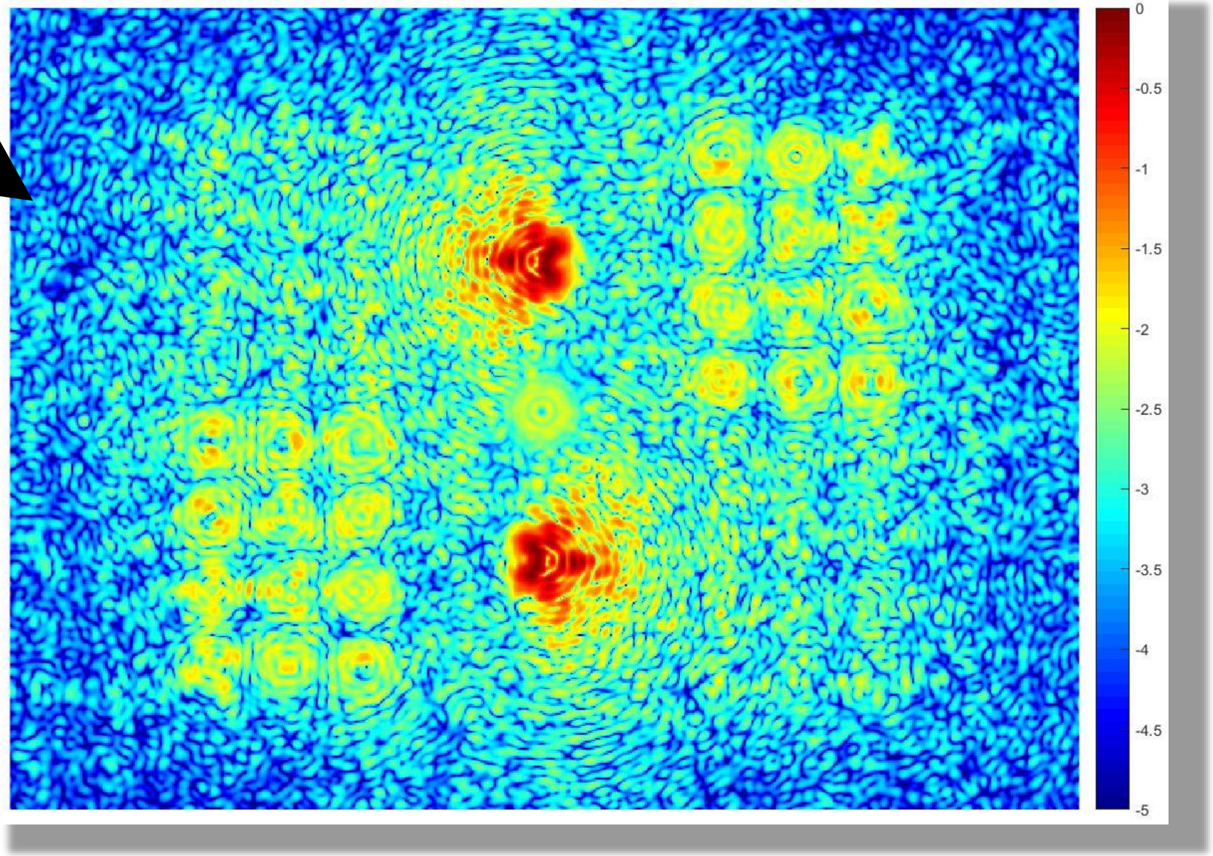

LDF agraph

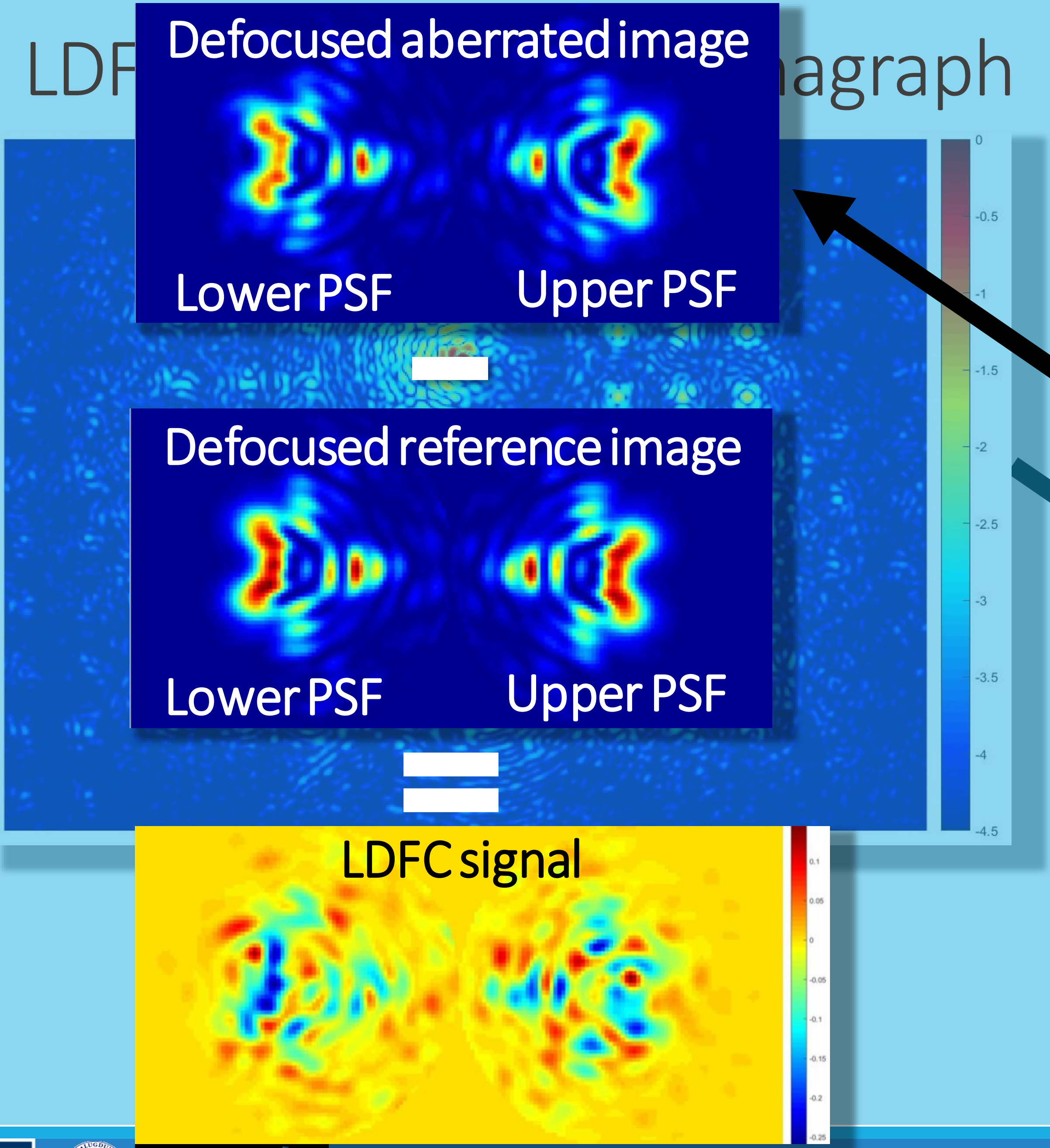

Defocused image

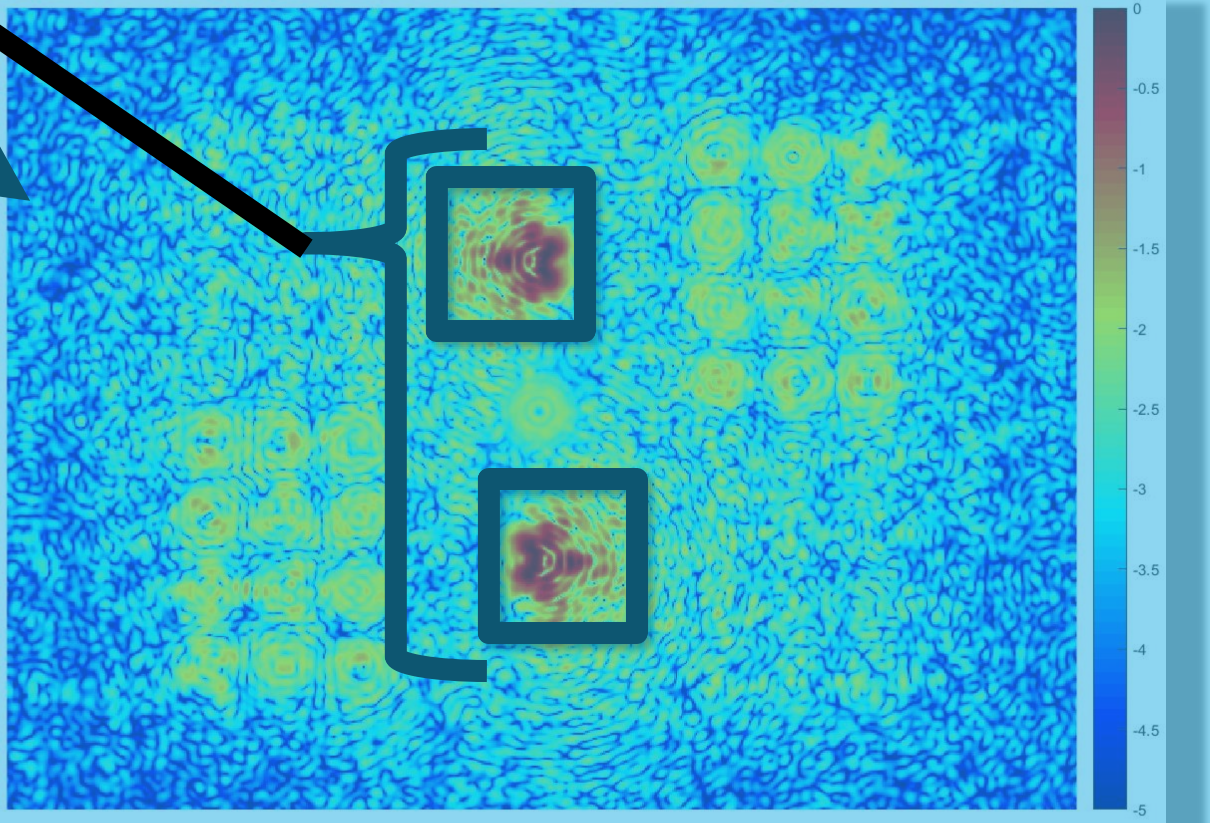

LDFC with a vAPP coronagraph

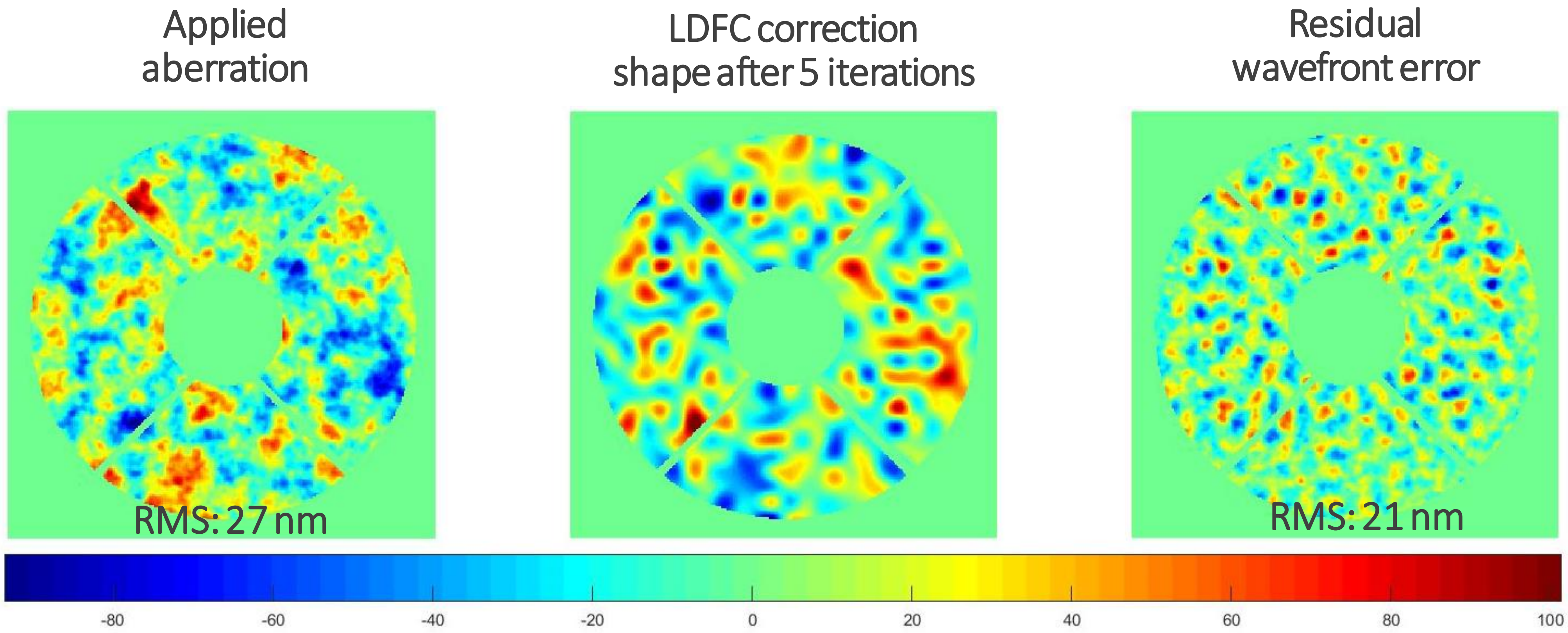

LDFC with a vAPP coronagraph

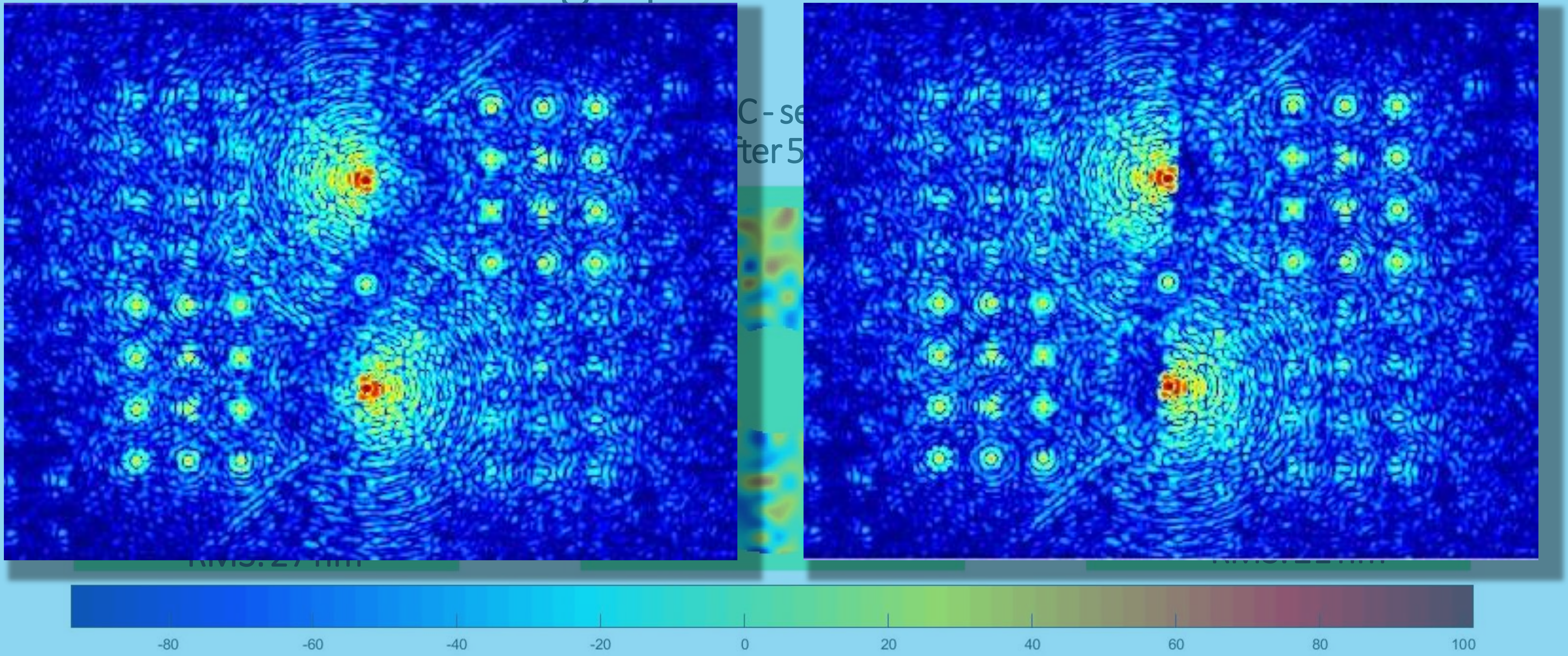

LDFC with a vAP

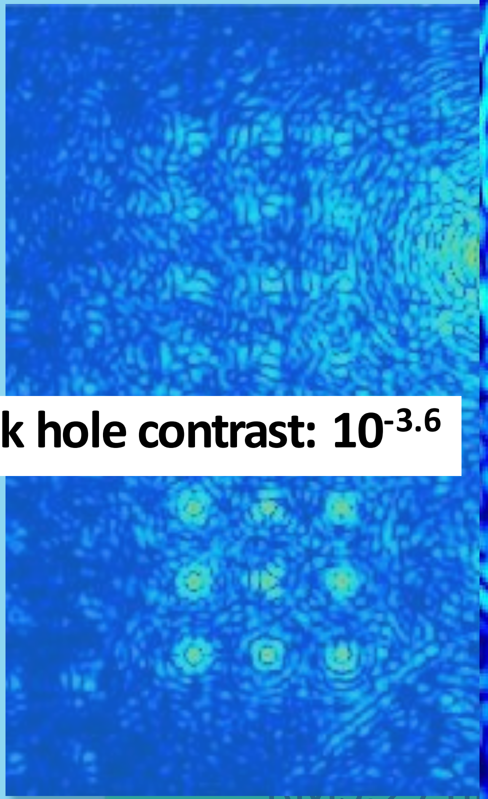

Dark hole contrast: $10^{-3.6}$

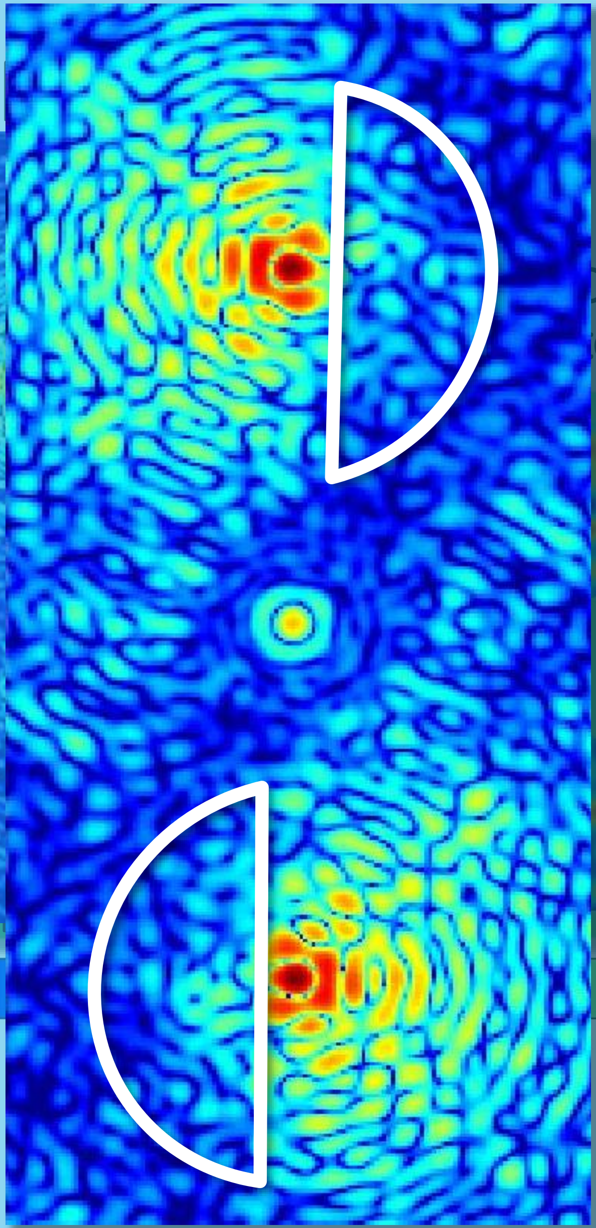

Aberrated PSF

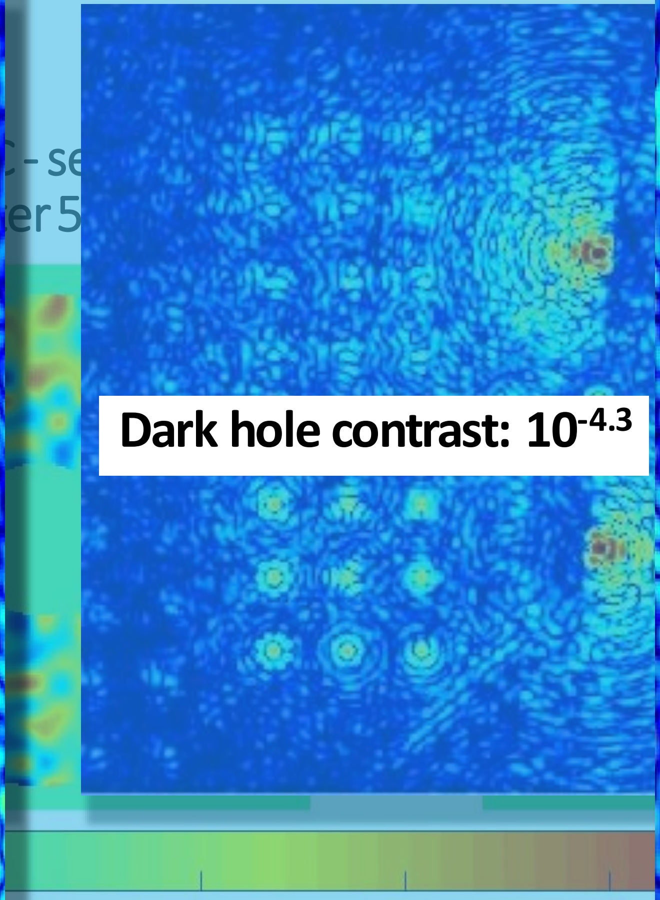

Dark hole contrast: $10^{-4.3}$

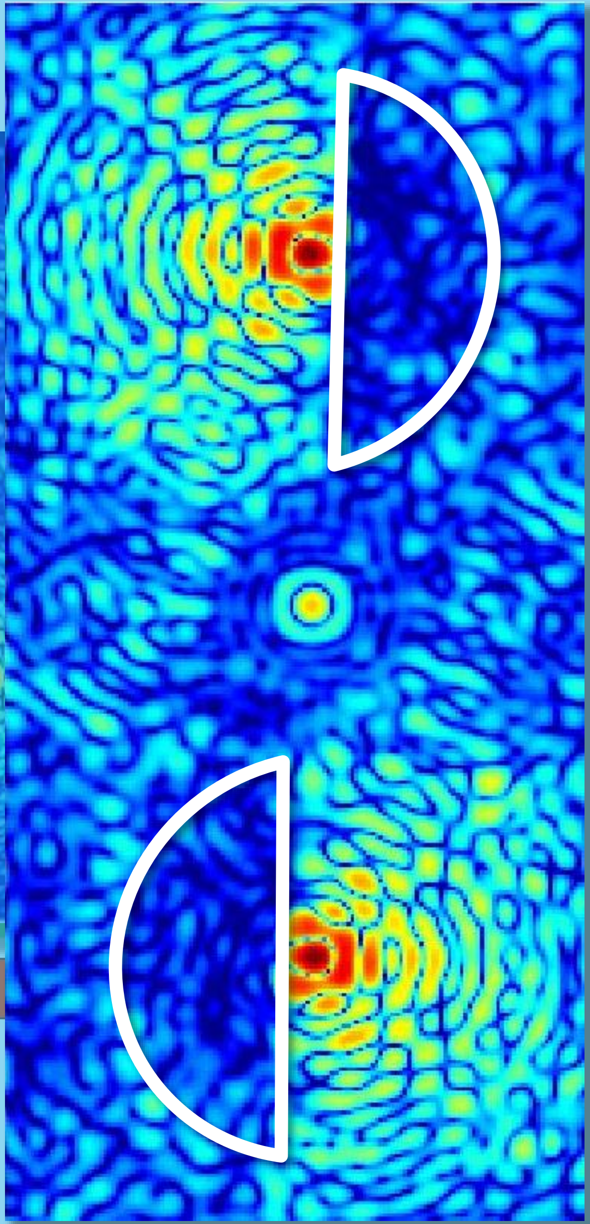

Corrected PSF

LDFC w/ a vAPP in the lab

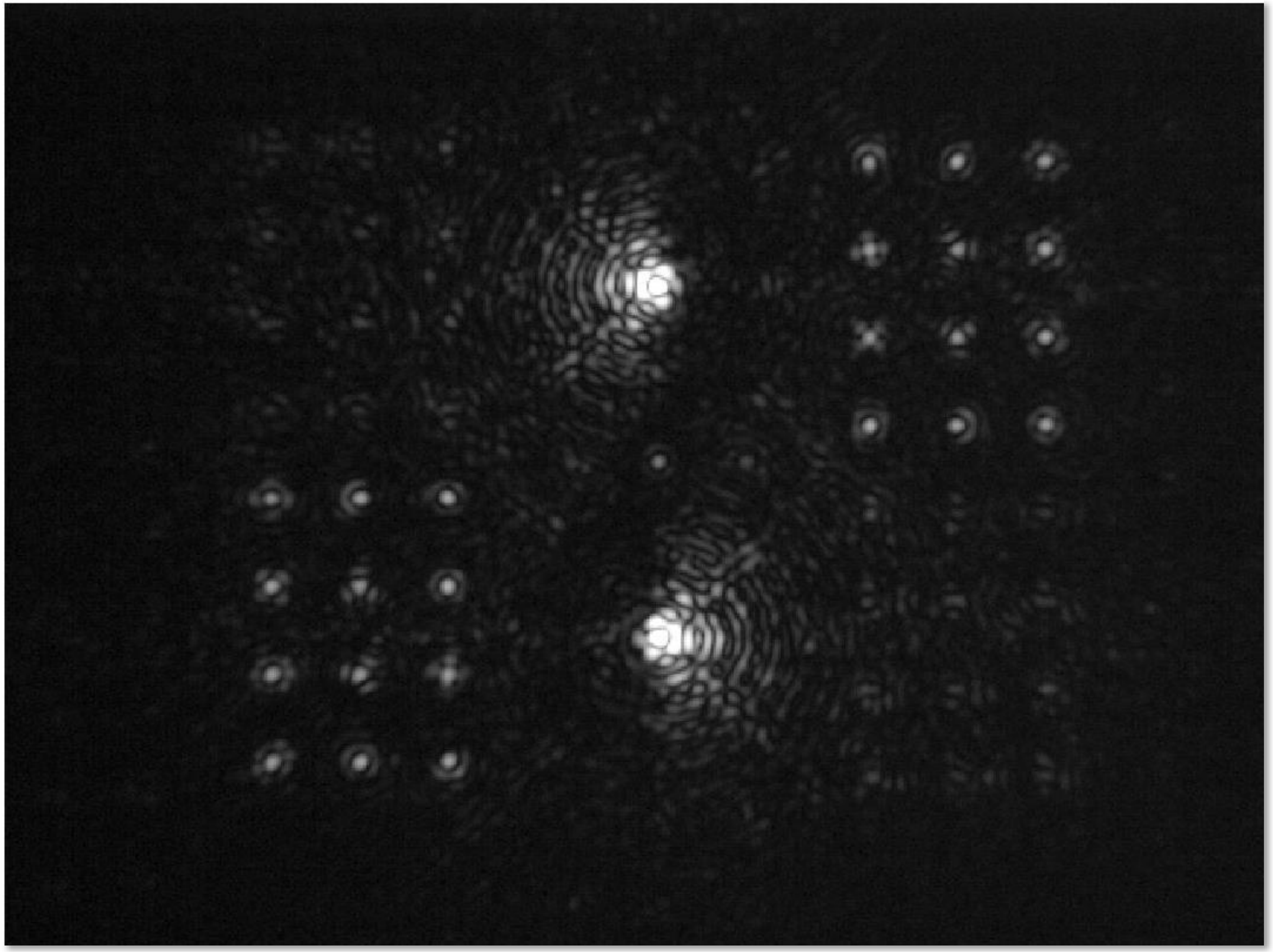

LDFC w/ a vAPP in the lab

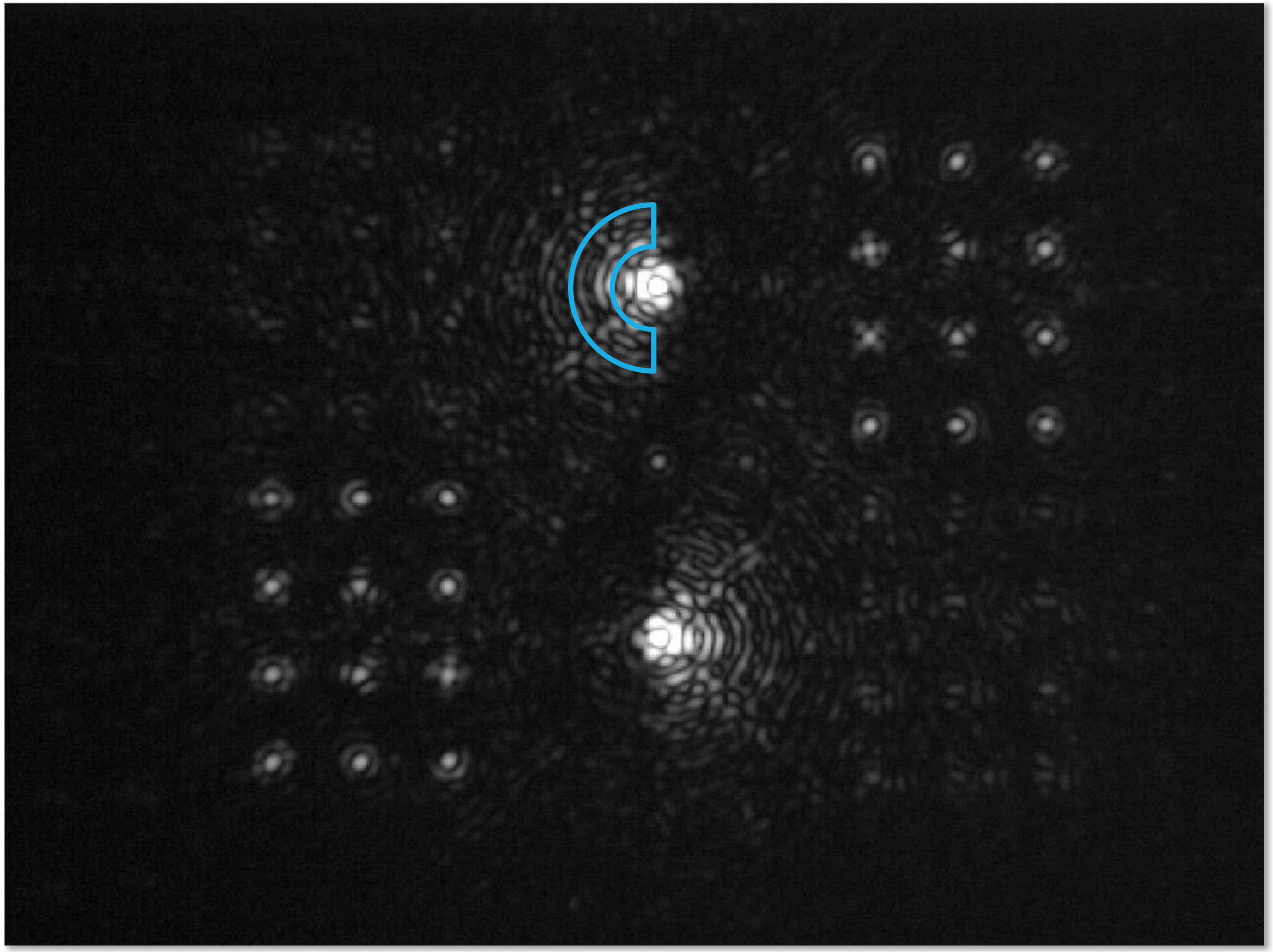

Bright field reference contrast: $10^{-2.4}$

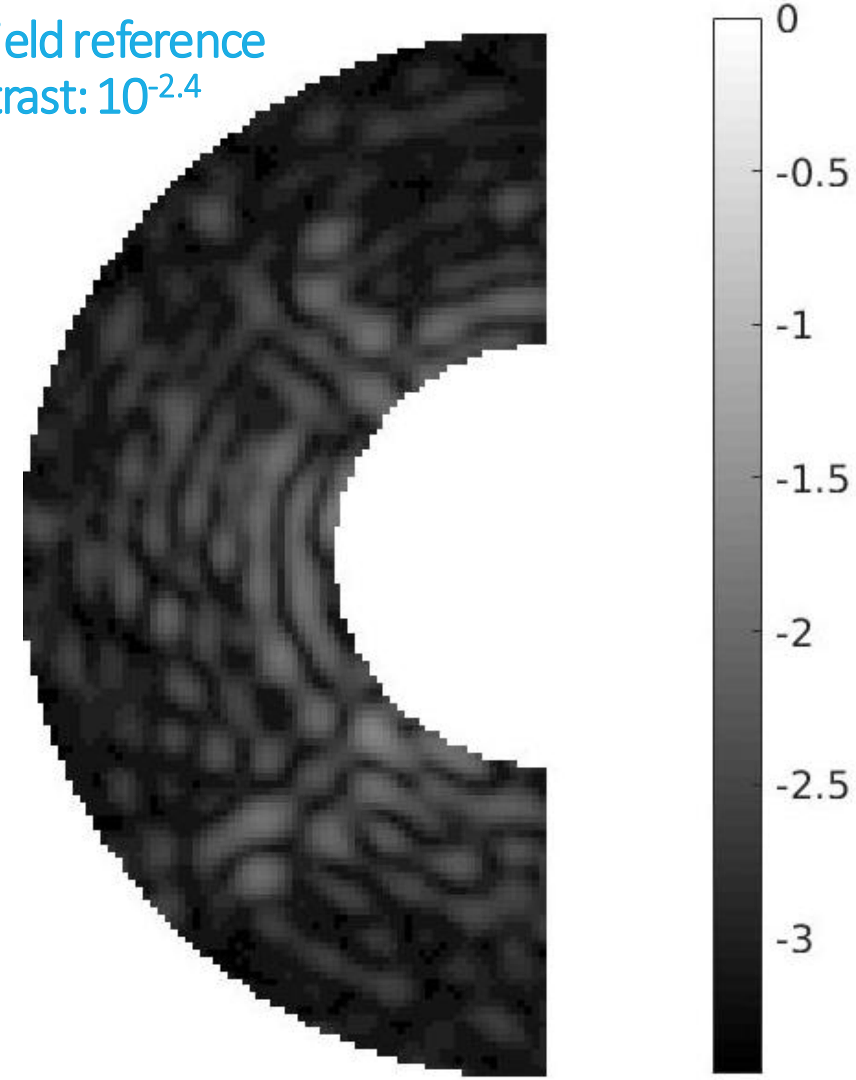

LDFC w/ a vAPP in the lab

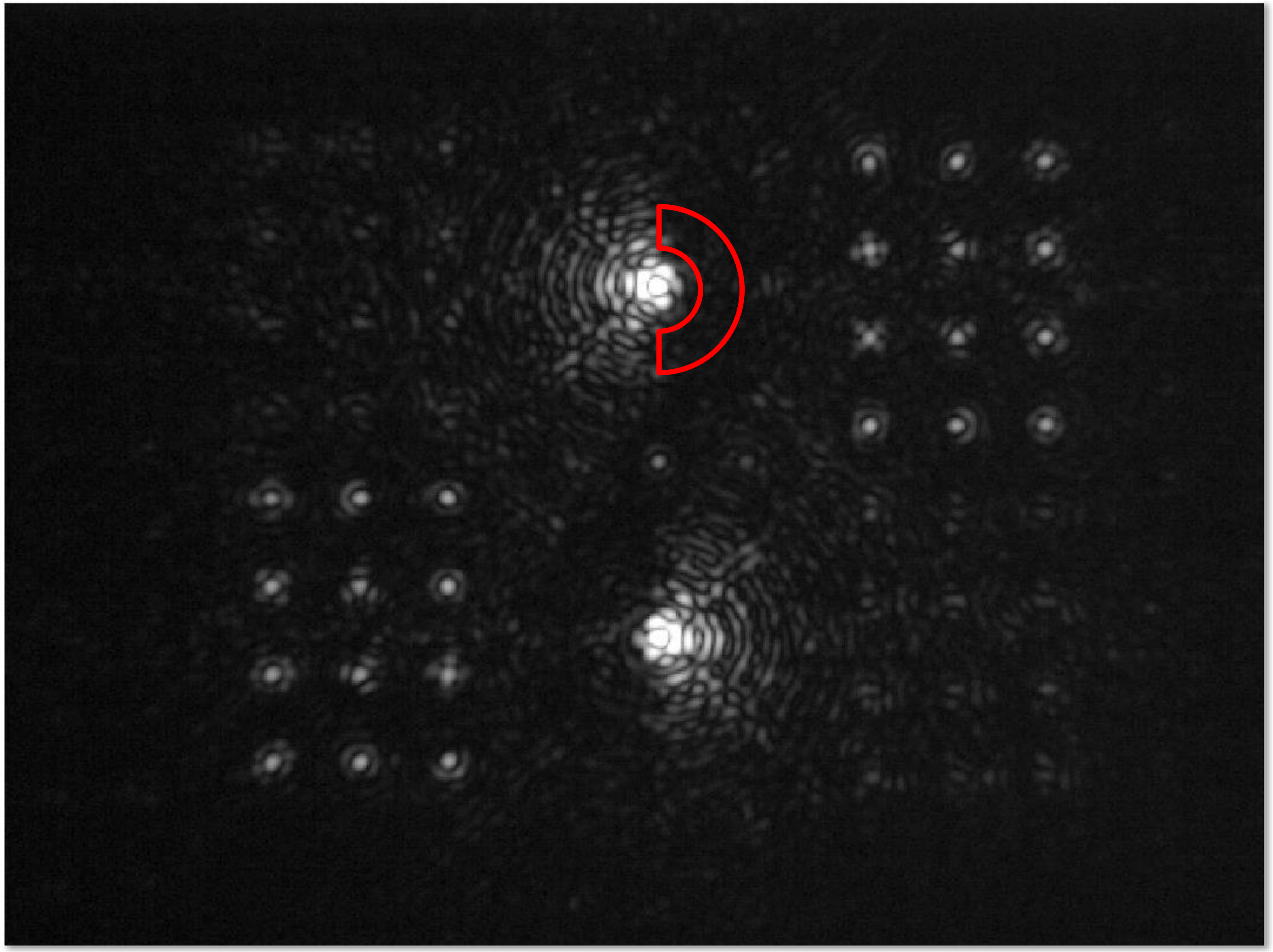

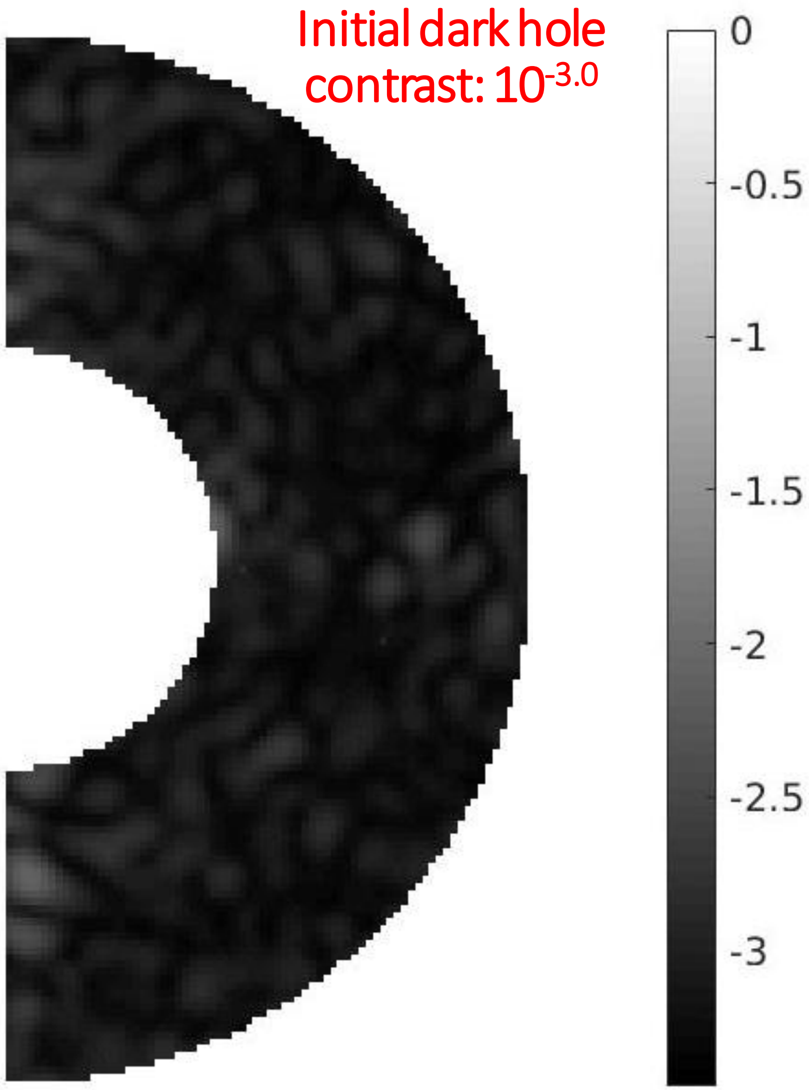

LDFC w/ a vAPP in the lab

Controlling 100 mid-spatial frequency mirror modes

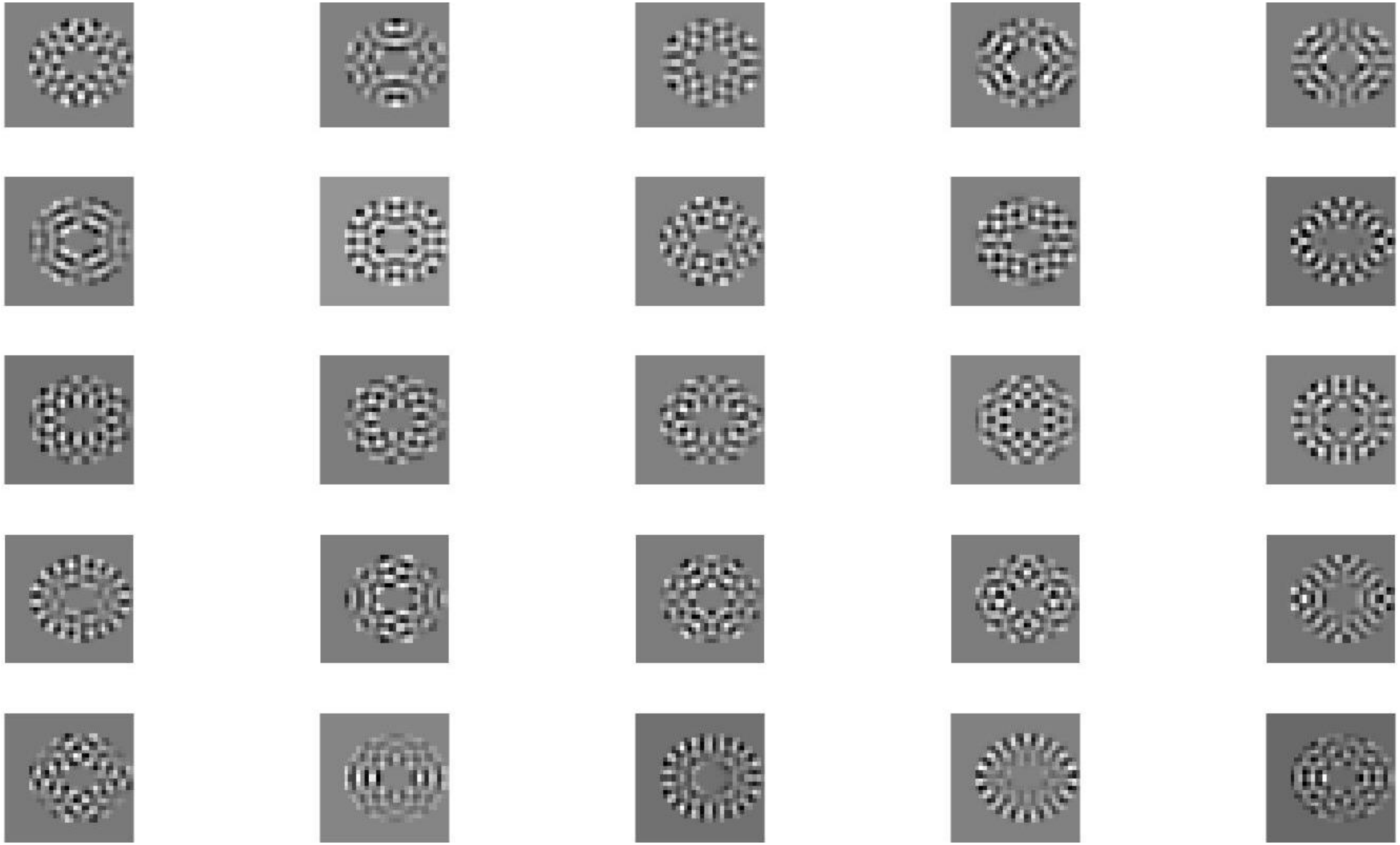

LDFC w/ a vAPP in the lab

Aberrated dark hole (LDFC off)

Corrected dark hole (LDFC on)

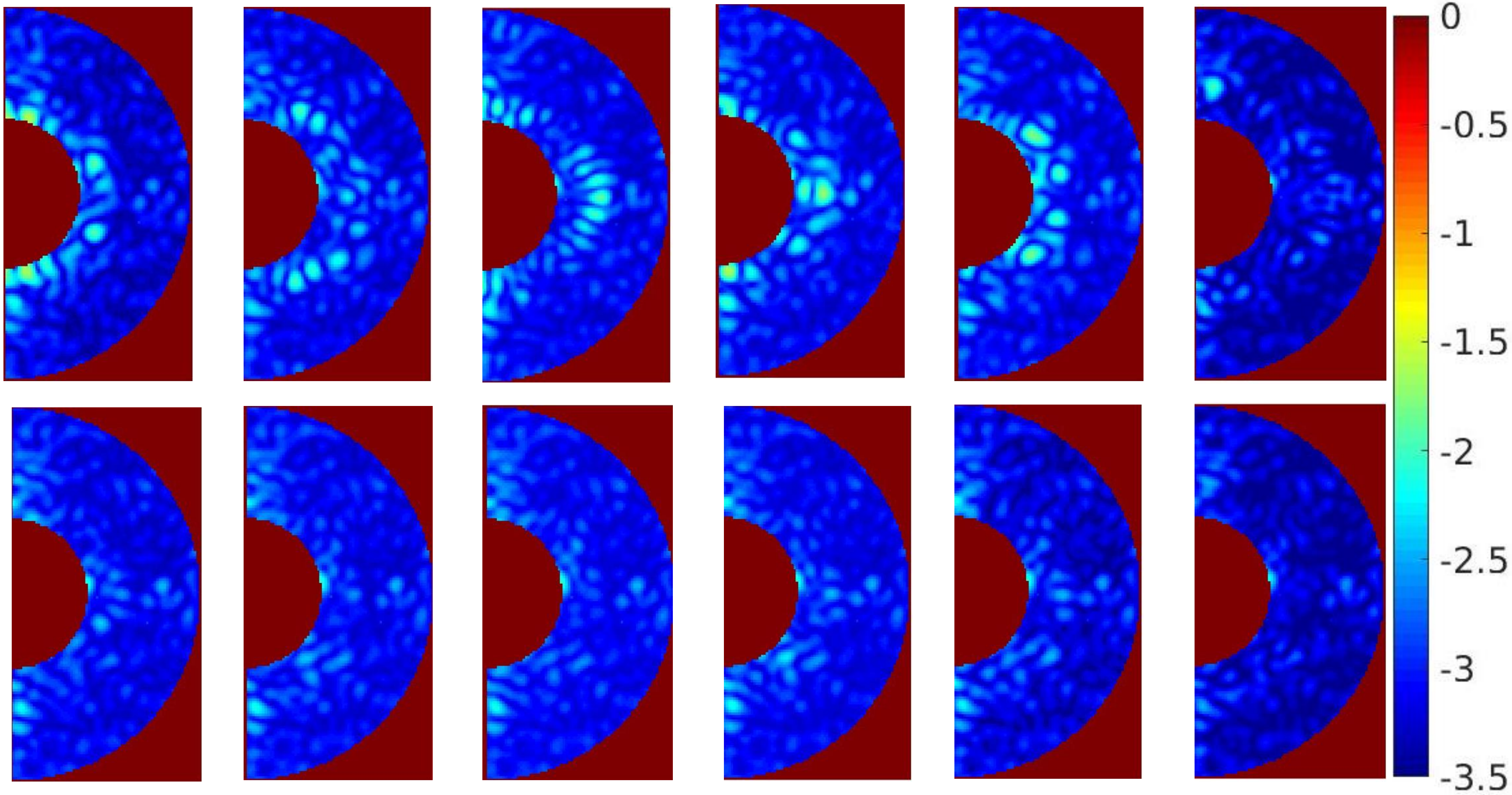

LDFC on MagAO-X

Future plans for implementing LDFC on MagAO-X

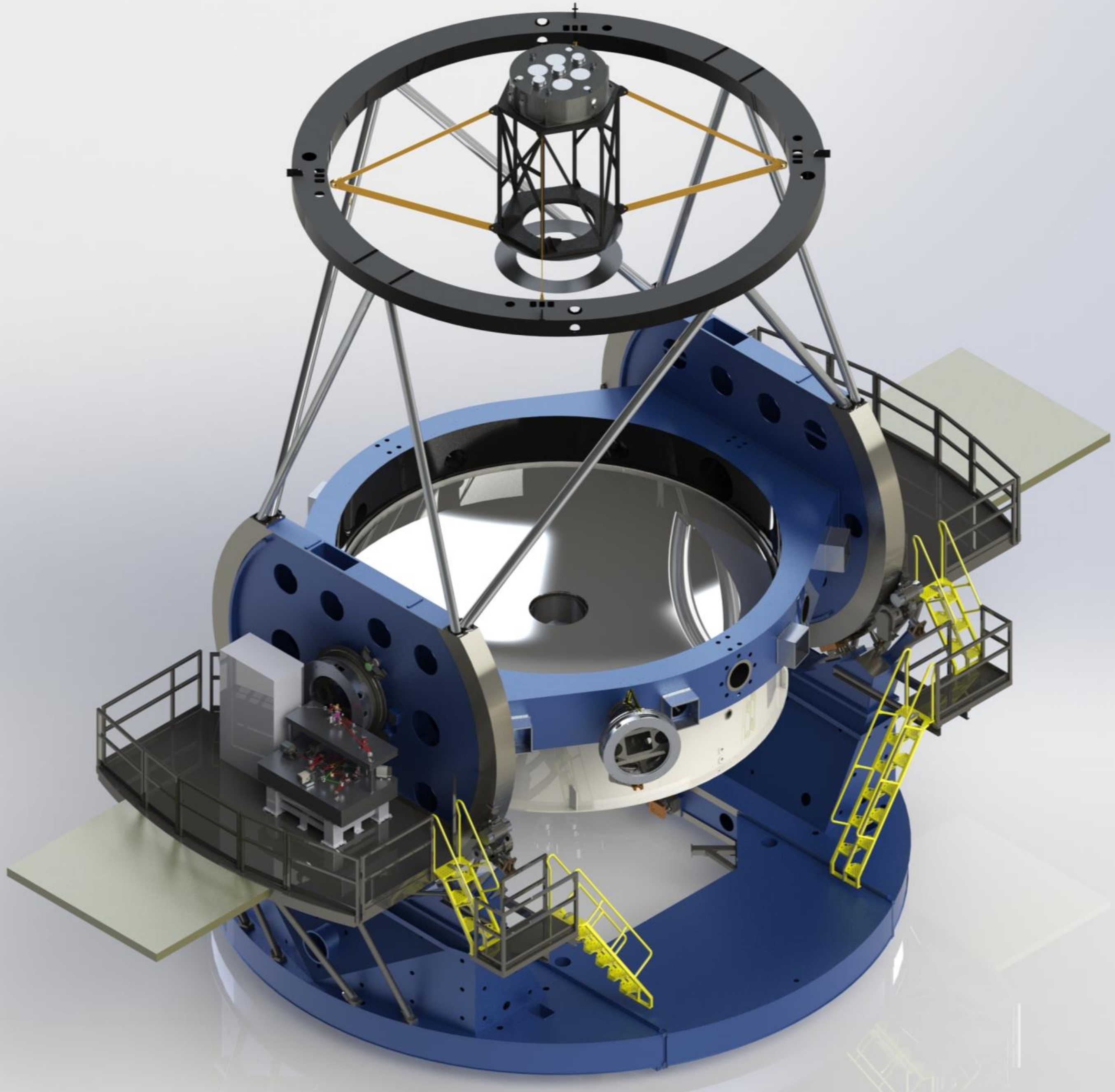

LDFC on MagAO-X

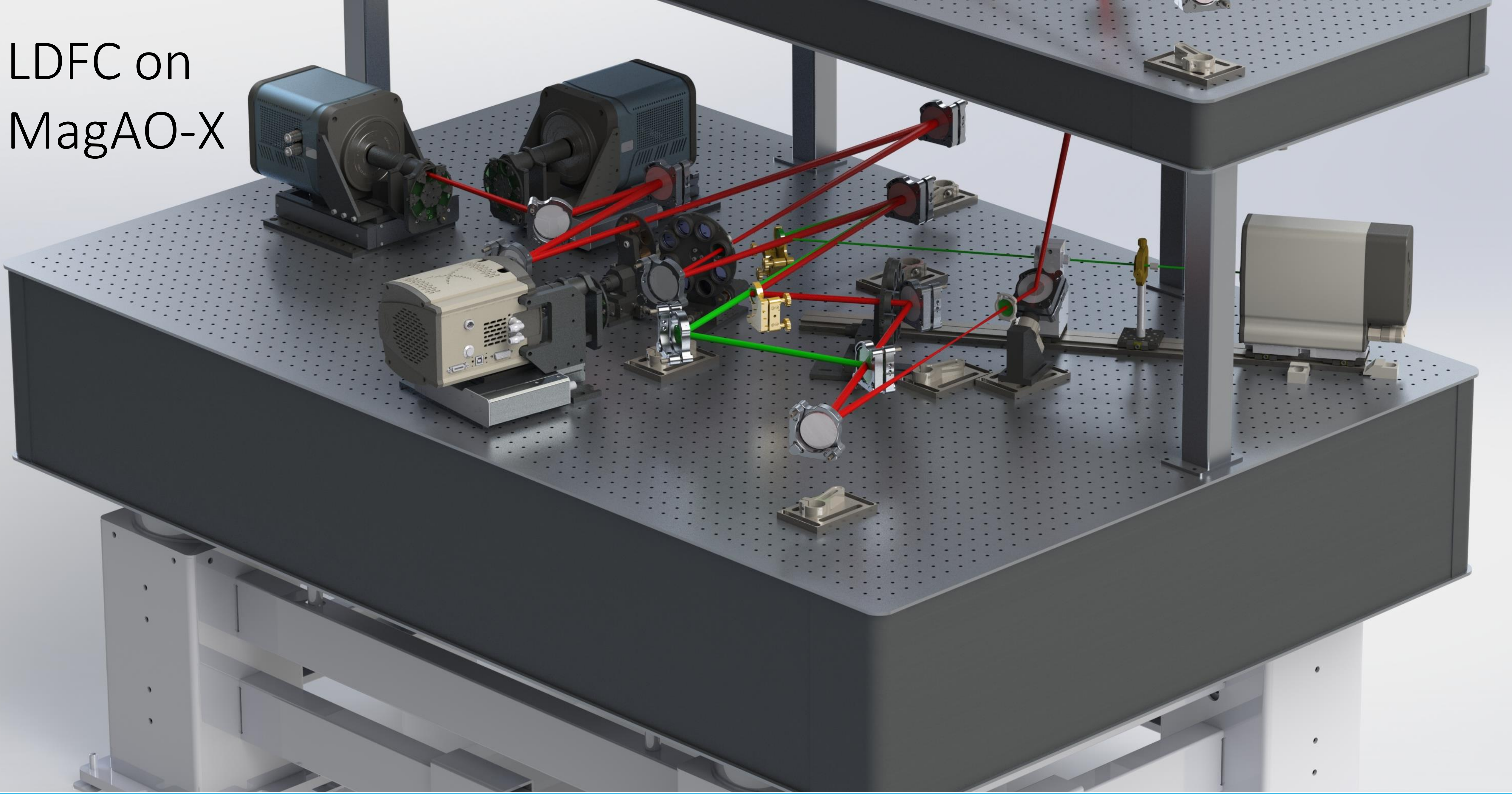

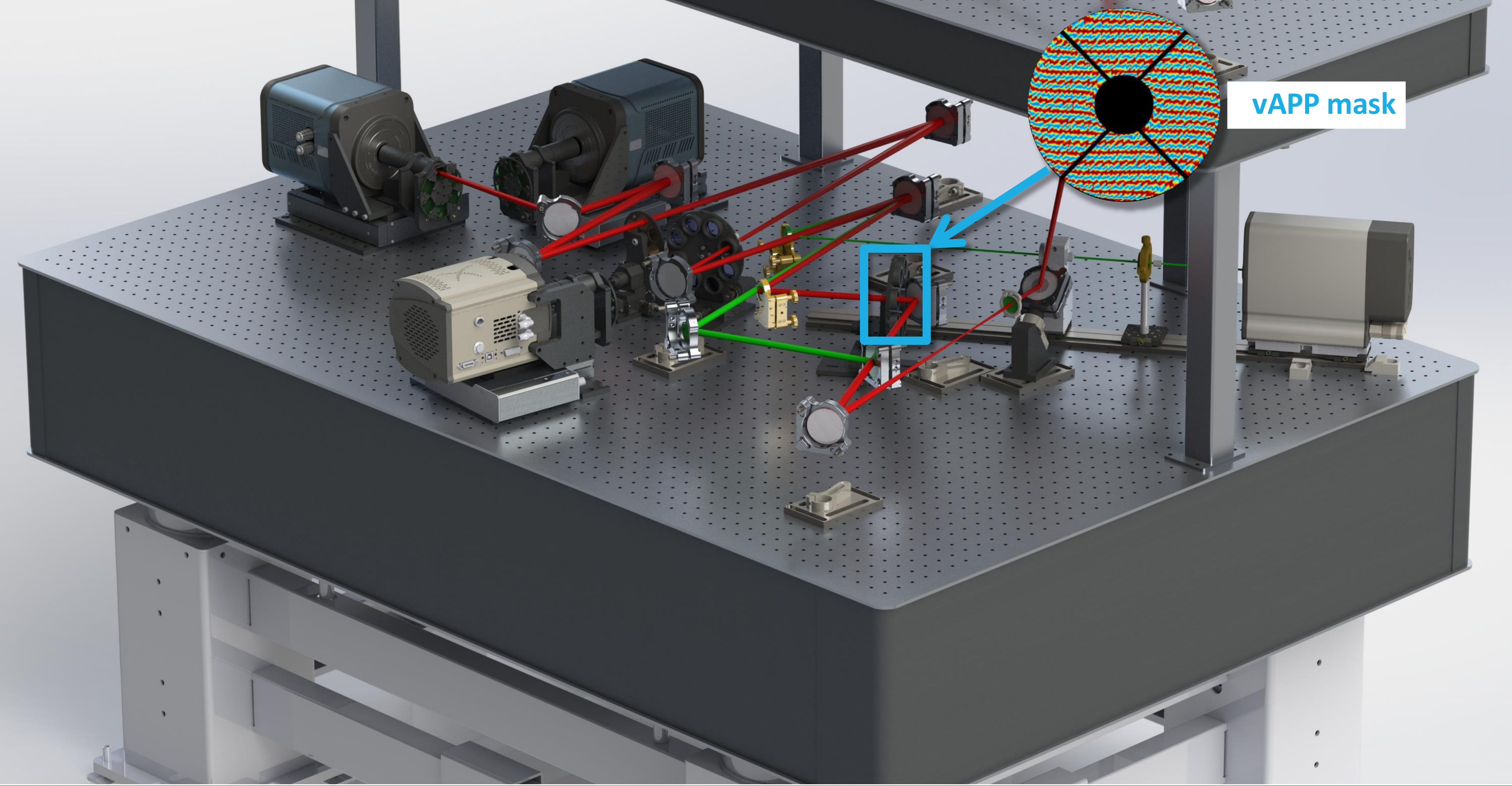
vAPP mask

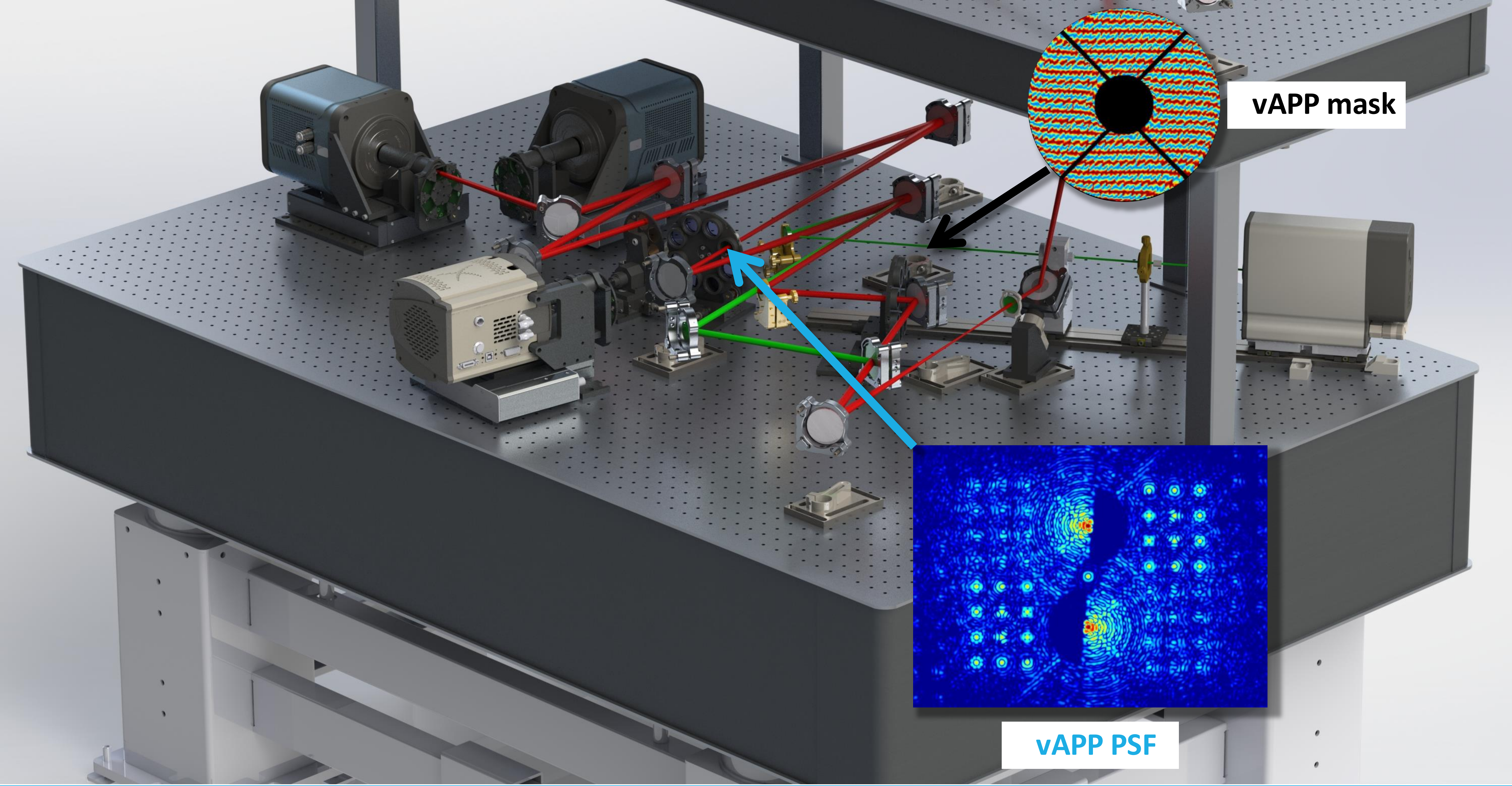
vAPP mask
vAPP PSF

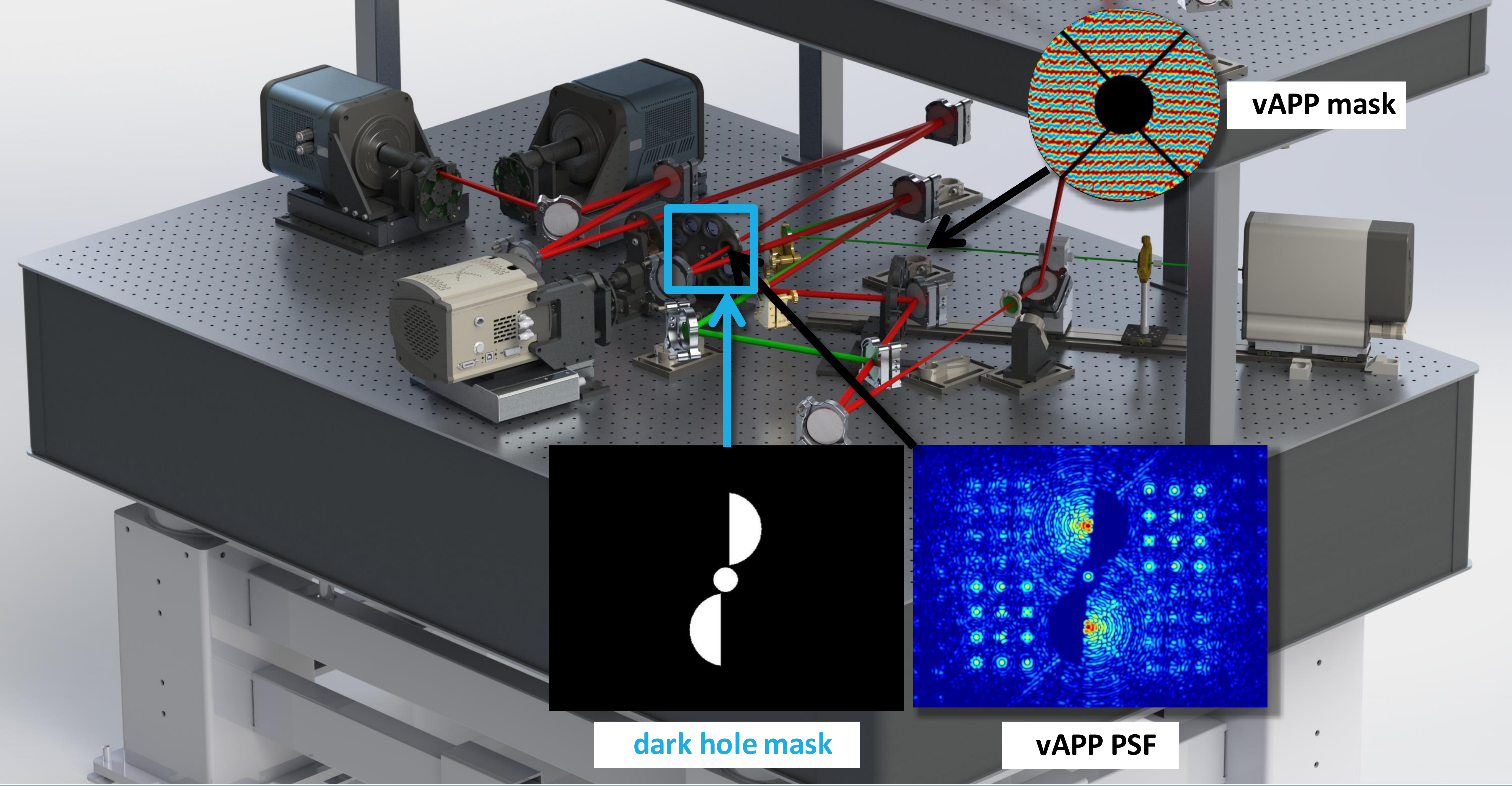
vAPP mask
dark hole mask
vAPP PSF

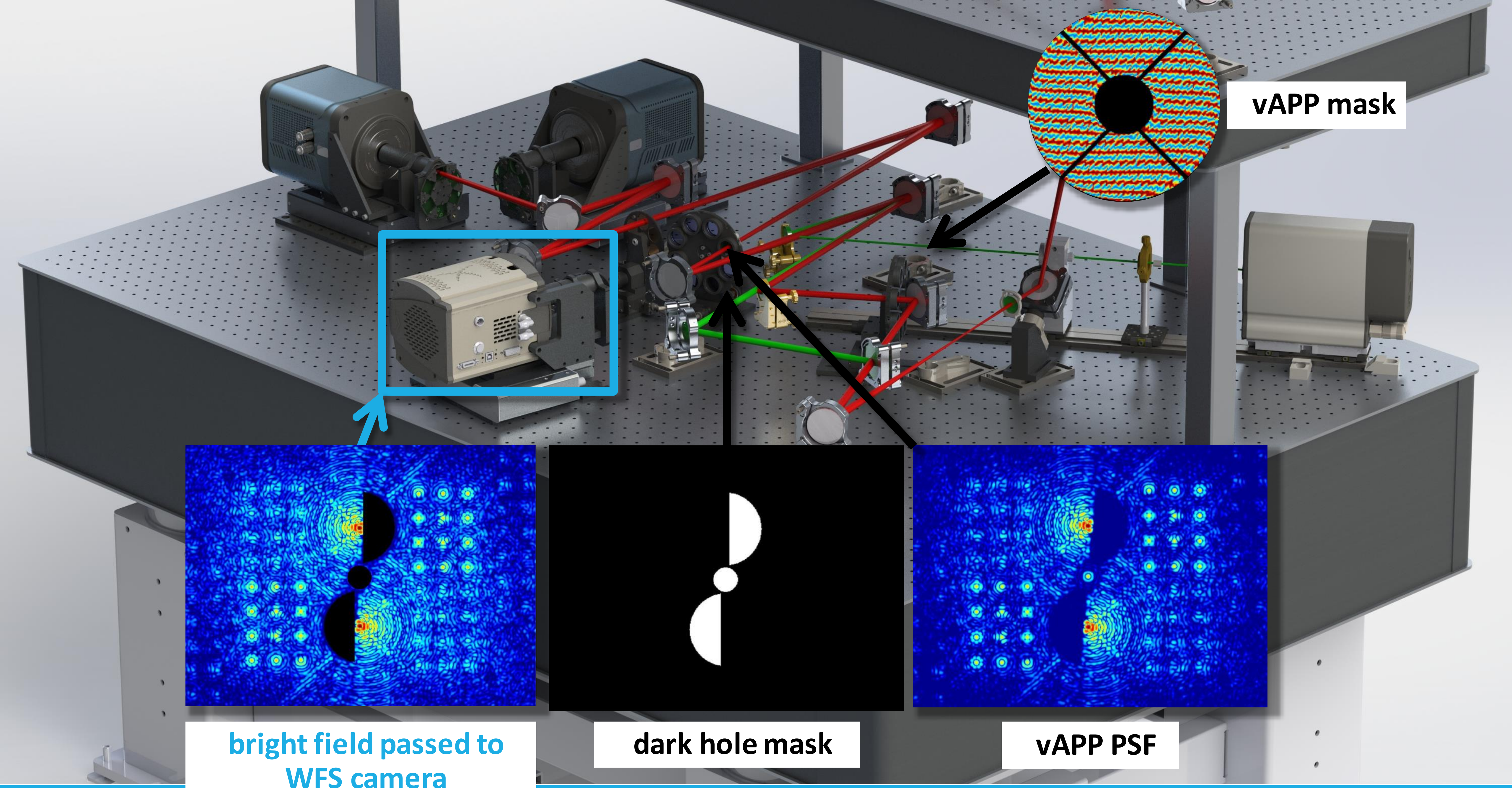
vAPP mask
bright field passed to WFS camera
dark hole mask
vAPP PSF
MagAOX
SPIE.

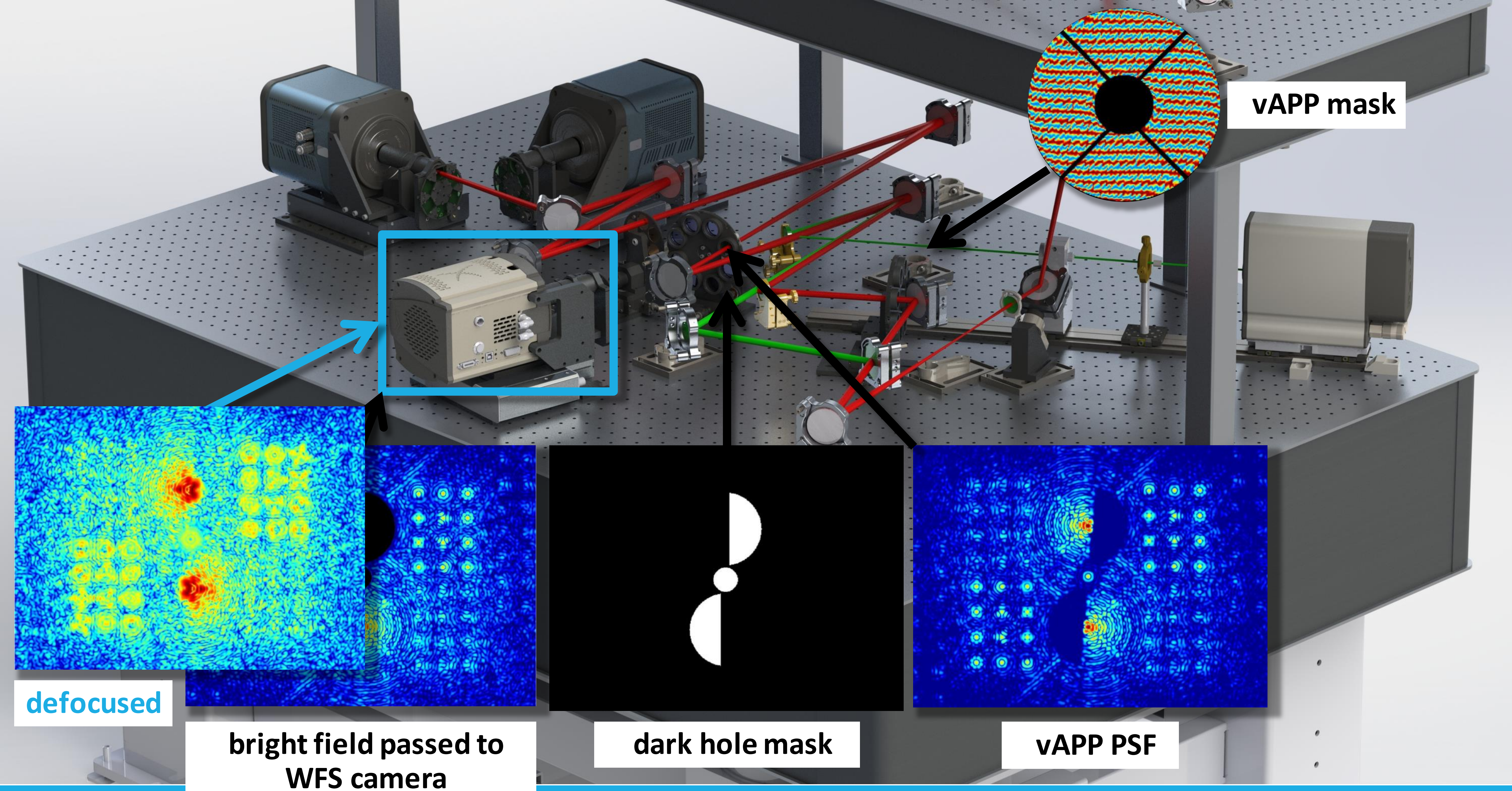
vAPP mask
defocused
bright field passed to WFS camera
dark hole mask
vAPP PSF

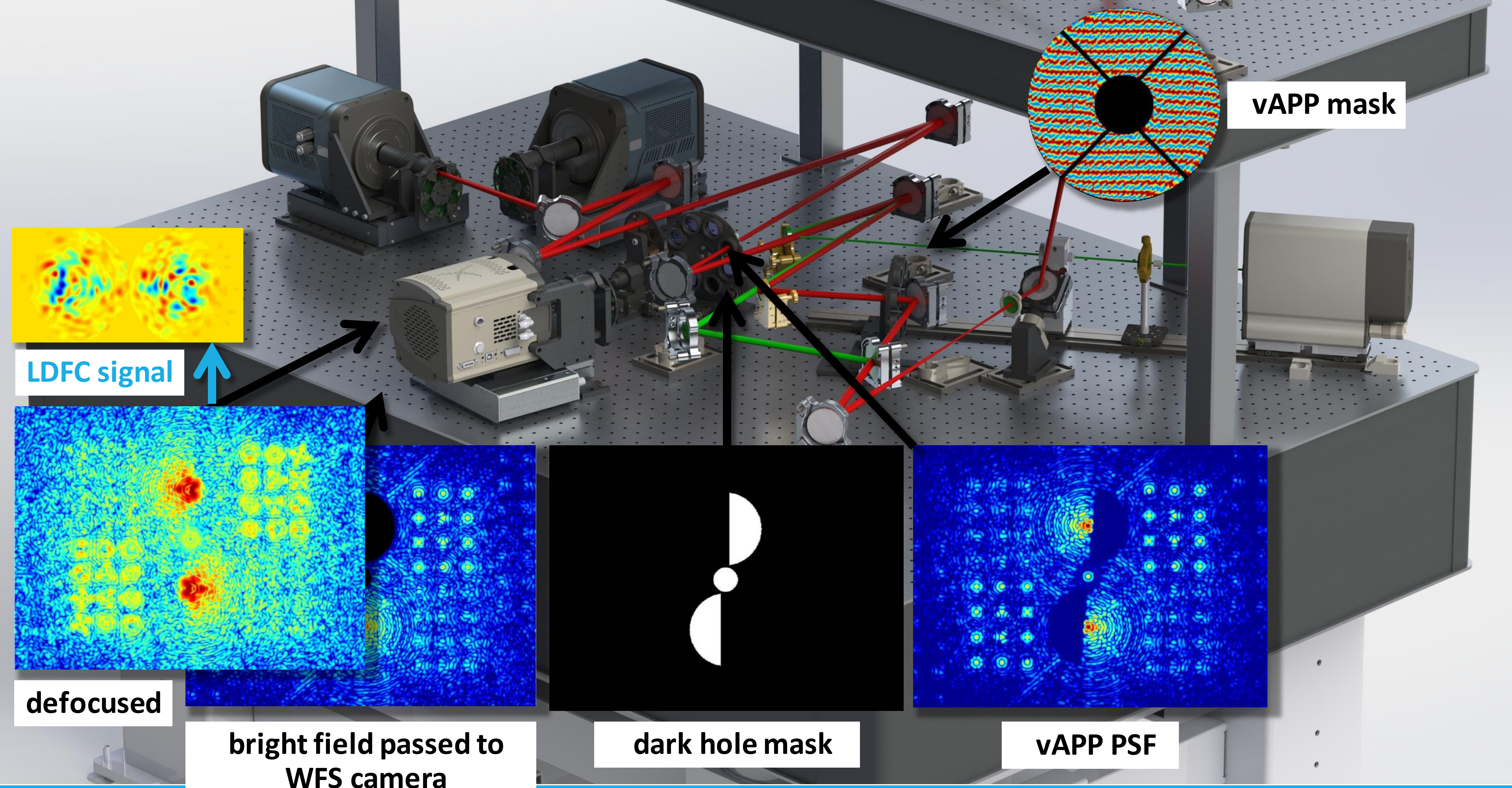

vAPP mask
LDFC signal
defocused
bright field passed to WFS camera
dark hole mask
vAPP PSF
MagAOX
SPIE.

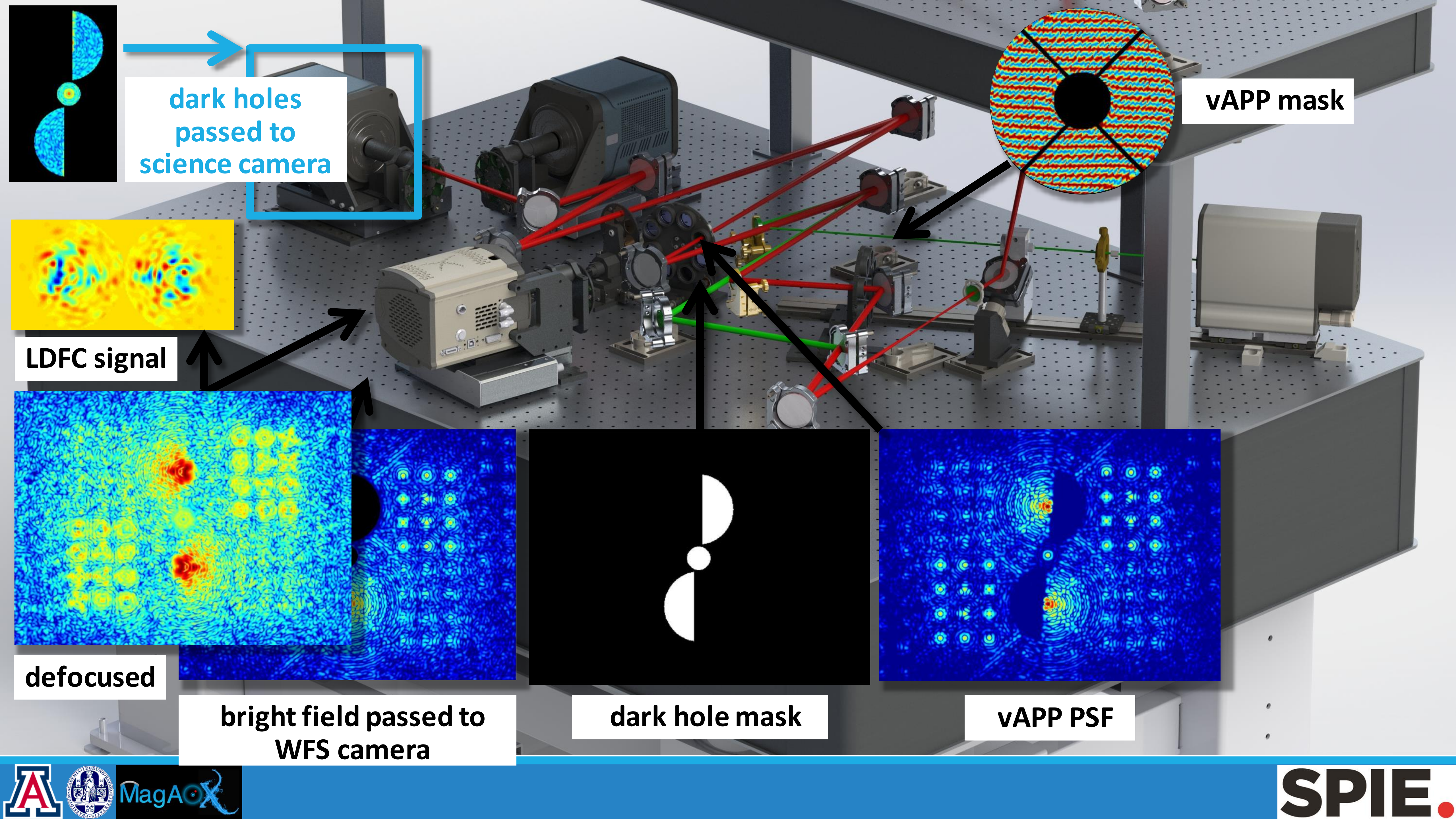
dark holes
passed to
science camera
vAPP mask
LDFC signal
defocused
bright field passed to
WFS camera
dark hole mask
vAPP PSF
MagAOX
SPIE.

Conclusions and ongoing work

- Further lab testing/demonstrations of LDFC
- Final selection of the MagAO-X vAPP coronagraph design
- Combining LOWFS with MWFS spots and LDFC into a single control loop for low and mid-spatial frequency control

Acknowledgements

This work was supported [in part] by NSF MRI Award #1625441 (MagAO-X)

Leiden University team:

Frans Snik

Christoph Keller

David Doelman

Emiel Por

Mike Wilby

Steven Bos

Matt Kenworthy

University of Arizona MagAO-X team:

Jared Males

Olivier Guyon

Chris Bohlman

Justin Knight

Alexander Rodack

Jhen Lumbres

Kyle van Gorkom

Laird Close

Maggie Kautz

Alexander Hedglen

Joseph Long

Katie Morzinski

Lauren Schatz

Thank you!

Backup slides

Primary wavefront sensor:

- Pyramid wavefront sensor (PyWFS)
- Operating at up to 3.63 kHz

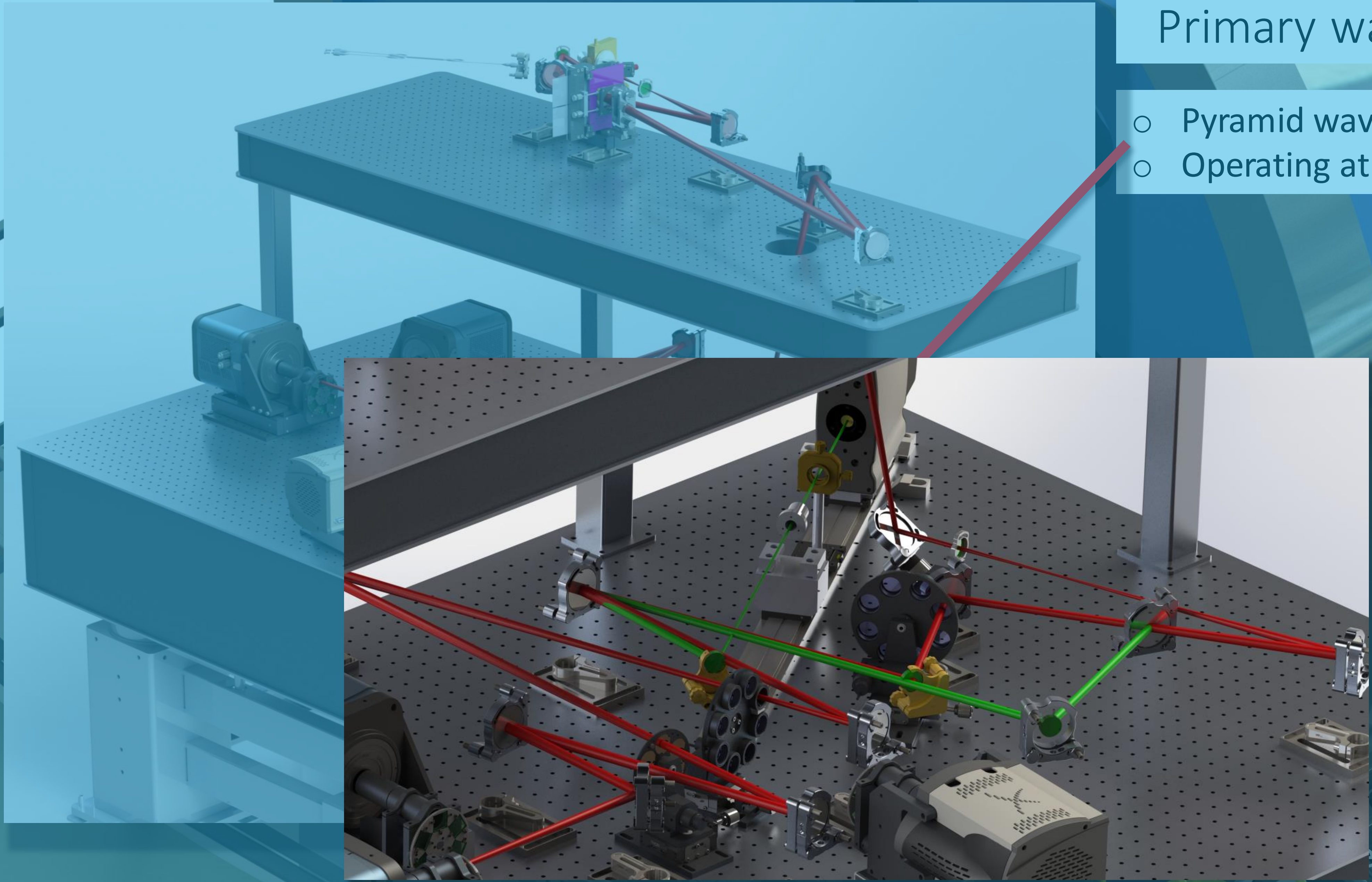

Magellan Clay Telescope

In-lab closed-loop MWFS LOWFS

Aberration: random phase aberration

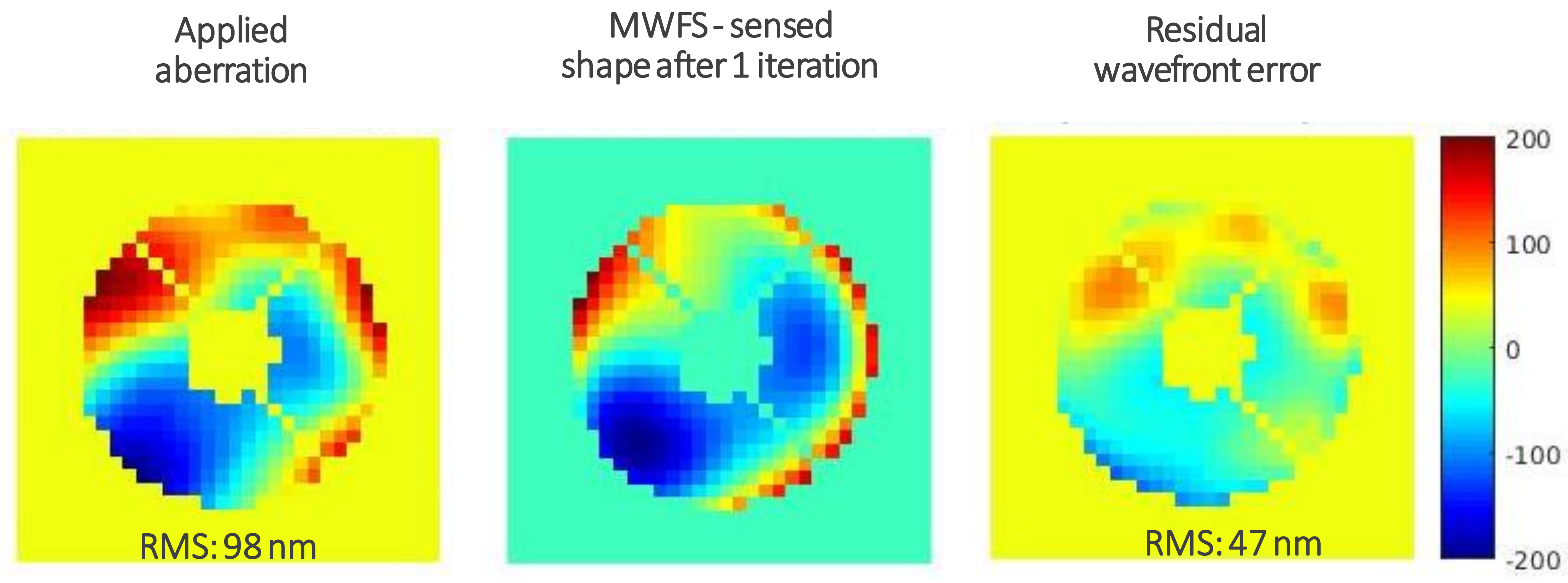

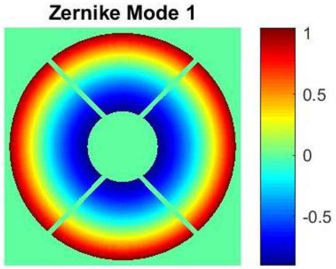
Zernike Mode 1
1
0.5
0
-0.5

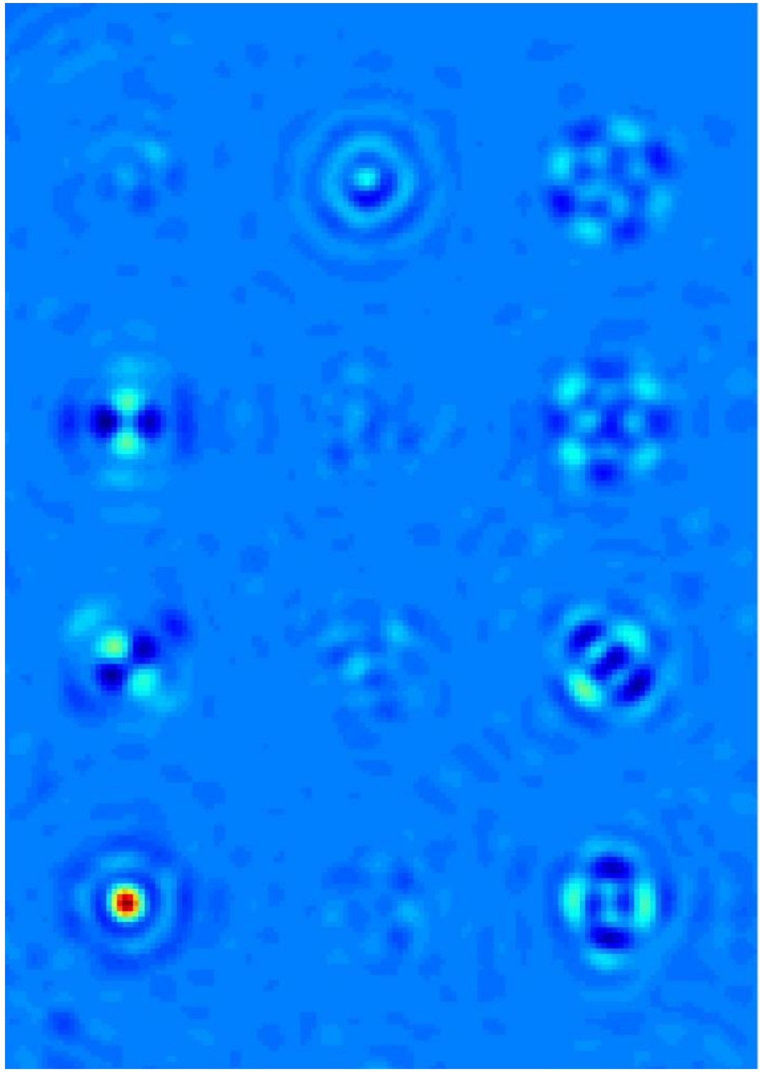

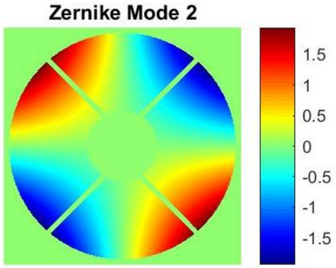
Zernike Mode 2
1.5
1
0.5
0
-0.5
-1
-1.5

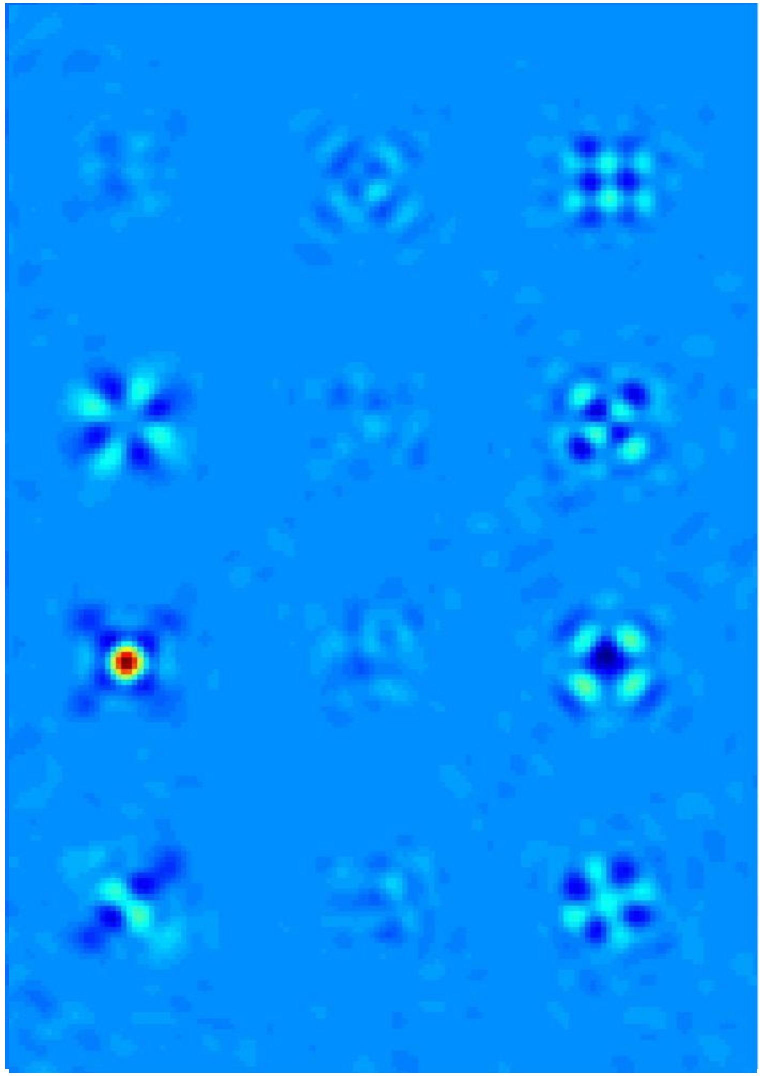

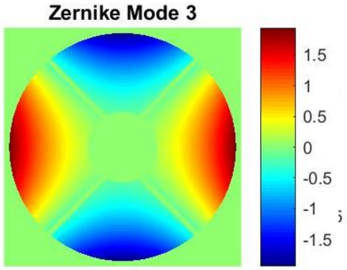
Zernike Mode 3
1.5
1
0.5
0
-0.5
-1
-1.5

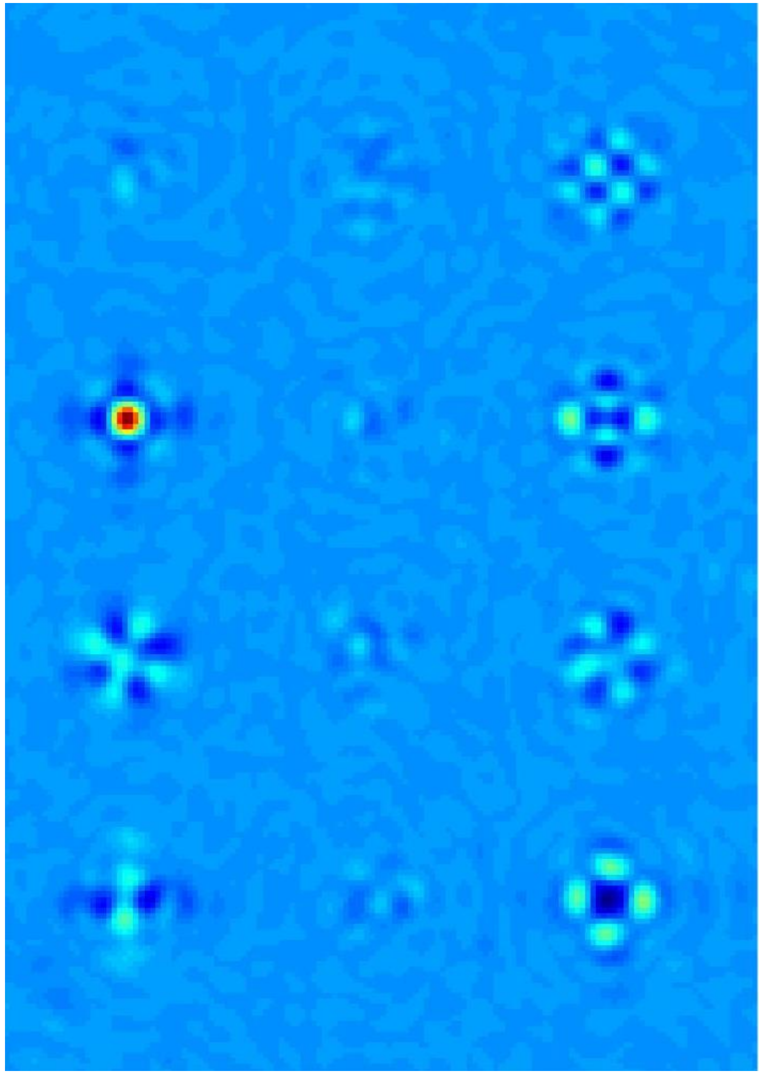

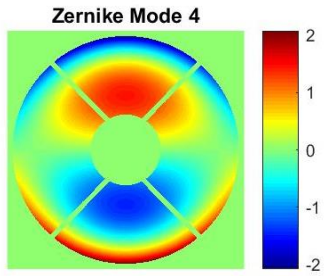
Zernike Mode 4
2
1
0
-1
-2

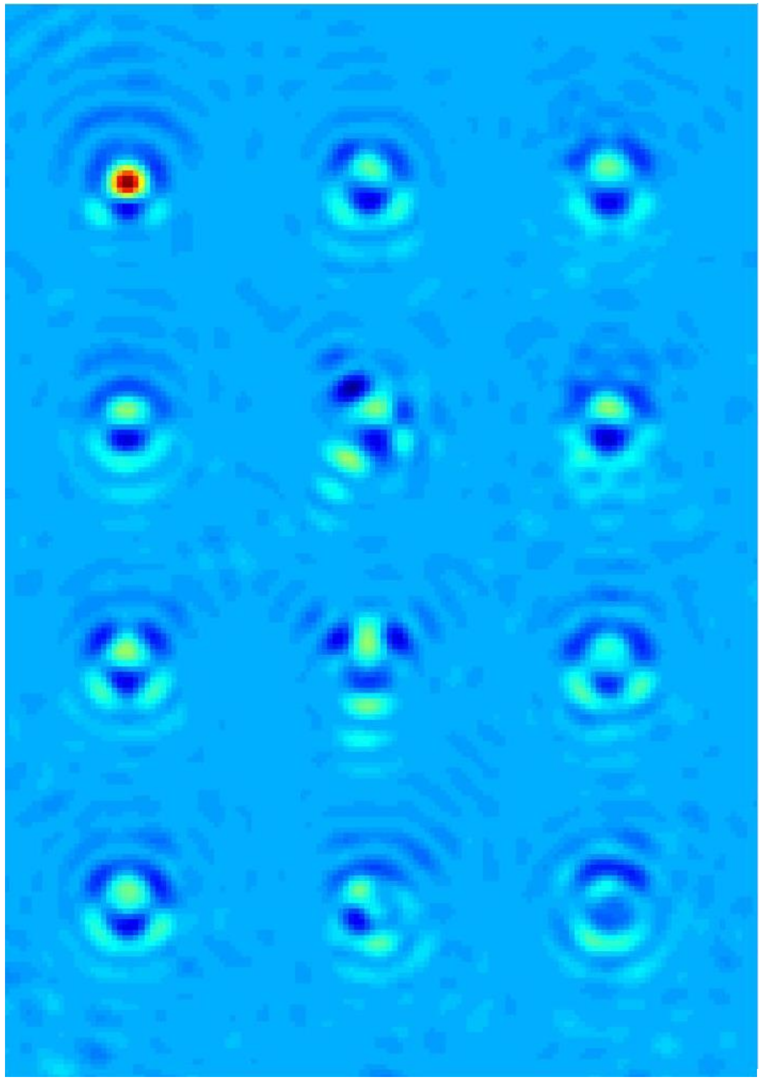

Simulated beam footprint
on the BMC Kilo-DM

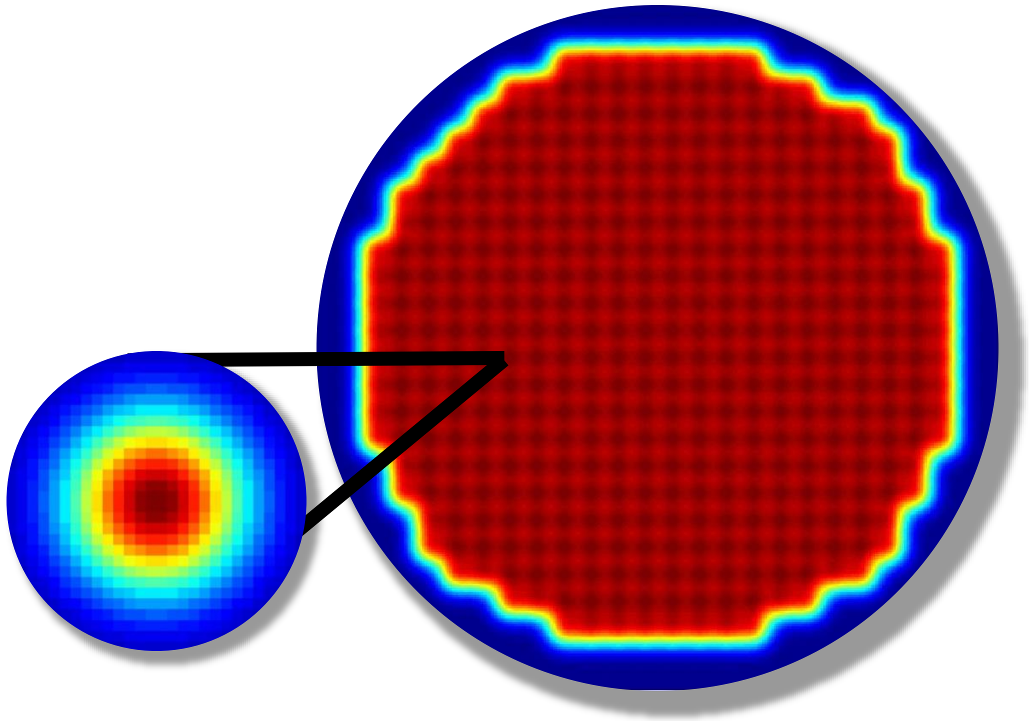

Table 6: Uncorrectable Common Path WFE (nm rms wavefront)

	No BMC				BMC 20 nm rms flat				BMC 13 nm rms flat			
OAPS Flats:	$\lambda/20$	$\lambda/50$	$\lambda/100$	$\lambda/200$	$\lambda/20$	$\lambda/50$	$\lambda/100$	$\lambda/200$	$\lambda/20$	$\lambda/50$	$\lambda/100$	$\lambda/200$
Vend. 1 Standard	229.1	218.7	217.1	216.7	231.2	220.8	219.3	218.9	230.0	219.6	218.1	217.7
Vend. 2 $\lambda/8$	219.2	208.2	206.6	206.2	221.4	210.5	208.9	208.5	220.1	209.2	207.6	207.2
Vend. 2 $\lambda/20$	113.1	90.1	86.3	85.3	117.3	95.2	91.7	90.7	114.9	92.3	88.6	87.6
Vend. 1 Precision	90.9	59.8	53.9	52.3	96.0	67.3	62.1	60.7	93.1	63.0	57.5	56.0
Vend. 1 High Prec.	79.2	39.8	30.2	27.3	85.0	50.4	43.2	41.2	81.7	44.5	36.3	33.9

Table 7: Non-Common Path WFE (nm rms wavefront)

	WFS Channel				Science Channel			
OAPS Flats:	$\lambda/20$	$\lambda/50$	$\lambda/100$	$\lambda/200$	$\lambda/20$	$\lambda/50$	$\lambda/100$	$\lambda/200$
Vend. 1 Standard	183.7	169.2	167.1	166.5	188.9	180.5	179.2	178.9
Vend. 2 $\lambda/8$	176.4	161.3	159.0	158.4	180.6	171.8	170.5	170.2
Vend. 2 $\lambda/20$	100.9	71.2	65.9	64.5	91.8	73.0	69.9	69.1
Vend. 1 Precision	86.5	48.8	40.6	38.3	72.9	47.1	42.1	40.8
Vend. 1 High Prec.	79.3	34.6	21.6	16.9	62.8	29.1	20.2	17.2